

Article

Mediterranean-Scale Drought: Regional Datasets for Exceptional Meteorological Drought Events during 1975–2019

Shifa Mathbout ^{1,*} , Joan Albert Lopez-Bustins ¹ , Dominic Royé ²  and Javier Martin-Vide ¹ 

¹ Climatology Group, Department of Geography, University of Barcelona, 08001 Barcelona, Spain; jlopezbustins@ub.edu (J.A.L.-B.); jmartinvide@ub.edu (J.M.-V.)

² Department of Geography, University of Santiago de Compostela, 15782 Santiago de Compostela, Spain; dominic.roye@usc.es

* Correspondence: shifamathbout@yahoo.com

Abstract: Drought is one of the most complex climate-related phenomena and is expected to progressively affect our lives by causing very serious environmental and socioeconomic damage by the end of the 21st century. In this study, we have extracted a dataset of exceptional meteorological drought events between 1975 and 2019 at the country and subregional scales. Each drought event was described by its start and end date, intensity, severity, duration, areal extent, peak month and peak area. To define such drought events and their characteristics, separate analyses based on three drought indices were performed at 12-month timescale: the Standardized Precipitation Index (SPI), the Standardized Precipitation Evapotranspiration Index (SPEI), and the Reconnaissance Drought Index (RDI). A multivariate combined drought index (DXI) was developed by merging the previous three indices for more understanding of droughts' features at the country and subregional levels. Principal component analysis (PCA) was used to identify five different drought subregions based on DXI-12 values for 312 Mediterranean stations and a new special score was defined to classify the multi-subregional exceptional drought events across the Mediterranean Basin (MED). The results indicated that extensive drought events occurred more frequently since the late 1990s, showing several drought hotspots in the last decades in the southeastern Mediterranean and northwest Africa. In addition, the results showed that the most severe events were more detected when more than single drought index was used. The highest percentage area under drought was also observed through combining the variations of three drought indices. Furthermore, the drought area in both dry and humid areas in the MED has also experienced a remarkable increase since the late 1990s. Based on a comparison of the drought events during the two periods—1975–1996 and 1997–2019—we find that the current dry conditions in the MED are more severe, intense, and frequent than the earlier period; moreover, the strongest dry conditions occurred in last two decades. The SPEI-12 and RDI-12 have a higher capacity in providing a more comprehensive description of the dry conditions because of the inclusion of temperature or atmospheric evaporative demand in their scheme. A complex range of atmospheric circulation patterns, particularly the Western Mediterranean Oscillation (WeMO) and East Atlantic/West Russia (EATL/WRUS), appear to play an important role in severe, intense and region-wide droughts, including the two most severe droughts, 1999–2001 and 2007–2012, with lesser influence of the NAO, ULMO and SCAND.

Keywords: climate change; drought event; Mediterranean basin; meteorological drought; SPEI; SPI; RDI; DXI



Citation: Mathbout, S.; Lopez-Bustins, J.A.; Royé, D.; Martin-Vide, J. Mediterranean-Scale Drought: Regional Datasets for Exceptional Meteorological Drought Events during 1975–2019. *Atmosphere* **2021**, *12*, 941. <https://doi.org/10.3390/atmos12080941>

Academic Editor: Luis Gimeno

Received: 7 July 2021

Accepted: 19 July 2021

Published: 22 July 2021

Publisher's Note: MDPI stays neutral with regard to jurisdictional claims in published maps and institutional affiliations.



Copyright: © 2021 by the authors. Licensee MDPI, Basel, Switzerland. This article is an open access article distributed under the terms and conditions of the Creative Commons Attribution (CC BY) license (<https://creativecommons.org/licenses/by/4.0/>).

1. Introduction

1.1. Climate Change and the Growing Risk of Drought Hazard

Climate change, in combination with accelerated population growth, has been described as the biggest human threat of the 21st century, putting natural systems and, thereby, sustainable human and environmental resource development at increased risk [1].

The intensive climate extremes are projected to result in a change in water availability, exacerbate carbon losses in terrestrial ecosystems, and further raise water vapor content in the atmosphere, thus amplifying the warming impacts and increasing mega-droughts worldwide [2–4]. Drought is one such recurring, widespread, complicated, costliest and disruptive climate extreme that frequently occurs as a result of differential responses to climate warming in different climatic regimes [5–7]. Recently, drought has begun to be seen not as a purely natural hazard, but partially as a result of human action, which has altered many of the characteristics of drought [1,8]. One-fifth of the global destruction caused by natural disasters can be attributed to droughts [9], where the dramatic population and economic growth has resulted in increasing demand for water that substantially intensified the frequency of global drought events [10]. Pandemics can potentially exacerbate drought impacts [11], as it was found that drought is among the most obvious reasons for displacement and disturbance during the coronavirus pandemic [12,13]. Droughts in the 21st century are identified as multifaceted, challenging natural disasters [14,15] and are characterised by longer duration, higher severity, larger spatial extent and hotter temperature that can potentially result in many deleterious impacts on ecological security, with non-linear alterations in ecosystem functions and resilience [3,4]. Systematic reviews [16,17] have indicated an accelerated transition to a more arid climate over several areas as the result of an increased tendency of frequent and intense droughts. Meanwhile, human-induced global warming and rapidly expanding human populations have already influenced water availability and storage, increasing pressure on water supplies, affecting the long-term ecosystem and increasing their sensitivity to droughts [4,18]. As a result of 1.5 to 2 °C global warming, two-thirds of the world population will experience increasing droughts; the drought magnitude is likely to double in 30% of the global land by the end of this century [19,20]. An important part of drought problem is that its current definitions refer to the drought only from the perspective of human dimensions, focusing primarily on meteorological, agricultural, socioeconomic and cultural impacts without addressing its ecological dimensions [21]. The occurrence of widespread drought in developing and developed societies has underscored the sensitivity of all communities to this natural hazard. It is not easy to know whether the drought frequency is increasing, or rather the community exposure to it. This tendency appears to be accelerating as a result of the increasing demand on both local and regional water resources [22]. The socioeconomically devastating impacts of frequent drought events have recently resulted in several global assessments of future drought conditions to better support populations and improve management plans in order to reduce direct and indirect cascading drought impacts [23–25]. Combining the natural and human dimensions of drought is one of the most fundamental steps in addressing the increased risk of drought in the 21st century [18,26].

1.2. Drought, Climate Change and the Mediterranean Context

The MED is identified as one of the most responsive hotspots of the climate system in the face of increased dryness at global warming levels beyond 1.5 °C [27]. The IPCC 1.5 degree Special Report (SR15) has pointed out that the increased anthropogenic warming in the MED has contributed to increased drying in the northern hemisphere mid-latitude areas including the MED [28,29]. Furthermore, with global warming of 2 °C, desertification is also predicted to occur in the MED by the end of the 21st century, resulting in an expansion of areas with significant decreases in water availability, with an accompanying increase in aridity, driving irreversible terrestrial biodiversity loss and affecting the Mediterranean ecosystem carbon storage in the coming decades [30]. The MED experienced more frequent and severe meteorological and hydrological droughts in recent decades, which is in line with the expected trend towards high frequencies of drought periods in a future warmer climate [31,32]. Above 2 °C, the MED could become more vulnerable to drought, calling for the development of a variety of adaptation mechanisms and the pursuit of drastic adaptive responses to cope with these extreme climate events, including mitigation strategies in addition to radical changes in the social structure and human communities [33,34]. The

complexity of the Mediterranean climate, with its high rainfall variability and its unequal seasonal distribution in addition to the observed dynamical and physical atmospheric process complexities [35,36], produced the conditions that have led to the high sensibility and vulnerability of this region to droughts [37]. Droughts are not spatially coherent in the MED [38] demonstrating different spatial patterns even at the regional scale [39,40].

The main goal of our study is to identify and characterise meteorological drought events over the MED by constructing a robust list of the most relevant drought events that occurred in the MED between 1975 and 2019, and analysing these events. The severity, intensity, spatial extent, peak month, area involved at peak month and the frequency of drought occurrence are the essential characteristics that we have investigated. Compared to the existing drought datasets, we have provided some important developments and novelties that include a new and detailed database of drought episodes over the MED. The importance of this dataset is that it deals in details with the drought events in the Eastern Mediterranean and Middle East (EMME), where drought studies are still relatively few. Based on quality-checked and homogenised data, three drought indices were applied in order to obtain detailed information and better understanding of drought events' features over the MED in addition to formulating a strong dataset of these events, taking into account the impacts of both precipitation (PP) and temperature (TEMP). The obtained drought events records have specific entries at both the country and subregional scales, which can then be used to extract the main drought characteristics for each subregion.

The remainder of this paper is structured into five main sections. In Section 2, we present the input data, study area and the selected drought indices. The main characteristics of different drought events and the new applied system for classifying the drought events are also demonstrated in this part. Section 3 displays the analysis results and discussion and describes, separately: the database structure; the collected records at the country and subregional scales; the biggest constructed drought events; and the drought dynamics in terms of large-scale teleconnection patterns. Finally, Section 4 derives some conclusions from the main results and includes some critical research questions for evaluating future studies of drought in the region.

2. Data and Methods

2.1. Study Area and Data

The Mediterranean basin, with latitude boundaries between 30° and 49° N and longitude boundaries between 10° W and 45° E, is the study area in this work. This study area reaches portions of three continents: Africa, Asia, and Europe. Climate is very variable within this area and characterised by warm to hot, dry summers and mild to cool, wet winters [40]. The daily meteorological datasets (1975–2019) used in this study are compiled by both the European Climate Assessment & Dataset (ECA & D; [41]) and the Global Historical Climatology Network (GHCN; [42]) Data for Syria, Lebanon, Algeria, and Jordan are directly obtained from national meteorological and hydrological services and some regional research projects. Main statistical characteristics of total annual precipitation and mean annual temperature for all stations are shown in Appendix A. After an initial quality check, the mean monthly maximum and minimum temperature (T_{max} , °C), (T_{min} , °C) were computed as an arithmetic average of daily maximum and minimum temperatures, respectively. The mean temperature values for any given month were considered if there were no more than three missing values in this month. Precipitation amounts (P) were transformed from daily values into monthly sums if no more than two daily values were missing. Monthly temperature and precipitation series have also undergone further quality checks and data errors and inhomogeneities are eliminated using the MASH V3.03 (Multiple Analysis of Series for Homogenization [43,44]) homogenization procedures and 312 stations were finally selected for our study. About 20% of total stations failed the homogeneity tests, more than 90% of which are located in Greece, Italy, Algeria and Turkey. Depending on these results, we discarded 78 stations and completed this study with 312 meteorological stations distributed evenly located at the west–east axis of

the Mediterranean basin (Figure 1). The values NOAA, EATL/WRUS and SCAND indices used in the study were obtained through the NOAA CPC website: <https://www.cpc.ncep.noaa.gov/data/teledoc/telecontents.shtml>, accessed on 21 July 2021 while the following websites have been used to obtain the values of the WeMO and ULMO, respectively: <https://crudata.uea.ac.uk/cru/data/moi/>, http://www.ub.edu/gc/data_base/, accessed on 21 July 2021.

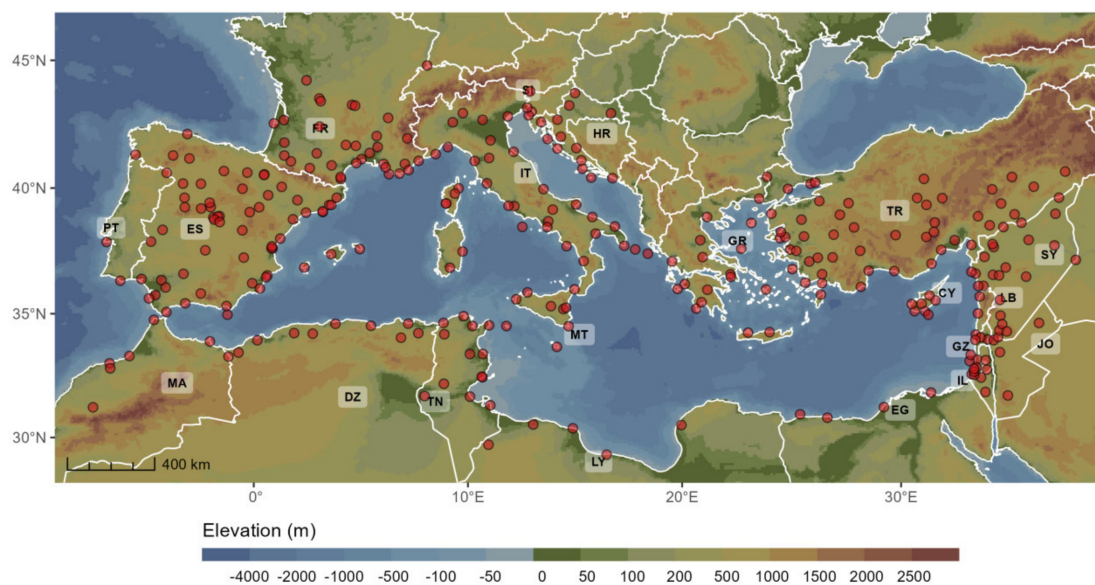


Figure 1. Geographical location map of meteorological stations with continuous monthly precipitation and temperature records in the Mediterranean Basin (MED) over the 1975–2019 period.

2.2. Selection of Drought Indicators: The SPI, SPEI and RDI

Drought indices are important and effective elements for providing a comprehensive picture of drought to plan, monitor, and quantify drought and its risk management [45,46]. Multiscale drought meteorological drought indices are commonly used as proxies for characterising soil moisture at different layers [47,48]. However, due to drought complexity, using a single index is not sufficient for precisely identifying the drought dimensions [49], and the combined use of several different drought indices would give an actual and clearer picture of drought conditions [50]. Drought is defined for each station using the Standardized Precipitation Index (SPI; McKee et al. [51–53]), which is based on precipitation data only and measures the normalised anomalies in accumulated precipitation through a given number of months. The SPI was recommended by the World Meteorological Organization (WMO) in 2012 to characterise the meteorological droughts and quantify the precipitation deficit at multiple time scales [54]. The later Standardized Precipitation Evapotranspiration Index (SPEI; [55,56]) is also applied. The SPEI is designed to represent climatic water balance (the difference between precipitation and potential evapotranspiration, PET), which captures the main effects on water requirement as a result of evapotranspiration. Using the ratio between cumulative precipitation and PET, the Reconnaissance Drought Index (RDI; [57,58]) is also used. The SPEI and RDI provide a more comprehensive representation of drought characteristics due to their inclusion of precipitation along with potential evapotranspiration that can be effectively used to compare the drought events under different climate conditions [59,60]. Droughts in the MED have very different dimensions and affect several sectors, but currently, the most important impacts relate to the hydrological one, which is largely affected by frequent droughts [61]. In this paper, the drought indices values are generated using a 12-month aggregation period because of its great importance in estimating the severity of hydrological droughts, determining the possibility of drought persistence conditions for long periods of time [62] and considering the management

of water supplies [40,63]. This paper focuses on long term drought indices (12-month timescale) because of their great importance in estimating the severity of hydrological droughts and determining the possibility of drought persistence conditions for long periods of time [62]. The input data are fitted to a two-parameter gamma probability density function for SPI-12 and RDI-12, whereas the SPEI-12 follows the log-logistic probability distributions. The PET is derived using the Hargreaves–Samani equation [64,65] which indirectly estimates extra-terrestrial radiation using T_{max} and T_{min} . Although the estimated evapotranspiration using temperature-based models may magnify the impacts of the current global warming [66], it has been indicated that drought indices provide reliable estimates of the true global drought trend when using the temperature-based models [67]. The temperature-based approaches, such as Thornthwaite, have produced reliable results [68]. The Hargreaves–Samani outputs show high correlation with Penman–Monteith method [56] and confirm high reliability in arid, semi-arid, Mediterranean, and very humid areas [69]. SPI-12 and SPEI-12 values are obtained using the SPEI package developed by Beguería and Vicente-Serrano (2017), available in R (Version.3.6.3, Development Core Team 2020) [70].

2.3. Drought Concepts and Characterisation, a Multivariate Perspective for a New Combined Index

A single index usually considers particular processes while ignoring others, leading to it not capturing an accurate picture of hydrological changes, and resulting in an incorrect interpretation [71]. To overcome the single-index problem, the three drought indices were integrated into one. For each station, a new combined drought index, DXI-12, was constructed by averaging the monthly values of the SPI-12, the SPEI-12, and the RDI-12 as a multivariate drought index to incorporate multiple drought-related values. The combination of multiple drought-related variables was successfully applied for drought monitoring [72], detecting [73,74], and prediction [75,76]. For example, results based on [77] have suggested a combined use of meteorological drought indices (SPI and SPEI) in the case of lack of streamflow measurements to provide the best performances in monitoring hydrological droughts. The development of a combined drought indicator gives a synoptic and synthetic overview and provides an integrated approach that fully describes the meteorological drought conditions across the MED [72]. The selected time scale relates to the time required for the effects of drought to appear on water resources and other different life sectors [78]. Recently, the use of multivariate indices has concretely increased [79], especially in cases that take into consideration the multiple characteristics of drought events. The combined index describes droughts in more detail, showing a set of drought characteristics such as intensity, severity, duration, start and end drought period, and areal extent for each region. Applicability of the combination of several drought indices is based on the fact that drought, as a natural phenomenon, results from a combination of different factors such as lack of precipitation, prolonged periods with below average rainfall, and increased evaporative demand as a result of temperature excess [80]. For each constructed drought event, we have identified the essential aspects of drought characteristics. In this paper, seven parameters (severity, intensity, duration, areal extent, peak area, peak month, area involved with peak month) were used to describe the constructed drought events. Details about the definition of these parameters can be found in Table 1. The degree of dryness (DDI) was also assessed as an indicator to evaluate the drought intensity for different drought categories in each area and for each subregion. More details about DDI calculation can be found in Salehnia et al. [81].

Table 1. Parameters used for a drought event evaluation as listed in the database.

Start event, month (ST)	The first month with an index value below a certain threshold
End event, month (EN)	The last month with an index value below a certain threshold
Drought duration (DD)	Number of consecutive months between drought start and drought end (length of drought event)
Drought severity (DRS)	Sum of the absolute values of drought indices during a drought event
Drought intensity (DRI)	The mean value of drought indices during a drought event (DRS/DD)
Drought frequency (DRF)	Number of drought events during specific interval, usually expressed as number of events every decade.
Areal Extent (AE)	Percentage of the region with indicator values below a certain threshold
Peak Area (PA)	The largest area exposed to drought during the event (%). Usually the PA is presented with its corresponding date in month and year (AMY)
Peak month and year (PM)	The month with the lowest value of the index over the drought event. This parameter is usually presented with severity value of this month.

2.4. Principal Component Analysis (PCA)

PCA is a multivariate technique that is extensively used in meteorological, climatological, hydrological studies, and drought regionalisation as a dimensionality reduction statistical method for extracting structural information in a dataset, and allowing a clearer interpretation of large datasets of dependent variables without losing much of the original information [82]. In this paper, the PCA was used to capture the major spatial patterns of drought across the MED by reducing dimensionality in a group of the DXI-12. Specifically, the S-mode PCA with the varimax orthogonal rotation was applied to the DXI-12 at 312 stations for identification of the regions within the MED that have homogeneous drought features and conditions. The S-mode PCA enables the analysis to describe the areas with close temporal fluctuations [83]. Using the REdaS R package developed in 2015, the Kaiser–Meyer–Olkin (KMO) test [84] was utilized to examine the quality of the principal components of the time series of all drought indices before the application of the PCA method, and thus, to check the suitability of the data for factor analysis. Both the scree plot of eigenvalues and the rule of thumb [85] were used to make the decision on how many loadings to retain for rotation. The PCA was performed using the “prcomp” function in R.

2.5. Definition of the Constructed Meteorological Drought Event Database

According to Henriques and Santos [86], a drought event occurs when the value of the variable falls below a fixed threshold. Many thresholds were selected for classifying drought events. McKee et al. [51] established that a drought event starts when the SPI value reaches -1 and ends when it becomes positive. Spinoni et al. [76] indicated that a drought spell requires at least two consecutive months with a negative drought indicator measured. Spinoni et al. [28,87] assumed that a drought event starts when the indicator values fall below a certain value corresponding to a given negative standard deviation ($X_i = -1\sigma$) for at least two consecutive months and ends when this value turns positive. In this study, drought durations for each country/subregion were constructed by creating sequences of the number of two or more consecutive months over which the value of indicator persists below a given threshold ($X_i = -1\sigma$). The time series of drought durations for each station was constructed by creating a succession of the number of consecutive months, at least two, over which the value of the drought indicator persists below this threshold. The drought event ends when the indicator value turns positive. Each drought event within the constructed database has its own property which reflects the drought dimensions and characteristics. We have investigated the drought events at the national and subregional level to determine the biggest droughts that occurred in each region over the MED during last four decades. Monthly series for DXI-12 during 1975–2019 were obtained for each station, and then the corresponding series for each country were

constructed. Finally, the subregional series was derived for each subregion. We have also assembled a list of the overall most relevant Mediterranean drought events that took place between 1975 and 2019 by also considering the events that involved more than one region (multi-subregional events).

2.6. Developing a New System for Classifying the Drought Events According to Three Different Attributes

Spinoni et al. [28] compared the drought events at different scales according to a special scoring system that was derived from an aggregation of six different parameters. To further identify the most exceptional drought events over the past 40 years, a similar approach will be applied using only the three most important parameters (severity, intensity and the areal extent) to describe and classify the drought events in different areas over the MED. Since the drought is a three dimensional interdisciplinary and multi-scalar phenomenon [73,88], our new approach to classification of the drought events is modified to incorporate these three drought parameters. The new classification is modified to evaluate the drought events depending on the previous grouped parameters. The main objective of this method is to identify coherent time and coverage structures through a three-dimensional array (severity, intensity, and areal extent) of drought period identified by the DXI-12 in order to transfer this qualitative classification into a quantitative one. In other words, a given parameter received grades from 1 to 6, relying on the event itself compared to others in the series, at a regional scale. While this approach has been tested for two different accumulation periods (3 and 12-month timescale), in this paper, we only present the results for 12-month accumulations. The percentile is used as a way to classify the status of each parameter and different percentiles are examined to assess the drought event condition through the combination of the three aforementioned indicators. Table 2 shows the classes of the three selected parameters and their respective grades, and this adopted drought events classification system has established the categories of “extreme drought events” for total grades from 18 to 15, “severe drought events” for total grades from 14 to 11, and “moderate drought events” for grades from 10 to 1 as a new attempt to classify the drought periods according to these attributes. The new classification is applied for each constructed drought event through the DXI-12.

Table 2. Drought parameters classes allocated to each drought event and their competent grades.

Grade	DP Status
6	DP > 95th percentile over the recorded events at the subregional and regional scale
5	90th percentile < DP ≤ 95th percentile over the recorded events at the subregional and regional scale
4	70th percentile < DP ≤ 90th percentile over the recorded events at the subregional and regional scale
3	50th percentile < DP ≤ 70th percentile over the recorded events at the subregional and regional scale
2	30th percentile < DP ≤ 50th percentile over the recorded events at the subregional and regional scale
1	DP < 30th percentile over the recorded events at the subregional and regional scale

2.7. Atmospheric Circulation–Drought Conditions Analyses

The MED is prone to the effects of the large-scale teleconnection patterns which considerably vary in their strength within the region [89]. Several studies have considered the association between fluctuations in the atmospheric teleconnection patterns (ATPs) and droughts [90–92] and their different impacts on the hydrological regime in the MED [91,93]. Here, we focus on the North Atlantic Oscillation (NAO) [94], the Upper-Level Mediterranean Oscillation index (ULMO) [95], the Western Mediterranean Oscillation (WeMO) [96], the East Atlantic/West Russia (EATL/WRUS) [97] and the Scandinavia pattern (SCAND) [98] because a preliminary analysis has showed that they are the best candidates among existing teleconnection indices which describe the drought conditions in the region of interest. Relationships between atmospheric circulation and the percent

area of drought based on SPI-12, SPEI-12 and RDI-12 were explored using Pearson's correlation analysis.

3. Results and Discussion

3.1. Loading Patterns of SPI-12, RDI-12, SPEI-12 and DXI-12 Derived from PCA

The SPI-12, SPEI-12, RDI-12 and DXI-12 were used to identify drought patterns for the 1975–2019 period. For all drought indices, five principal components (PCs) were retained identifying five regions that are well-structured and spatially coherent and show the highest values of loadings and explain the highest variance. The obtained regions are characterised by different drought variability due to different precipitation and temperature regimes in these areas.

High values obtained in the KMO test (>0.71) suggest that all proposed drought indices are adequate for the PCA, which also indicates that we can apply the PCA method to all selected time series. The KMO measures of sample adequacy applied to the drought indices are, respectively, 0.71, 0.95, 0.69, and 0.92 for the SPI-12, SPEI-12, RDI-12 and DXI-12, suggesting that all are adequate for PCA analysis (KMO test > 0.50). Applying the varimax rotation to the PCs has allowed the identification of subregions within the MED that have homogeneous drought conditions. Generally, there is a spatial coherence in the distribution of stations associated with each PC. Some stations have shown the highest correlation with more than one component identified in the PCA analysis. Generally, the main spatial patterns of all drought indices' variability characterise the MED uniformly. The patterns were harmonious and had a coherent spatial structure that was consistent with climate influences over the MED. Although the general drought patterns existing over the MED are captured by all indices, the proportions of variance by the leading PCs are relatively higher in the case of the SPEI-12, RDI-12, and DXI-12, indicating the significant role of PET and the large response of drought to temperature variations. This means that the sensitivity of a purely precipitation-based drought index to drought variability differs from the precipitation and temperature-based indices.

The percentages of the total variance explained by the first retained loadings for the previous drought indices, which explain 10.34%, 15.53%, 17.78%, and 17.58% of total variance, respectively, clearly exhibit consistent spatial structures as well as temporal variation. The second rotated loadings account for 10.08%, 10.5%, 10.49%, and 10.99% of the total variance, respectively, with a mean cumulative variance of almost 59.9% for the five PCs for all indices. Thus, the rotated loadings for SPI-12, SPEI-12, RDI-12 and DXI-12 successfully reflect a coherent structure with five distinct subregions that are characterised by different drought variability levels, which are possibly related to the different rainfall regimes in these areas. The spatial patterns of the first five principal components are almost the same for SPI-12, SPEI-12 and RDI-12 but, in the case of the SPEI-12 and RDI-12, the loadings are higher and correspond to a wider extent than SPI. Therefore, our study is based on the analysis of the drought-event records, which are constructed according to DXI-12 for five subregions spread over 20 countries along the Mediterranean area (Figure 2 and Table 3).

Table 3. The five subregions identified by five PCs for DXI-12 over the MED.

PCs	Code	Regions	Country
PC1	IBE-NWA	Iberian Peninsula–Northwest Africa	Spain–Portugal–South France–Morocco–Gibraltar
PC2	EMME	Eastern and Middle East	Syria–Lebanon–Israel–Palestine–Jordan–Cyprus–North Egypt–North Libya–South and South-East Turkey
PC3	AEG	Aegean Sea	Greece and West Turkey
PC4	BLK-FR	Balkans–France	France–Croatia–Slovenia–Central and North Italy
PC5	NA	North Africa and south Italy	Algeria–Tunisia–Malta–Tyrrhenian Sea

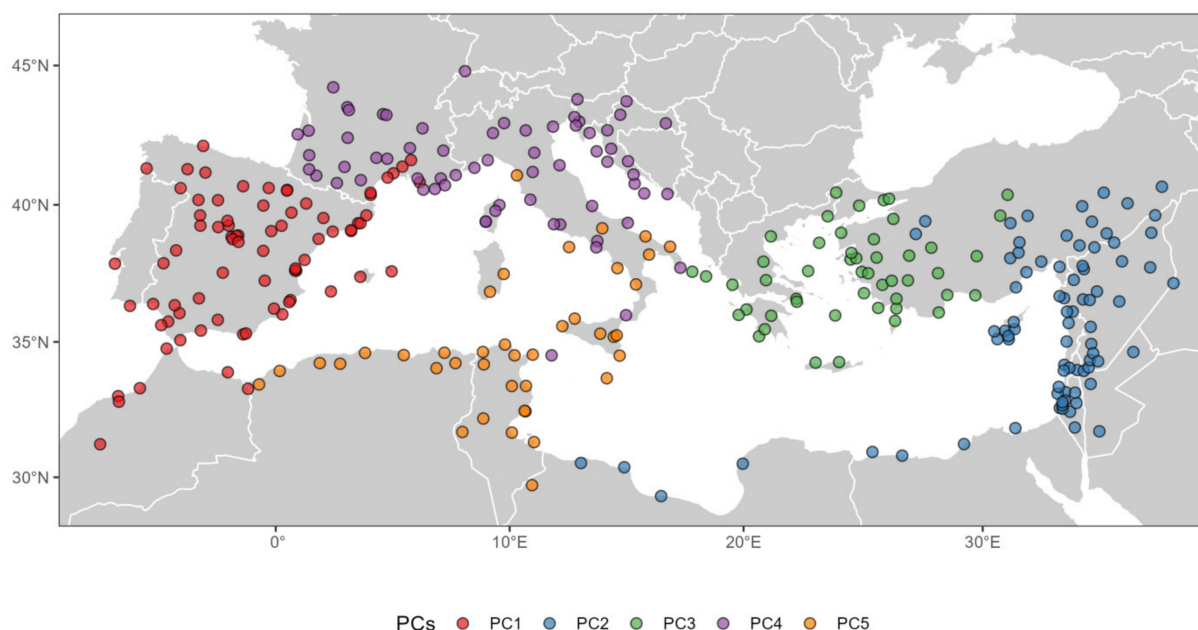


Figure 2. Spatial patterns of the rotated loadings of the five principal components (PCs) based on the principal component analysis (PCA) on the DXI-12.

3.2. Meteorological Drought Events Identified by DXI-12 and Their Characteristics at Country and Subregional Scales

Based on the analysis of the DXI-12, a new dataset of meteorological drought events was constructed during the period between 1975 and 2019. The overall number of drought events is 375, 169 of which occurred after 1996 at the country level. Any drought event that involved more than one country was allocated to represent its subregion. At the subregional scale, 19 drought events are detected in IBE-NWA, whereas the dataset has reported 20, 13, 13 and 15 drought events in EMME, AEG, BLK-FR and NA, respectively. The spatiotemporal characteristics of each drought event, including its duration, severity, intensity, areal extent and area involved with peak were examined at the country and subregional scales. Considering that the area affected by drought is a very important drought characteristic to evaluate the drought risk, we first reported the widest drought events in each region that hit more than one country with a peak regional area that exceeded 50% (Table 4). The corresponding Degree of Dryness (DDI) values for the peak year for each drought event at the subregional scale are also presented.

Table 4. List of the widest drought events detected by the DXI-12 and their corresponding areal extent, the area involved by the peak month, and the Degree of Dryness (DDI) of widest area at the subregional scale during 1975–2019.

Region	Period	DRS	DRI	Peak Event		Area Involved with PM %	DDI	AE %	Widest Area	
				PM (Mon/Year)	DRS				PA%	Mon/Year
IBE-NWA	1981–1983	20.1	1.4	11/1981	2.4	57.3	3.6	21.1	57.1	11/1981
	1989–1992	20.3	1.4	04/1992	2.8	50.0	4.8	20.3	50.0	04/1992
	1994–1995	28.7	2.2	12/1995	3.1	52.1	11.3	36.2	78.1	10/1995
	1999–2000	27.5	2.3	06/1999	3.2	50.1	7.1	51.0	58.4	05/1999
	2004–2005	25.4	2.1	01/2005	3.3	30.1	11.9	52.7	74.2	08/2005
	2012	17.6	1.5	03/2012	2.8	57.0	8.5	46.6	70.0	07/2012
	2014–2016	20.2	1.7	04/2014	2.8	33.8	4.6	32.0	58.4	01/1016
	2017–2018	35.3	2.0	11/2017	3.7	41.0	6.2	33.5	74.3	12/2017
	2019	17.0	1.5	07/2019	2.9	45.5	5.9	45.0	57.1	11/2019

Table 4. Cont.

Region	Period	DRS	DRI	Peak Event		Area Involved with PM %	DDI	AE %	Widest Area	
				PM (Mon/Year)	DRS				PA%	Mon/Year
EMME	1999–2001	30.5	2.5	07/1999	2.8	70.0	14.3	51.0	80.3	12/1999
	2007–2012	40.6	2.2	05/2008	3.3	61.3	9.8	33.2	80.0	01/2009
	2014–2018	53.6	2.2	01/2017	3.3	60.0	10.5	35.1	67.9	12/2017
AGE	1977	14.4	1.3	08/1977	2.3	22.4	2.9	50.0	51.0	11/1977
	1989–1991	31.9	2.3	01/1990	3.3	59.2	11.3	52.4	77.6	11/1990
	1992–1993	33.0	1.5	08/1992	2.5	36.7	6.3	30.0	51.0	12/1992
	1999–2001	37.0	2.1	10/2001	2.9	65.3	9.0	50.0	65.3	03/2001
	2006–2009	44.0	2.1	06/2008	3.2	42.9	13.0	51.0	78.0	10/2007
	2013–2014	40.1	1.7	02/2014	3.3	50.0	4.1	20.0	51.0	02/2014
	2015–2018	43.1	1.7	09/2017	3.8	30.0	6.8	35.0	55.0	10/2016
BLK-FR	1989–1991	39.2	1.8	10/1989	3.3	52.2	9.4	48.6	66.7	09/1990
	2001–2002	35.4	1.5	12/2001	2.8	30.0	7.9	50.0	71.6	04/2002
	2003	15.0	1.4	11/2003	2.4	46.3	3.9	31.0	50.0	12/2003
	Winter (2003–2004)	5.7	1.6	01/2004	2.5	49.3	4.0	43.8	50.7	02/2004
	2006–2008	45.4	1.6	12/2006	2.9	38.8	7.2	26.0	53.7	10/2007
	2011–2012	33.3	2.4	11/2011	3.1	39.3	8.4	38.6	71.5	03/2012
	2016–2018	40.6	1.5	10/2017	3.2	62.7	9.2	37.8	65.7	11/2017
NA	2019	20.0	1.5	06/2019	2.7	37.3	4.9	30.0	50.1	03/2019
	1980–1982	50.1	2.1	08/1981	2.9	35.9	4.9	30.0	50.2	12/1981
	1988	15.0	1.4	05/1988	2.1	53.8	5.8	37.8	53.8	05/1988
	1999–2002	51.2	2.2	10/1999	3.4	64.1	8.5	36.0	64.1	02/2002
	2004–2005	44.0	2.1	12/2004	3.8	43.6	4.9	28.7	50.0	12/2004
	2016	17.1	1.4	01/2016	2.2	30.8	2.8	38.0	51.3	11/2016
	2017–2018	26.0	1.5	01/2018	3.9	61.5	6.6	30.3	61.5	01/2018

Bold refers to the highest values at the subregional scale.

The areal extent of annual droughts (Table 4) shows many wide droughts over the MED that have struck more than 40% of the area. The exceptional multi-year drought event (1999–2001) might be marked as critical in all subregions, as the MED was exposed to drought episodes which affected the wider area by more than 50% in the IBW–NWA, EMME and AEG, while 37% of the area of NA was affected by this exception event. In terms of individual drought events and their other main characteristics, the differences were also significant between subregions. The meteorological drought events in the MED usually exhibit spiky behavior, inherently related to the high temporal variability of precipitation in this region. Generally, the most pronounced drought events in the last two decades experienced larger areas than other periods, compared with the late 1970s and 1980s. Sub regional drought area reached its highest level in several years after 2015 with severe and large coverage drought episodes during 2015–2018. Considering both the average of involved area and DDI values, the 1999–2001 period is the period of the broadest drought spell in the MED as a whole and the driest period in the EMME, with the drought also extended until 2002 in the NA, at which point it had the largest severity and highest intensity (Table 4). These findings reinforce what is already established by Hoell et al. [99] and Barlow et al. [100] who considered the catastrophic 1999–2001 droughts to be one of the worst drought periods in the EMME and the period with the widest drought impacts in the Southeastern Mediterranean. Furthermore, it appears that drought distribution within a multi-year is one of the most important factors in determining the severity of drought episodes. In Europe as a whole, a very spatially extensive event was shown between

2017 and 2018 that covered at least 35% of the total area and peaked in December 2017 with 74.3% in the Iberian subregion. The highest severities were also recorded during the 2017–2018 drought incidents in the IBE–NWA, as shown in Table 4. These results are in agreement with other studies [101] that ranked the 2017 drought period as one of the most severe drought events in Europe since 1979. In the IBE–NWA, an extensive coverage drought period (52.7%) was also notable in the mid-2000s, typified by high severe conditions (DDI = 11.9), and peaked at 74.2% in August 2005. The same degree of dryness was identical for the AEG in 1990, with a peak area of 77.6%. Severe drought events with high percentage areal extent were experienced in the AGE through the 1990s (59.2% in 1990), 2000s (65.3 in 2001) and mid 2010s (50% in 2014), with an almost complete lack of wide drought events in 1980s.

A wide drought event was recorded in the BLK–FR in the early 1990s, covering more than 50% of this area and followed by multiple periods of large drought extent in the mid-2000s with more 45% of spatial coverage that were not repeated until the late-2010s. Moreover, large sectors of the Adriatic and west central Mediterranean (BLK–FR) suffered from a persistent spring and summer drought in 2003 affecting 31% of this area and reaching its largest coverage in December 2003 (50%). This intensive drought episode was accompanied with an exceptional heatwave that broke the temperature record, particularly cross southern and central France [102,103], indicating a very good example of a compound drought and heat event. In the NA, drought events have been recorded in different periods and there was a succession of wide drought events since the 1980s but the most severe and widest drought event was recorded in the late 1990s, a period characterised by extremely severe long-lasting droughts. The latter half of the twentieth century also emerged as the driest of the last nine hundred years in the NA [104]. Furthermore, the multi-year drought (1999–2002) in the NA was reported as the most severe of the last five centuries [105].

Additionally, it is apparent that the late 1980s drought episode in the IBW–NWA, AGE, and NA droughts are not such extreme events compared with other drought episodes. The results suggest they display considerably lower severity and intensity with respect to the multi-year 1999–2001, 2005–2007 and 2015–2018 droughts. Table 5 and Figure 3 list the top five drought events that struck each subregion ranked by duration, severity, intensity, areal extent and degree of dryness. Several drought hotspots were indicated during last two decades along the MED. The most severe and intense droughts of the 1990s and late 2010s are clearly visible for the region as a whole.

Table 5. The top drought events (most severe, most intense, longest, widest dry events) and the highest degree of dryness in each subregion according to DXI-12 during 1975–2019.

Subregion	Most Severe		Most Intense		Longest Event			Widest Area		Highest Degree of Dryness	
	Period	DRS	Period	DRI	Period	DD	AE%	Period	DDI	Year	
IBE–NWA	1989–1990	57.5	1999	2.7	1989–1990	41	71.3	2017–2018	11.9	2005	
EMME	2008–2012	95.4	2005–2007	2.8	2008–2012	47	75.6	2008–2009	14.3	1999	
AEG	2015–2018	77.2	2016–2018	2.7	2015–2018	36	67.0	2007	13.0	2007	
BLK–FR	2015–2018	72.7	2004–2006	2.7	2015–2018	37	67.2	2002	10.4	1990	
NA	1999–2004	84.6	2006–2007	2.7	1999–2004	51	62.8	2002	8.5	1999	

Bold refers to the highest values at the subregional scale.

The 1990s and 2000s also stand out in terms of spatial area in drought. The most spatially extensive events were two of the five long-lasting droughts (2008–2009) in the southeastern Mediterranean across the EMME, and in 2002 in NA. The multi-year drought in 2015–2018 displayed a highly unusual spatial pattern that affected huge parts of Europe including the AEG and BLK–FR, as shown in Table 5. Dry conditions were reported in over 90% of central-western Europe, which hit record-breaking values in more than 25% of the area [100]. Furthermore, the spatial coverage of the top drought events in all subregions

has displayed large affected areas with the highest coverage in the EMME ($\approx 76\%$) in the late 2000s.

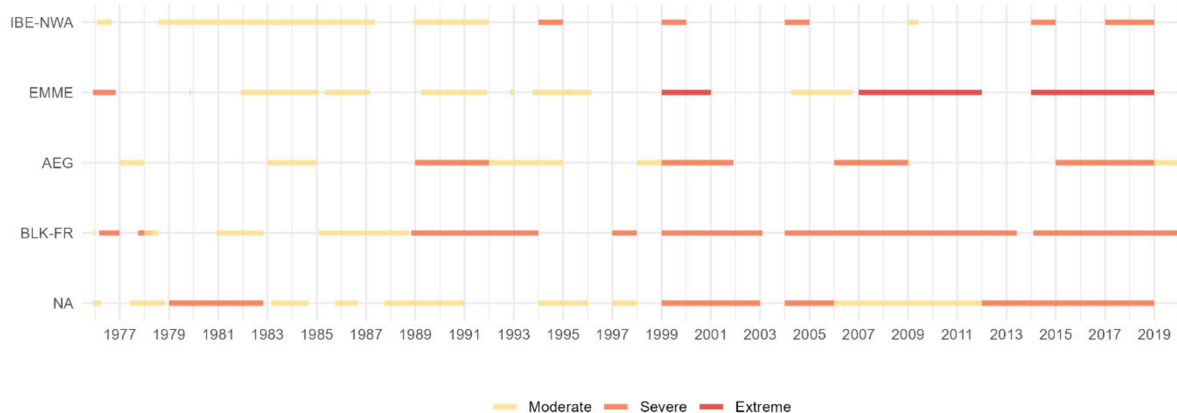


Figure 3. Subregional drought events in 1975–2019 identified by the DXI-12.

For the same period, this area also displayed its most long-lasting drought event, lasting 47 months, which was the longest drought episode in the last 900 years in the EMME [38]. This prolonged drought episode (2007–2012) was one of the worst long-term droughts in modern history, and was associated with the steepest decline in crop productivity in thousands of years [100]. With this continuous harsh drought phenomenon, hundreds of thousands of people have been displaced in the Euphrates and Tigris catchment basins, leading to an increased risk of regional conflicts, and thus contributing to the outbreak of war and helping to spark the Syrian Civil War [106,107]. The most intense drought events were recorded in the late 1990s and mid-2000s in the IBE-NWA, EMME, and NA, whereas the late 2010s experienced the most intense events in the AEG. Results have revealed top drought clusters in specific decades such as the mid-2000s and late 2010s, and more widespread events were most notable during the 2000s, with the highest degrees of dryness also shown after 1990 in the region as a whole. The highest degree of dryness was recorded in the 1990s in the EMME, NA and AEG, while the other subregions recorded their highest scores in the mid-2000s. These results are in line with other previous ones which confirmed that there is clear evidence of a strong drying trend in the EMME starting in the early 1960s, with the lowest precipitation amounts associated with the driest years in the late 1990s [99,108]. Very similar findings have been obtained by computing the DDI to describe the area affected by the droughts in the AEG. This result was also reported by Korner et al., 2005 [109], who indicated that the most crop yield declined in the Aegean area, namely in Greece, during the 1990s due to the consecutive severe droughts that hit this area. Varol and Ertugrul, 2015 [110] have also reported an increase of 14.75 times in the burned forest area in the Aegean region after 1990 due to increased droughts in this area. Finally, the results suggest the MED as a region which is characterised by a marked and high spatial variability of drought events, even for the most extreme and exceptional episodes recorded in the region, which is consistent with the results of previous observation [111]. The higher values of the DDIs during the last two decades also represent the trends toward drier conditions in all subregions (Figure 4).

Figure 4 presents the temporal variations in the DDIs over the MED during the 1975–2019 period. The results demonstrate that the MED has exhibited a high drought tendency during the past four decades with more frequent and severe droughts occurring after the 1990s and in the 2000s, and fewer droughts in the 1980s. Based on Figure 4, the DDIs change in the MED exhibits a large subregional increase over the past four decades, with a remarkable upward (drying) shift since the late 1990s. Generally, the MED displays the highest tendency toward extreme dry conditions, represented by higher DDIs values (>10) in the IBE-NWA, EMME and AEG, where the highest DDI was recorded in 1999 in

the EMME (14.3). Large dry conditions were also present for the other four subregions in the 2000s, while relatively small dry conditions were present from the early-1980s into the mid-1990s.

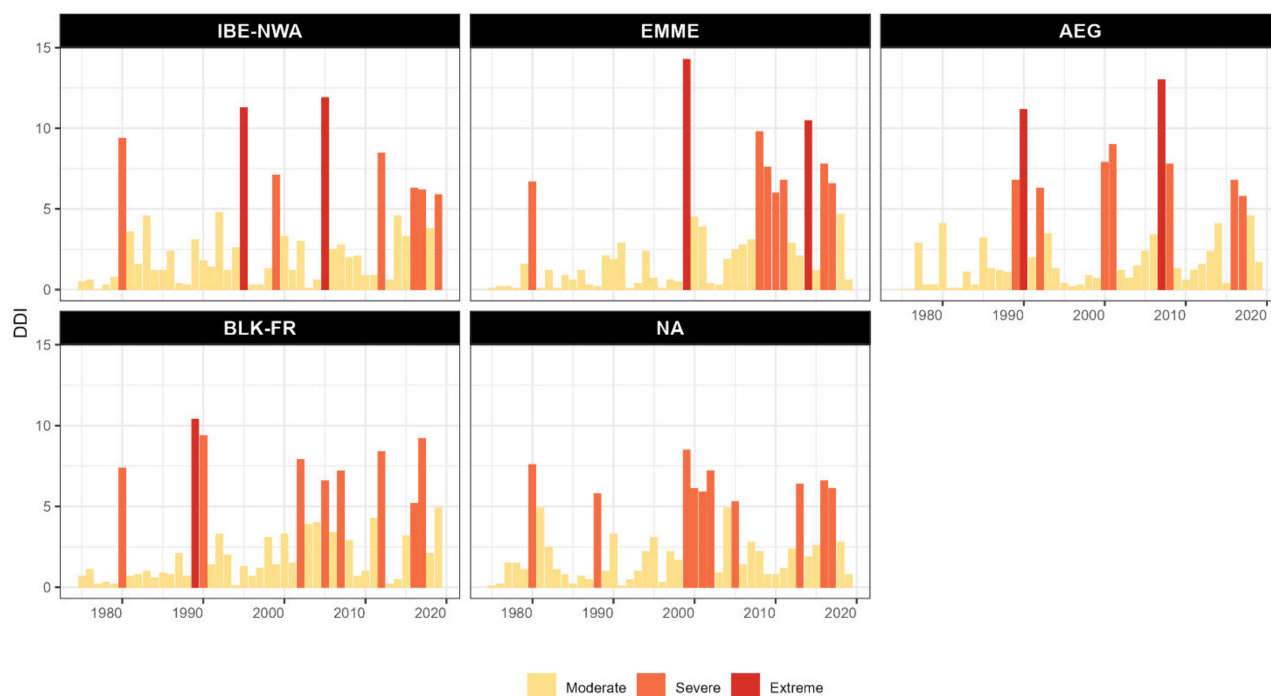


Figure 4. Temporal variations of the degree of dryness (DDIs) over all subregions during 1975–2019.

3.3. Three-Dimensional Identification and Characterisation of Meteorological Drought Events at Subregional and Regional Scales

According to the new classification system that we previously described, multiple drought events have been recorded between 1975 and 2019 at the national and regional scales. Following the new classification, the meteorological drought events were firstly investigated at the country scale (Table 6), as the impacts of drought, corresponding damages and other economic losses are generally recorded at the national scale for each drought event [112]. Then, all events at the country scale which involved more than one country have been grouped to create a new list of drought events at the subregional scale (Table 7). Only drought events with high grade (>13) during 1975–2019 have been considered for both the national and regional scales. In order to prove the effectiveness of our approach in extracting drought periods, we have listed some scientific literature and scientific text-based reports that discussed single or several drought case studies across the MED. Generally, the literature is not as extensive about all drought events in the MED, particularly in southern and southeastern areas. However, all the drought events reported in Tables 6 and 7 has been previously documented. The spatial patterns of the obtained drought events in this study are in good agreement with most of the major drought events presented in the international database of text-based reports and add a series of other drought events, particularly in the Eastern Mediterranean and Maghreb countries. As shown in Table 6, the largest numbers of droughts occurred from the 1990s up to the present and are considered to be exceptional events. All countries have experienced extreme drought events becoming more severe and more intense in the last two decades. The areal extent of annual droughts (Table 6) shows that many wide droughts, in all Mediterranean countries, have struck more than 50% of the area. The period after the late 1990s might be marked as critical, as the MED was exposed to drought episodes which affected more than 90% of countries in the wider area. For example, the event in 1989–1991 was the most severe one in Greece, Italy, and Croatia over the last four decades and the

area under these very dry conditions has dramatically expanded to reach its maximum (97%) in Croatia in this exceptional drought spell. The late 1990s were characterised by very exceptional events that hit the Southern Levant countries (Syria, Lebanon, Israel, Jordan, Palestine, and Turkey), two of them ending in the early 2000s (Syria and Turkey). The 1999 widespread drought also affected neighboring Jordan and Israel, which were hit by their worst drought over the past 100 years in 1999 [113]. The highest drought severity ever recorded at the country level was detected in Algeria in the late 1990s, namely between 1999 and 2002 (Table 6). The recent drought (1999–2002) in the Mediterranean parts of Algeria and Tunisia was classified as the longest period of consecutive drought years since at least the middle of the 15th century and the worst drought event that struck these two countries since at least the middle of the 15th century [105,114]. The period between 2000 and 2001 included very severe and prolonged droughts in France, Italy, and Greece, which started in 1999 in Greece. This period is seen as the most serious event in Italy since the 1920s [115]. The extensive and persistent droughts in the mid-2000s significantly exceeded the other events in their spatial extent to include all the Mediterranean countries. Table 6 shows many wide droughts that struck more than 40% of the area, such as the event which spanned between 2003 and 2004 in Croatia and affected 74% of the entire country. The results display that around 34% of the area that was hit by drought in 2006 and substantial parts of Morocco and Spain (50 % and 70%, respectively) were also drought-prone between 2004 and 2005. Very dry conditions occupied several western and eastern countries in the mid and late-2010s as one of the most recent exceptional drought periods was consistent with a major drought in Spain, Italy, France, Algeria, and Cyprus and severe drought from 2016 to 2018 in Turkey. Based on these results, the two decades of 2000–2010 can be classified as a period with the most severe and long-lasting droughts during the last 50 years that appear in all Mediterranean countries [87,116]. More specifically, the droughts of the late 1990s, mid-2000s, and the multi-year drought series around 2015, appear to be the most serious and large spatial extent drought episodes, which covered almost all Mediterranean countries and reaching high severity levels. It should be noted, however, that recent droughts at particular locations (e.g., Algeria and Tunisia) are more severe than in other Mediterranean countries, as Algeria and Tunisia recorded the highest drought severity in 2002 and 1981, respectively. Although the other countries have a broader spatial extent, the NA experienced droughts in the late 20th century that were exceptional in the context of the prior 500 years [117].

Table 6. List of subregional exceptional drought events across the MED detected by DXI-12 at the country level that were identified according the new grade classification, 1975–2019.

Country	ST	EN	DRS	DRI	AE %	Widest Area		Grade	Mentioned by
						PA%	AMY		
Spain	06/1994	12/1995	30.2	2.1	50.1	83.3	10/1995	15	[118]
	12/2004	05/2006	28.7	2.7	50.0	78.3	08/2005	15	[62]
	04/2017	08/2018	35.3	1.9	34.1	71.7	01/2018	14	[102,119]
Portugal	12/2004	01/2006	23.7	2.0	93.0	100.0	09/2005	18	[107]
Morocco	10/2004	12/2005	30.3	2.3	69.9	83.3	10/2005	16	[120]
	01/1995	11/1995	28.2	2.3	48.5	50.0	10/1995	14	[105,121]
	12/1998	11/2000	25.4	2.0	55.0	83.3	09/1999	15	[121]
Cyprus	02/2008	01/2009	33.3	2.2	57.1	85.7	08/2008	15	[122]
	12/2013	12/2014	20.2	1.7	83.5	100.0	12/2013	15	[123]
	01/2017	11/2018	22.4	1.9	57.1	85.7	11/2018	14	[124]
Israel	11/1998	12/1999	29.7	2.2	95.1	100.0	3–12/1999	18	[100]
Jordan	01/1999	12/1999	22.2	1.9	88.9	100.0	11/1999	14	[99]

Table 6. Cont.

Country	ST	EN	DRS	DRI	AE %	Widest Area		Grade	Mentioned by
						PA%	AMY		
Syria	10/2007	10/2011	45.0	1.9	70.0	87.5	02/2009	16	[38,125]
	11/1998	11/2000	25.6	2.1	70.0	91.7	12/1999	14	[99,100]
	01/2014	03/2015	37.0	2.3	31.7	45.8	04/2014	14	[120]
Turkey	01/2007	01/2009	43.3	2.0	57.7	91.3	01/2008	15	[126]
	02/2016	01/2018	40.8	2.0	36.5	65.2	10/2016	14	[126]
	04/1989	04/1990	34.9	1.9	39.4	67.4	12/1989	14	[127]
	05/1999	11/2001	37.0	2.1	42.6	69.6	10/2001	14	[126,127]
Greece	02/1989	01/1991	42.0	2.8	51.1	77.3	11/1990	15	[28]
	09/1999	06/2002	41.1	1.8	39.4	68.2	07/2000	14	[128]
	12/2006	01/2009	37.1	1.8	34.3	59.1	09/2007	14	[28]
Croatia	09/2011	10/2012	23.0	1.9	71.4	84.6	12/2011	16	[129]
	01/1989	11/1990	37.1	1.6	70.0	97.0	09/1990	15	[111]
	08/2003	04/2004	15.6	1.8	74.0	100.0	12/2003	14	[130]
France	09/2001	09/2002	23.1	1.8	40.0	65.0	04/2002	14	[111]
	03/1989	11/1990	37.0	2.0	42.8	86.5	10/1989	14	[131]
	12/2015	04/2018	48.1	1.8	41.3	89.2	11/2017	15	[101]
Italy	07/1988	12/1991	44.7	1.5	20.0	40.0	03/1989	14	[132]
	10/2001	09/2002	20.0	1.7	48.4	70.3	04/2002	14	[115]
	11/2015	11/2016	25.6	1.9	35.3	48.6	01/2016	14	[101]
	02/2017	05/2018	25.0	1.8	43.8	65.0	01/2018	14	[101]
Algeria	04/2017	03/2018	23.5	1.9	50.4	66.7	08/2017	15	[133]
	08/1999	11/2002	67.0	1.8	37.5	89.9	02/2002	14	[134]
Tunisia	04/1999	07/2000	28.7	1.7	58.2	92.3	10/1999	15	[105,114]
	02/1979	03/1982	50.1	1.7	42.7	69.2	08/1981	14	[120]

Table 7. A list of exceptional subregional drought events across the MED detected by DXI-12 that were identified according to the new grade classification during 1975–2019.

R	ST	EN	DRS	DRI	AE %	PA %	AMY	Score	Mentioned by
IBE–NWA	09/1994	12/1995	28.7	2.2	36.2	78.1	10/1995	14	[87]
	01/1999	03/2000	27.5	2.3	45.0	58.4	05/1999	15	[87,100]
	11/2004	12/2005	25.4	2.1	52.7	74.2	08/2005	15	[101,111]
	01/2012	12/2012	20.2	1.5	46.4	68.9	07/2012	13	[111]
	03/2014	11/2016	30.6	1.6	25.8	58.4	01/2016	13	[135]
EMME	04/2017	09/2018	35.3	2.0	33.5	74.1	12/2017	14	[136,137]
	11/1998	02/2001	30.5	2.3	51.0	80.0	12/1999	15	[100,138]
	01/2007	12/2012	40.6	2.2	33.2	80.0	01/2009	14	[38,126]
AEG	12/2014	01/2019	53.6	2.1	35.1	67.9	12/2017	14	[120]
	11/1989	01/1991	31.9	2.3	52.4	77.6	11/1990	16	[28,57]
	11/1999	04/2001	37.0	2.1	41.7	65.3	03/2001	15	[87]
	12/2006	01/2009	44.0	2.1	51.0	78.0	10/2007	16	[87,139]
	12/2015	01/2018	43.1	1.7	35.0	55.0	10/2016	14	[126,136]

Table 7. Cont.

R	ST	EN	DRS	DRI	AE %	PA %	AMY	Score	Mentioned by
BLK-FR	12/1988	10/1991	39.2	1.8	48.6	65.7	09/1990	14	[28]
	12/2001	09/2002	41.1	2.6	50.0	71.6	04/2002	15	[28,140]
	07/2003	05/2004	11.7	1.9	37.0	50.7	02/2004	13	[137]
	01/2005	12/2005	20.1	1.9	30.0	38.8	08/2005	13	[140]
	05/2006	10/2008	42.7	1.5	30.1	53.7	04/2007	13	[87]
	07/2011	10/2012	33.3	2.5	38.6	71.6	03/2012	15	[129]
	11/2015	04/2018	38.1	1.5	37.8	65.7	11/2017	14	[101,135]
NA	02/1980	03/1982	50.1	2.1	27.7	50.2	12/1981	14	[135,141]
	01/1999	12/2002	22.3	1.5	36.0	64.1	02/2002	14	[45]
	02/2004	10/2005	44.2	2.1	28.7	50.0	12/2004	14	[120,142]
	01/2012	07/2018	27.6	1.9	23.6	61.5	01/2018	13	[133]

It should be noted, however, that recent droughts at particular locations (e.g., Algeria and Tunisia) are more severe than other sites, although the others have broader spatial extent as the NA experienced droughts in the late 20th century that were exceptional in the context of the prior 500 years [117]. Compared to previous works on global-scale drought change [28,66], we provide, through this paper, a more comprehensive and detailed drought-event dataset for the MED by considering multiple meteorological drought indices to identify drought in this region. Table 7 reports a corresponding compiled list of the extraordinary, extreme and severe drought events, with scores exceeding 13 at the subregional scale between 1975 and 2019 identified by the three-dimensional array system, and presents twenty-four multiregion severe events detected by the DXI-12. Moreover, Table 7 is based on input data up to December 2019, but a few drought events were still ongoing at the end of 2019. These updates will be included in the coming dataset in future research.

A notable uneven temporal distribution of the drought events is detected as most events occurred after the 2000s, which have been characterised by increasing and more severe and extreme rainfall events mixed with prolonged dry conditions [40,143]. In the 2000s, 17% of the global population (1.1 billion people), who mostly live in the Middle East, North Africa, and South and East Asia, experienced critical water deficiency and high water stress [33] with 61–89% of the population under water shortage. Severe, intense, wide, and long-lasting drought events are frequent in all subregions across the MED over the last decades and were more pronounced in the Middle East and some parts of the Eastern Mediterranean. The largest drought severity was recorded in the EMME (>53) with very high intensity (>2.1) between 2014 and 2019. The multi-drought event in the mid-2000s also experienced high severity (>40) with very high intensity (2.2). The common pattern of drought occurrence displays marked spatial variability of the Mediterranean drought events, as droughts in this region seldom affect the area as a whole; the matter could be explained through the east–west climate dipole as the dominant component of variability between western and eastern sites of the MED [144]. Moreover, the EMME reflects transition between summer subtropical in the north and semi-arid climates in the south, making it more vulnerable to climatic sensitivity [141]. Combining the results reported in Tables 6 and 7 and Figure 4 makes it possible to clearly identify the “hotspots” hit by more severe, more intense and wider meteorological drought events at the national and regional scales during 1975–2019. The recent drought in the Levant region between 2008 and 2012 was probably the worst drought of the past nine centuries. It was 50% drier than the worst drought period of the previous 500 years and 20% drier than the driest spell over the past 900 years [38]. A very severe drought period struck the northern parts of Africa between 2004 and 2005, leading to a reduction in the economic growth rate by 2.2% [142].

In 2005, severe droughts were recorded in the west of the Iberian Peninsula, southeast France, which is consistent with the results supported by Quintana-Seguí et al. [141].

In 2017, one of the worst drought periods in 150 years hit large parts of Europe and threatened the Balkans, eastern and southern Spain, and most of the Italian peninsula. Table 7 shows that exceptional droughts occurred in the 2010s and encompassed five subregions with grades higher than 13, while the AEG experienced the most exceptional drought events in the early 1990s and the mid-2000s with grade (16).

3.4. Evaluation of Different Drought Events Parameters during Two Subperiods

3.4.1. Change in Severity, Intensity and Frequency of Drought Events between 1975–1996 and 1997–2019

According to DXI-12, the number of drought events for each subregion was assessed for two consecutive periods 1975–1996 and 1997–2019. Their average values for duration, severity and intensity, and the degree of dryness were computed (Table 8). Table 8 illustrates the number of drought events at the regional scale and their average duration, severity, intensity and their spatial extent identified by the DXI-12.

Table 8. Subregional drought parameters for two subperiods according to the DXI-12.

Subregion	Average Number of Events (N)		DD		DRS		DRI		AE (%)		DDI (%)	
	1975 1996	1997 2019	1975 1996	1997 2019	1975 1996	1997 2019	1975 1996	1997 2019	1975 1996	1997 2019	1975 1996	1997 2019
IBE–NWA	5	14	6.1	6.5	9.1	9.8	1.3	1.4	12.4	18.6	2.5	3.6
EMME	9	11	4.4	10.4	6.0	16.8	1.1	1.5	5.5	23.8	1.1	4.4
AEG	5	8	6.8	8.3	10.1	13.1	1.4	1.4	12.1	18.2	2.3	3.5
BLK–FR	5	8	6.2	7.3	9.5	11.1	1.3	1.4	10.5	20.2	2.2	3.7
NA	6	9	6.3	8.0	8.9	12.6	1.3	1.4	10.1	18.3	1.9	3.6

Bold refers to the highest value between the two periods.

The average degree of dryness was also reported in Table 8. In order to evaluate the spatial and temporal patterns of drought events, we have compared the average severity and intensity (Figure 5), frequency and spatial extent through the two subperiods. The drought periods identified by the DXI-12 were longer, wider, most severe, most intense and most frequent over 1997–2019 (Table 8 and Figure 5). The DDI values have also exerted visible upward tendency in all subregions. The Table 8 shows the frequency of the drought events in all subregions has increased from 1975–1996 to 1997–2019. The same applies to other parameters, as the drought intensity, severity and spatial coverage experienced a remarkable change in all subregions. Additionally, the DXI-12 identified dryer conditions and an increase in the area affected by droughts over all subregions. A more remarkable change is shown across the EMME, which indicates the highest drought exposure in the second period. The arid and semi-arid areas over the EMME are generally characterised by high dry conditions induced by increases in temperature and evaporation [38,107]. The highest increase in the different drought parameters was demonstrated in this subregion, while the change towards largest number of drought events mainly occurred in the IBE–NWA. Furthermore, the dry climate of EMME has not only tended to experience more intense drought events over the last two decades, as shown in this research, but also more prolonged and long-lasting events. This was confirmed by Tabari and Willems (2018) [145], who found evidence that the number of dry days is increasing and the drought episodes will be longer (up to 90%) over 80% of the Middle East. The most relevant decrease in severity was clearly evident in some parts of BLK–FR area and NA, mainly in Croatia, southeast France and Spain, and Tunisia. The results have shown a clear correspondence

between the severity and intensity of drought events, particularly in the Levant area and Turkey.

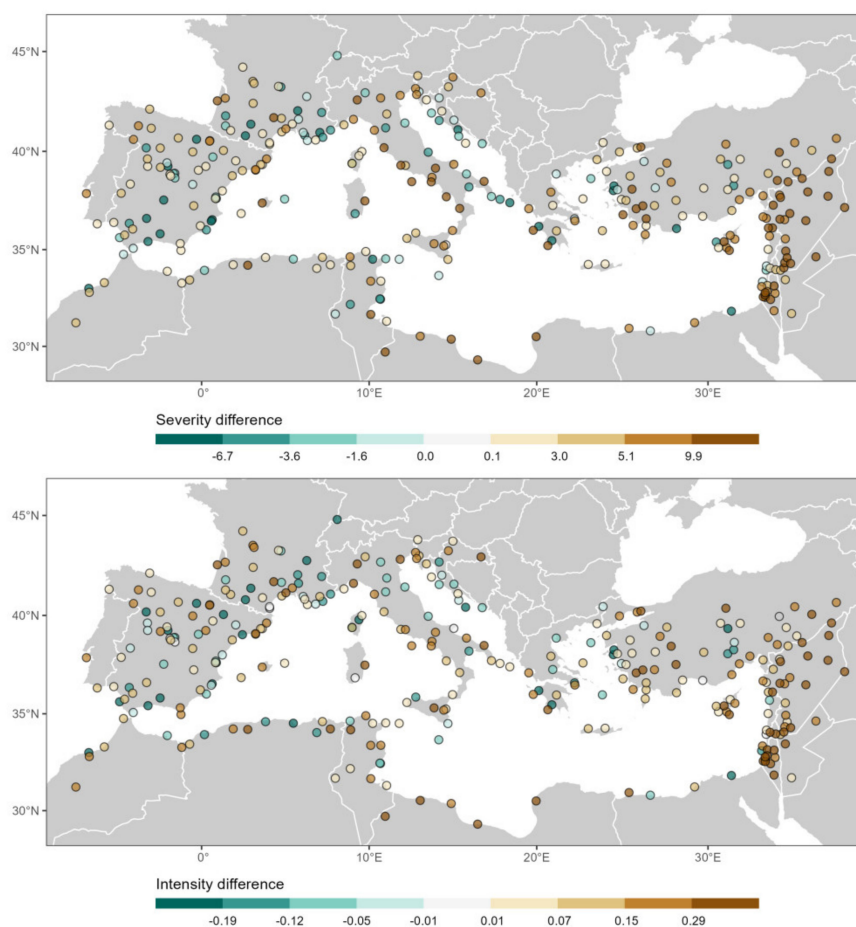


Figure 5. Difference of average severity of drought events (DRS) and average intensity drought events (DRI) between 1975–1996 and 1997–2019 according to the DXI-12.

Based on the DXI-12, a significant change towards larger frequencies of moderate, severe and extreme drought events was evident, in all subregions, in 75%, 81% and 82% of the total stations, respectively (Figure 6).

The increases in the number of droughts over the MED have been detected between the subperiods 1975–1996 and 1997–2019 in all subregions at different categories. During the second period (1997–2019), the increasing trend in drought frequency based on DXI-12 was experienced over the majority of the MED. The results revealed a clear signal concerning the increase in the average number of drought events over the MED by 1.36 events per decade (not shown). The EMME demonstrates the highest increase in drought occurrence by more than one event per decade (+1.9 event/per decade), where Syria and Israel show the highest increase in drought frequency (more than two events per decade). On a spatial basis and based on the DXI-12, the frequency of moderate droughts shows similar patterns for all subregions, but the moderate drought events display a larger increase in the last two decades than both severe and extreme ones. The EMME retained the largest share of the increase in all extreme, severe and moderate events, with increases of almost one moderate event, 0.7 severe events, and 0.3 extreme events per decade (Figure 6). The AEG, for example, experienced a pronounced increase in severe drought events by 0.2 and 0.3 events per decade in severe and drought events, respectively. A very clear increase in the moderate events was also evident in the BLK–FR during 1997–2019, with an approximate increase of 0.6 events per decade. The increase in extreme periods was clear, at 1.2 events per decade, in some localised areas over Italy, Greece, Tunisia and Levant countries, while some other

areas in south France and Spain have experienced an eminent increase in severe droughts by 1.1 events per decade. Such results confirm what has been reported by Spinoni et al. and Dai [28,76] following different approaches (Figure 6).

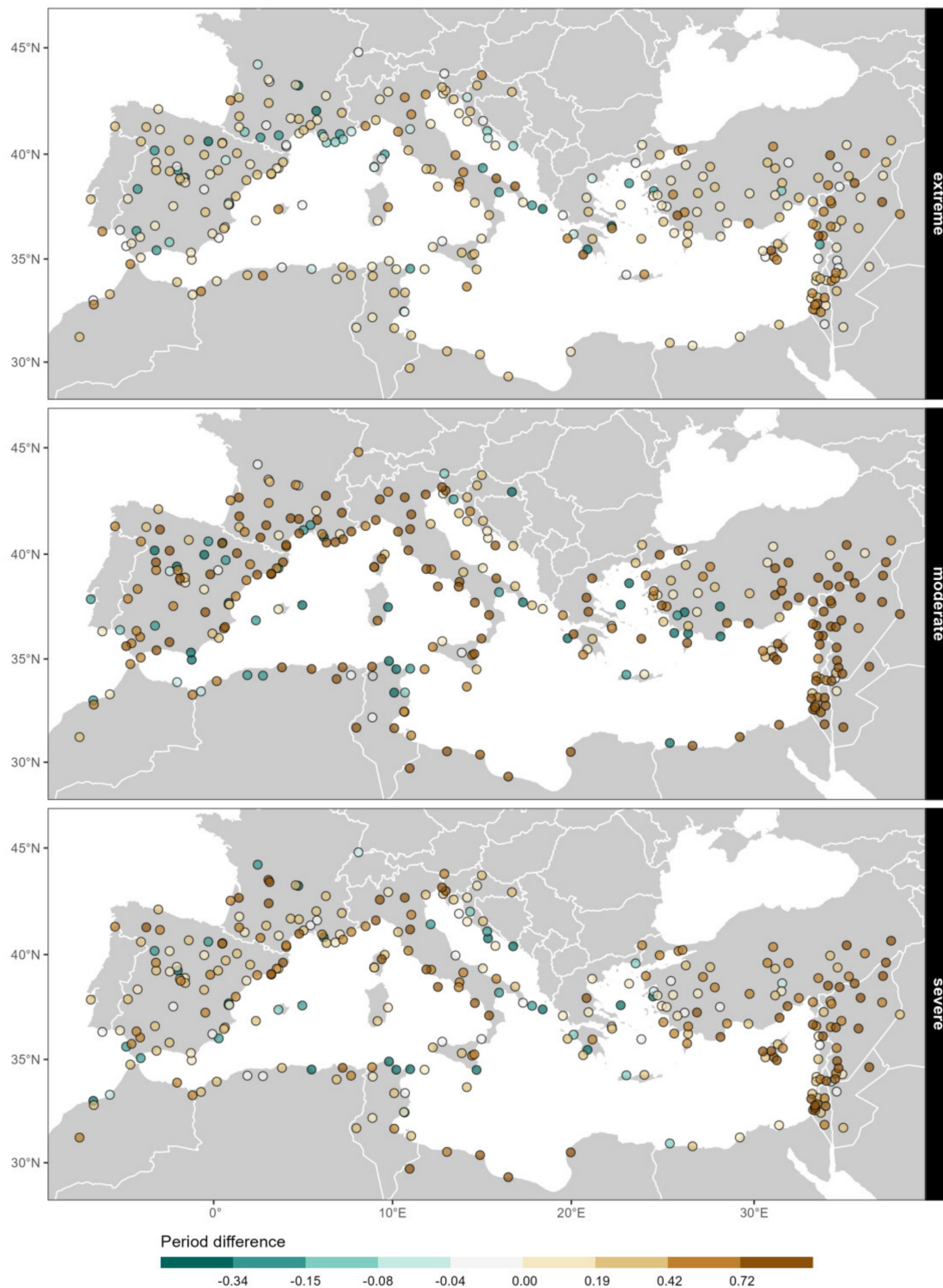


Figure 6. The expressed difference (per decade) of extreme, severe and moderate drought frequency (DRF) between 1975–1996 and 1997–2019 based on DXI-12.

Thus, drought occurrence has shown an increasing trend in addition to more prolonged and frequent periods, in last two decades, at the regional level (Table 8). The change

in drought event frequency was also assessed according to the SPI, SPEI-12 and RDI-12 between the subperiods 1975–1996 and 1997–2019 (Figure 7). An overall increase in the frequency of dry spells appears over the MED for all the combinations of SPI-12, SPEI-12 and RDI-12 during 1997–2019, with clear spatial patterns, suggesting that droughts were more frequent in the last two decades. Based on the SPI-12, SPEI-12 and RDI-12, the results indicated that 70%, 96% and 84% of the total stations have reported an increase in the frequency of drought periods during 1996–2019, respectively (Figure 7).

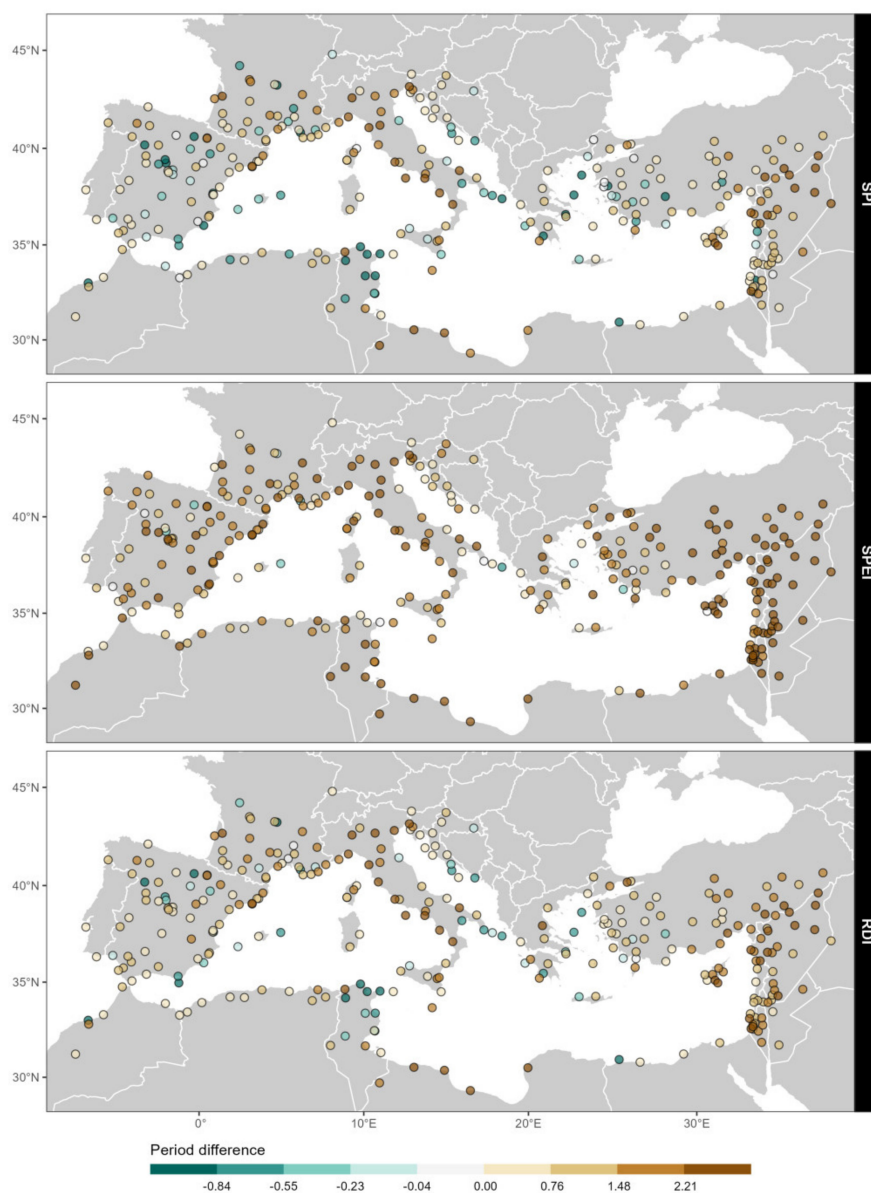


Figure 7. Drought frequency identified by SPI-12 (upper map), SPEI-12 (middle map) and RDI-12 (lower map) between 1975–1996 and 1997–2019.

Although there is a coherent change in the characteristics of the original drought events, which was identified by all indicators, there is a general increase in the frequency of the drought events that were studied using SPEI-12 and RDI-12 compared with those obtained by the SPI-12. Therefore, their capacity to detect drought conditions is potentially higher than the SPI-12 due to their incorporating of the influence of temperature on multi-temporal drought. The representation of the full water balance by SPEI and RDI makes them superior to SPI in terms of the accurate assessment of meteorological droughts with

increasing climate [146–148]. Most parts of the Iberian Peninsula have also displayed consistent characteristics and experienced a drought frequency increase identified by the different drought indicators, and these were more evident when measured by the SPEI-12 and RDI-12. The results further suggest that drought events could exhibit entirely different characteristics when we include the influence of the temperature in the drought indices.

3.4.2. Change in Precipitation (PP) and Potential Evapotranspiration (PET) between 1975–1996 and 1997–2019

Changes in precipitation amounts and PET values between 1975–1996 and 1997–2019 were analysed to explore whether the dry and wet tendency reflected by the SPI-12, SPEI-12 and RDI-12 was driven by the precipitation or temperature anomalies—that were included in PET—, or both (Figure 8a,b). It is not easy to understand the actual roles of both temperature and precipitation variations in drought changes over the MED during the last two decades. This is due to nonlinear interactions among temperature, precipitation, and droughts. Although an extended period of reduced precipitation plays an important role in producing drought conditions over the MED, the effect of increased temperature is notable as a significant factor in enhancing drought by enhancing the evapotranspiration rate. According to SPI-12, 62% of total stations experienced a drying tendency. In the last two decades, some areas across west Turkey, south Spain, and the Adriatic experienced a wetting tendency. The more extreme negative values for both the SPEI-12 and RDI-12 compared with the SPI-12 (not shown), particularly in the semi-arid areas in the southeastern Mediterranean, indicate the impacts of temperature that may initiate or increase drought via the enhancement of PET. Although the RDI-12 identified dryer conditions in the last two decades compared with the SPI-12, the SPEI-12 displays the highest contribution of PET to drought conditions compared with the SPI-12 and RDI-12, particularly in the Balkans, north-east Tunisia, and west Turkey. It was concluded that the DXI-12 was able to provide a physically sound, temporally flexible index, which can be directly combined with all possible variants and linked to the climate conditions, that allowed us to list hundreds drought periods and characterise several exceptional drought events between 1975 and 2019. In this sense, DXI-12 can evaluate the actual drought conditions and effectively lessen overestimation of any drought conditions by SPEI-12 in terms of drought duration and intensity. All drought events detected by the DXI-12 were previously confirmed and documented at both the country and subregional scales, while some drought accidents, especially the moderate and short ones, could not be detected by SPI-12 and RDI-12 as well.

According to the SPEI-12, the dry conditions across the MED have been enhanced in recent years as a result of increases in temperature and decreases in precipitation in approximately 63% of total stations. The findings also show that approximately 28% of the total stations experienced drier conditions which resulted only from positive temperature anomalies over the last two decades, where the SPI-12 showed an increasing trend, while the rest of the indicators showed a significant decreasing trend (Figure 8). There is a detectable and significant decreasing trend of precipitation and increasing temperature over the Mediterranean and Middle Eastern countries [33,100,107]. Thus, this result indicates that the positive trend of precipitation is not strong enough to outweigh the temperature increase in this area, and that the drought exhibits a larger response to temperature variations, which is more than its response to the precipitation anomalies in these areas. This proportion decreases to approximately 15% for RDI-12. Generally, the MED as a whole displays a clear example of the worst drying combination (decrease in precipitation amount associated with increase in the PET).

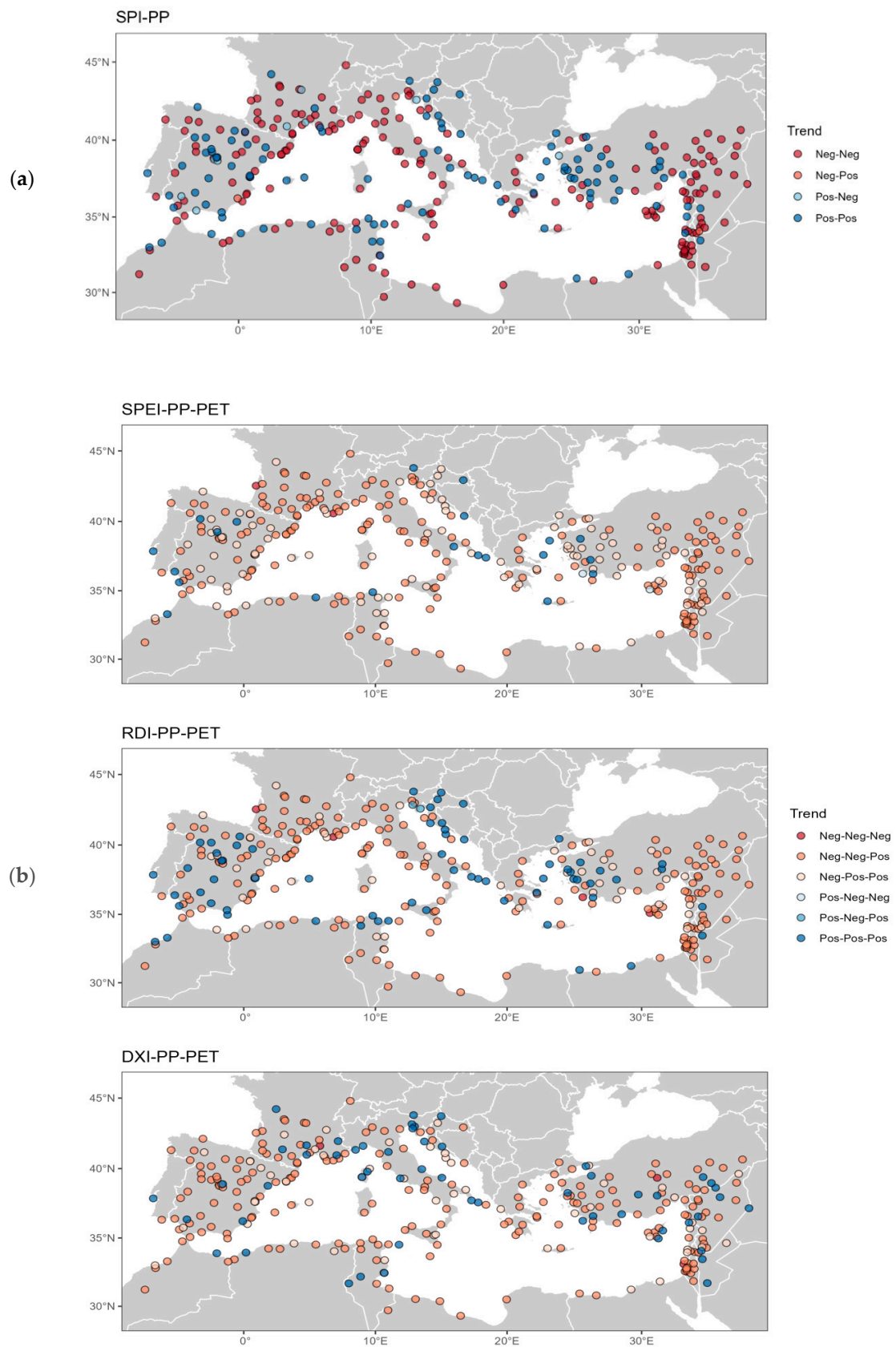


Figure 8. Drought tendencies from 1975–1996 to 1997–2019 according to the SPI-12 (a), SPEI-12, RDI-12 and DXI-12 (b) at a 12-month timescale and corresponding increases or decreases in precipitation amounts (PP) and evapotranspiration (PET).

3.5. Drought Dynamics, Large Scale Atmospheric Controls of Widespread Drought Events over the MED

The correlation of the annual percent of drought area extent based on the SPI-12, SPEI-12, RDI-12 and DXI-12 indices with large-scale atmospheric fields over the whole study period (1975–2019) is investigated. The correlation analysis gives a more detailed evaluation of the processes linking large-scale atmospheric variation to Mediterranean meteorological droughts. In addition to the general relationship between the percentage of MED experiencing meteorological droughts and ATPs (Table 9), the widespread droughts and their atmospheric drivers were also investigated. The spatial pattern of correlation is virtually identical for the SPEI-12, RDI-12 and RDI-12, with positive correlations with NAO and ULMO and negative ones with WeMO, EATL/WRUS and SCAND (Table 9).

Table 9. Correlation coefficients between the percent areas in drought identified by SPI-12, SPEI-12 and RDI-12 and ATPs (only coefficients significant at 95% confidence level are shown).

Subregion	NAO				ULMO				WeMO				EATL/WRUS				SCAND			
	SPI-12	SPEI-12	RDI-12	DXI-12	SPI-12	SPEI-12	RDI-12	DXI-12	SPI-12	SPEI-12	RDI-12	DXI-12	SPI-12	SPEI-12	RDI-12	DXI-12	SPI-12	SPEI-12	RDI-12	DXI-12
IBE-NWA													−0.5	−0.3	−0.5					
EMME									−0.3	−0.4	−0.4	−0.5	−0.3	−0.5	−0.4	−0.5				
AEG													−0.3	−0.3	−0.4					
BLK-FR					0.3	0.3	0.3	0.4	−0.5	−0.5	−0.4	−0.5					−0.3	−0.4	−0.3	−0.4
NA	0.3				0.3								−0.3	−0.4	−0.5					

Despite the similarity of the spatial patterns of correlation coefficients presented in Table 9, the correlation of the area in drought with the NAO is the weakest. Generally, the areas in drought obtained by the SPEI-12 and RDI-12 are better related to the ATPs in comparison to SPI-12 and detected the highest correlations with DXI-12 (Table 9). Statistically, the WeMO and EATL/WRUS are remarkably correlated with the area in drought identified by SPEI-12, RDI-12 and DXI-12. The widespread dry conditions over central and Western Europe (BLK-FR) were associated with negative phases of WeMO and SCAND and a positive phase of ULMO, as shown in Table 9. The results presented here show a major role played by the WeMO in drought within the EMME and BLK-FR. The negative phase of the WeMO generally shows very wide spatial coverage of drought over the EMME and BLK-FR. The large area under drought noted over the EMME during 2011–2012 (47%) was often linked with severe negative values of the WeMO. The severe negative phase of the WeMO (< -1.5) over 2017 was also connected with the largest percentage of the affected area in the EMME. Similarly, the ongoing negative annual phase of the WeMO between 1985 and 1991 was associated with very large area under drought in the BLK-FR. This affected area spanned over large territories in France and Croatia which were hit by severe drought episodes and involved 61.2% of the entire subregion. The consecutive low annual negative values of the WeMO between 2002 and 2018 were found to be associated with very high percentages of the area under drought in the BLK-FR. With the exception of the BLK-FR, the negative phase of EATL/WRUS was often associated with large drought spatial coverage within the MED. The persistent negative anomalies in the EATL/WRUS values in the late 2010s (July 2017–September 2018) were associated with high spatial coverage (40%) in the IBE-NWA. Furthermore, the exceptional multi-year 2007–2012 drought in the EMME was developed in a predominantly negative phase of both the WeMO and EATL/WRUS patterns. The combination of the negative phase of WeMO and EATL/WRUS over 2008 resulted in a strong influence on the drought areal extent in the EMME (76%), as shown in Table 5.

The major drought episodes that occurred between 1999 and 2002 in the NA were driven by qualitatively similar conditions with the complete domination of the negative EATL/WRUS, which had the largest mean drought area in 2002. The negative phase of the EATL/WRUS is usually linked to below-average precipitation and above-average tem-

peratures in these areas [148,149], which clearly explains the strong negative relationship between the EATL/WRUS and the area in drought except for the BLK–FR.

The impact of the ULMO significantly appeared through both the 1994 and 2012 exceptional droughts. The very large areas of the IBE–NWA affected by droughts during 1992, 1999 and 2012 (52%, 44% and 62%, respectively) were concordant with the positive phase of ULMO. The widest affected area in in the BLK–FR during 2002 (Table 5) was remarkably associated with a large predominance of negative values of the WeMO, SCAND and positive values of the ULMO. These findings perhaps suggest that the WeMO and EATL/WRUS patterns show most potential role in explaining the spatial evolution and characteristics of large-scale drought over the MED with lesser influence of the NAO ULMO, and SCAND. In NA, the EATL/WRUS may determine the climatic water balance drought, while the NAO and ULMO play a significant role in regulating the internal rainfall variability, and thereby the spread of drought events. These results correspond with previous findings [150,151], which indicated high drought conditions during the positive phase on the NAO in southern Europe and North Africa.

At the regional scale, similar correlation patterns have been detected with drought severity, intensity and area in drought. Correlation patterns of all selected ATPs indicate relationships of Mediterranean drought severity, intensity with atmospheric circulation at the regional level (Figure 9). High drought intensities and severities are significantly associated with the negative phases of both WeMO and EATL/WRUS across the MED. The results confirm the higher capability of the SPEI-12 and RDI-12, and DXI-12 compared with SPI-12 in improving climatic water deficit detection in the MED, which confirms the capacity of temperature in detecting drought conditions. The drought intensities and severities obtained by the DXI-12 showed the highest negative correlation coefficient values with EATL/WRUS and WeMO, respectively.

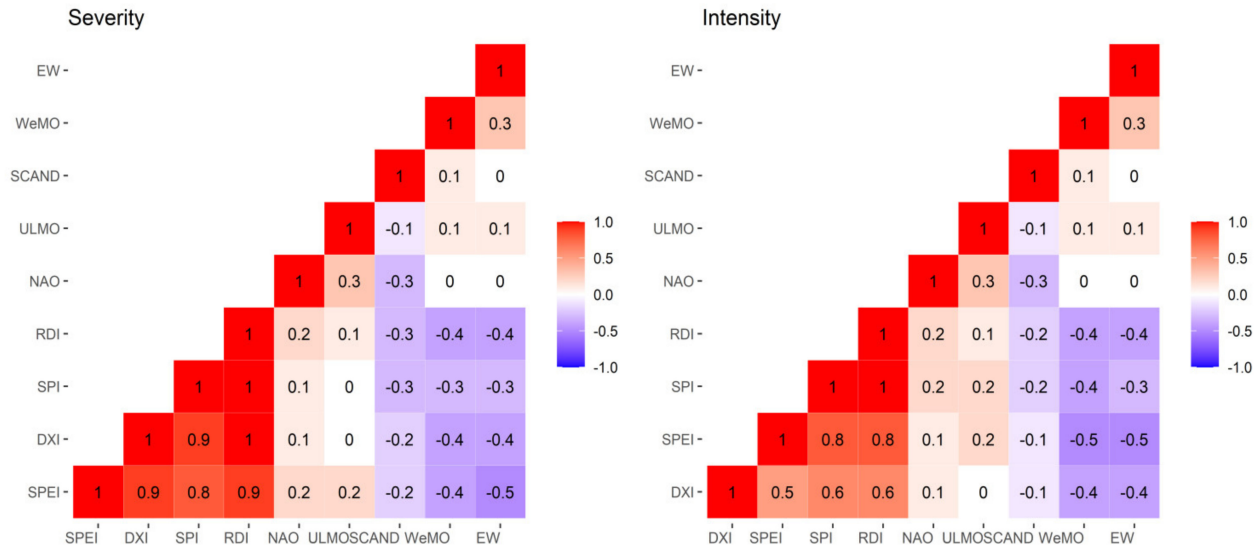


Figure 9. Values of the matrix correlation of drought severity and intensity identified by SPI-12, SPEI-12, RDI-12 and DXI-12, and the ATPs over the MED. (Values greater than or equal to the absolute value of 0.3 are significant.).

4. Conclusions

This study has provided a comprehensive dataset of exceptional meteorological drought events over the Mediterranean during the 1975–2019 period that contains hundreds of constructed drought events at the national and subregional scales. Three drought indices were computed at 12-month accumulation scales and a new combined indicator was obtained (DXI-12) as the average of these three indices to identify the meteorological drought due to both rainfall shortage and climatic water balance. The drought event databases are identified by monthly series of the DXI-12 at the national and subregional scales. Based on

the drought-event dataset, we have also investigated in detail the main characteristics of the obtained drought events in different subregions across the MED, including duration, severity, intensity, spatial coverage, peak month, area involved at peak month and the frequency of drought occurrence. This new approach has proved to be effective in detecting the most relevant Mediterranean drought events at the national and subregional scales as it is based on data obtained with high-quality control, a multi-indicator method, and a strong statistical setting. The evaluated drought quantification, which includes these three indices, gives a more reasonable estimation of water demand as a result of including evapotranspiration. Generally, our newly developed DXI-12 provides better information about drought identification and more realistic characteristics of dry spells compared to a single drought index and, thereby, provides a better tool for monitoring water resources, especially in semi-arid and arid ecosystems. According to the results presented in this study, the MED is shown to be a region that is water-stressed and prone to severe and exceptional droughts. The drought episodes show that the EMME and most areas of the NA and southern Europe, including south Italy and Spain, underwent a drying phase during the study period, with the highest drought severity and intensity from the late 1990s onwards. These findings are in line with recent scientific literature [28,101]. The combination of individual indicators depicts the spatial extent of a drought situation across the MED and gives an overview of the drought drivers. The DXI-12 indicates that droughts over the MED were mainly driven by temperature increases with the inherent increase in the PET, particularly in the humid area, whereas rainfall did not change appreciably. A new grade classification approach for identifying the most relevant extreme events is identified by the three-dimensional array (severity, intensity and spatial coverage). The new classification approach and database extracted from combined indices the time series have listed twenty-four multi-region big drought events, which were previously documented. The new classification has allowed us to discover the most hotspots that have displayed the highest severity and intensity and included the largest area over the MED. The significant trends towards larger drought areas and higher drought severities and intensities in all subregions and mainly occurred in the EMME. Although the actual precipitation anomalies exhibit relatively large effects on drought occurrence, we can also conclude that the rapid warming of the MED in recent decades presents a relatively greater role in determining droughts than that of precipitation variations in several areas, especially in the Balkans and west Turkey.

In this paper, we have detected several drought hotspots that have tended to experience more severe, intense wide and more long-lasting drought events between the subperiods 1975–1996 and 1997–2019 in all subregions. Dynamically, the region lies at a crossroads of large-scale influence from the Atlantic Ocean and the Mediterranean Sea, which results in regionally severe and prolonged droughts. Dynamically, the region is a junction of regional influence from the Mediterranean Sea, Europe, and Asia, as well as large-scale influence from the Atlantic Ocean and the Mediterranean Sea. A complex range of atmospheric circulation patterns influences have been shown to have at least some influence on the droughts of the MED, both nationally and regionwide, particularly the WeMO and the EATL/WRUS.

The WeMO pattern and the EATL/WRUS appear to play the strongest role in forcing wide droughts at the subregional scale, including the two widest and most devastating droughts of the last 40 years (1999–2001 and 2007–2012). A relative role is played by the NAO and ULMO in the NA in these episodes; in addition, a relationship between the SCAND and the area in drought in western and the Adriatic is found. The drought event datasets produced by this study still need to be improved in some respects. The extension of the data to drought events to include more historical data is significant for studies of climatic dynamics and ATPs in order to understand the long-term variation of droughts and develop monitoring and forecasting tools to help to adapt to and mitigate drought. Moreover, including realistic socio-economic data will strongly improve the prospects for drought risk assessment in the future as many combined meteorological, hydrological, and social drivers contribute to drought occurrence. Finally, these constructed exceptional

drought events at the national and subregional scales can help researchers and relevant stakeholders in dealing with the multitude of such drought events and assess their risk by investigating the correlation between the severity and duration of each event and documented impacts in different sectors. As an initial possible application, we are planning to exploit this dataset in exploring the synergy and combination between these exceptional droughts and heatwaves across the MED.

Author Contributions: Conceptualization, S.M. and J.A.L.-B.; methodology, S.M.; software, S.M. and D.R.; formal analysis, S.M. and D.R.; data curation, S.M.; writing—original draft preparation, S.M.; writing—review and editing, J.M.-V., J.A.L.-B., D.R. and S.M.; supervision, J.M.-V. and J.A.L.-B. All authors have read and agreed to the published version of the manuscript.

Funding: This research was supported by the Spanish CLICES project (CGL2017-83866-C3-2-R, AEI/FEDER, UE).

Institutional Review Board Statement: Not applicable.

Informed Consent Statement: Not applicable.

Data Availability Statement: The historical climate data are available at the European Climate Assessment & Dataset (ECA&D; <https://www.ecad.eu/>; accessed on 21 July 2021) and the Daily Global Historical Climatology Network (GHCN; <https://www.ncdc.noaa.gov/data-access/land-based-station-data/land-based-datasets/global-historical-climatology-network-ghcn>, accessed on 21 July 2021). The values NOAA, EATL/WRUS and SCAND indices were obtained through the NOAA CPC website: <https://www.cpc.ncep.noaa.gov/data/teledoc/telecontents.shtml>, while the following websites have been used to obtain the values of the WeMO and ULMO, respectively: <https://crudata.uea.ac.uk/cru/data/moi/> and http://www.ub.edu/gc/data_base/, accessed on 21 July 2021.

Acknowledgments: This study was achieved within the framework of Climatology Group of the University of Barcelona (2017 SGR 1362, Catalan Government) and the Spanish CLICES project (CGL2017-83866-C3-2-R, AEI/FEDER, UE).

Conflicts of Interest: The authors declare no conflict of interest.

Appendix A

Table A1. Main statistical characteristics of total annual precipitation over the MED during 1975–2019.

ID	Long	Lat	Mean	Med	Max	Min	Sk	Ku	CV%	LCL	UCL
ST01	7.48	36.50	656.4	622.4	1126.6	61.7	−0.2	2.9	26.3	606.0	706.9
ST02	1.20	36.12	384.2	400.1	618.0	61.7	−0.2	0.0	30.4	350.0	418.3
ST03	3.25	36.68	604.2	606.6	884.9	269.0	0.0	−0.8	26.6	557.2	651.1
ST04	2.14	36.18	729.1	726.9	1069.6	61.7	−0.6	0.6	29.5	666.3	791.9
ST05	−0.60	35.63	338.6	324.5	546.5	61.7	−0.2	0.3	28.7	310.2	366.9
ST06	18.08	42.65	1120.3	1051.3	1911.6	726.1	0.9	0.5	24.2	1041.2	1199.4
ST07	15.36	44.55	1404.3	1367.6	2552.5	683.3	1.1	5.1	20.5	1320.0	1488.6
ST08	16.45	43.16	736.9	711.9	1257.8	383.7	0.7	0.8	24.8	683.5	790.2
ST09	16.20	44.03	1031.8	1007.4	1450.2	494.3	0.0	−0.3	20.1	971.1	1092.5
ST10	16.90	42.76	637.7	639.1	967.9	368.0	0.0	−0.4	23.2	594.4	681.0
ST11	15.23	45.26	1549.5	1489.7	2244.1	1103.2	0.5	0.7	14.7	1482.8	1616.1
ST12	18.38	45.32	679.5	654.6	1010.7	317.0	0.2	0.1	21.7	636.5	722.5
ST13	14.27	45.20	1574.7	1565.4	2105.2	991.4	0.0	−0.7	18.2	1490.8	1658.6
ST14	16.43	43.51	803.1	767.7	1203.7	486.6	0.1	−0.7	22.1	751.2	855.0
ST15	16.38	46.30	849.3	858.9	1310.9	481.2	0.4	1.4	18.4	803.7	895.0
ST16	15.12	44.07	895.9	907.1	1359.7	508.8	0.1	−0.2	20.6	841.8	949.9
ST17	15.98	45.81	879.0	864.0	1229.6	520.8	0.0	0.6	15.5	839.2	918.8
ST18	14.59	44.49	1983.9	1977.7	2629.5	1302.1	−0.2	−0.5	15.8	1892.5	2075.4
ST19	32.98	34.58	362.5	344.2	650.7	61.7	0.3	−0.2	35.9	324.4	400.5
ST20	32.92	34.93	839.2	899.4	1400.8	22.0	−0.5	0.1	35.4	752.5	926.0
ST21	33.36	34.88	335.4	310.8	663.0	160.7	0.9	0.3	37.3	298.9	371.9

Table A1. Cont.

ID	Long	Lat	Mean	Med	Max	Min	Sk	Ku	CV%	LCL	UCL
ST22	33.00	34.70	401.7	383.4	703.1	164.6	0.4	−0.3	32.6	363.4	439.9
ST23	33.40	35.15	315.6	304.1	571.1	133.5	0.4	−0.2	32.8	285.4	345.8
ST24	32.48	34.71	431.8	414.5	814.8	189.9	0.6	0.8	29.3	394.8	468.7
ST25	32.43	35.03	448.5	446.4	814.8	189.9	0.7	1.0	28.3	411.5	485.6
ST26	29.95	31.20	195.5	186.6	516.1	24.5	1.1	1.8	49.3	167.3	223.6
ST27	27.21	31.33	141.3	134.1	286.2	28.7	0.7	0.5	37.1	126.0	156.6
ST28	32.29	31.26	85.1	61.0	423.4	6.9	3.1	11.0	94.6	61.6	108.6
ST29	8.80	41.91	646.4	648.8	925.8	373.8	−0.1	−1.1	24.6	599.8	692.9
ST30	1.40	43.64	642.4	627.9	1010.0	423.2	0.6	0.1	22.0	601.2	683.7
ST31	9.48	42.55	807.8	773.2	1375.2	550.8	0.8	0.3	23.2	753.1	862.6
ST32	1.20	45.90	1020.8	1006.5	1448.5	721.2	0.4	0.8	14.1	978.6	1063.0
ST33	−1.46	35.01	345.8	339.0	723.0	139.0	0.8	1.8	32.3	313.1	378.5
ST34	9.28	42.33	766.4	726.9	1171.3	453.3	0.3	−0.9	24.6	711.5	821.4
ST35	6.43	43.50	666.1	681.2	1027.3	397.3	0.2	−0.5	24.6	618.2	714.1
ST36	5.56	43.04	644.0	589.8	1115.4	304.1	0.5	−0.1	30.8	586.0	701.9
ST37	3.16	45.78	578.2	572.6	825.8	353.4	0.2	−0.4	19.5	545.3	611.1
ST38	6.50	44.56	673.8	668.5	944.7	267.2	−0.4	0.0	22.6	629.4	718.2
ST39	1.40	44.75	834.5	809.0	1047.5	544.6	−0.1	−0.6	15.3	797.2	871.9
ST40	5.33	45.36	926.5	929.1	1412.5	499.9	0.2	0.3	20.5	871.1	981.9
ST41	12.61	44.03	659.5	610.4	1097.3	312.9	0.4	−0.6	31.4	598.9	720.0
ST42	5.23	43.45	514.8	515.1	839.0	259.9	0.2	−0.7	29.1	471.0	558.6
ST43	−0.70	44.83	910.3	922.2	1230.6	560.6	−0.1	−0.8	20.2	856.5	964.2
ST44	3.01	44.11	725.5	716.6	1034.2	438.0	0.3	−0.4	19.2	684.9	766.2
ST45	3.58	44.11	1880.7	1801.6	3527.4	919.9	0.9	0.8	29.1	1720.8	2040.6
ST46	−0.50	43.91	952.0	917.2	1665.0	708.7	1.6	4.6	18.5	900.4	1003.6
ST47	4.73	44.58	915.0	895.2	1583.0	512.1	0.6	0.5	25.1	847.8	982.1
ST48	3.96	43.58	641.2	609.8	1148.4	310.8	0.6	0.1	29.0	586.7	695.6
ST49	7.20	43.65	767.9	787.4	1254.0	265.9	−0.1	−0.5	29.6	701.5	834.4
ST50	4.40	43.86	734.5	720.0	1173.9	329.2	0.3	−0.4	27.1	676.4	792.6
ST51	4.83	44.13	701.2	676.9	1303.8	253.2	0.7	1.3	27.7	644.3	758.0
ST52	2.89	42.69	550.7	509.0	1009.1	299.5	0.9	0.3	29.2	503.7	597.6
ST53	14.91	37.41	571.0	509.3	1338.6	197.8	1.1	0.7	49.2	488.8	653.1
ST54	3.68	43.40	541.0	521.2	978.1	249.5	0.5	−0.3	34.3	486.8	595.2
ST55	1.10	43.00	988.3	965.6	1329.8	648.6	0.3	−0.1	15.2	944.4	1032.2
ST56	5.35	43.31	604.3	593.1	1128.3	302.0	0.8	0.6	31.4	549.0	659.7
ST57	0.00	43.18	1072.5	1033.8	1423.4	735.3	0.2	−1.1	16.9	1019.6	1125.4
ST58	−7.66	33.56	388.4	378.0	992.0	148.5	1.7	6.2	36.6	346.9	429.9
ST59	3.34	45.76	546.5	525.3	865.4	180.3	0.1	0.3	25.4	505.9	587.2
ST60	7.51	47.60	786.5	740.4	1436.6	467.3	1.2	2.1	25.2	728.6	844.5
ST61	2.87	42.77	541.8	517.1	883.7	293.1	0.6	−0.7	29.0	495.9	587.7
ST62	−1.25	44.63	785.3	771.9	1115.8	440.2	−0.1	0.1	19.2	741.4	829.3
ST63	6.66	43.25	764.4	789.9	1254.0	289.6	0.0	−0.4	29.2	699.1	829.6
ST64	−0.41	43.38	1072.5	1045.2	1554.7	738.1	0.5	−0.4	17.6	1017.3	1127.8
ST65	15.28	40.01	676.4	659.9	1205.2	344.4	0.4	−0.2	30.6	613.8	739.0
ST66	6.15	43.09	685.0	663.7	1699.3	286.8	1.5	4.1	38.0	608.9	761.1
ST67	1.30	45.80	1020.8	1006.5	1448.5	721.2	0.4	0.8	14.1	978.6	1063.0
ST68	8.79	41.92	678.4	668.4	1076.7	369.8	0.3	−0.4	27.3	624.3	732.4
ST69	6.61	36.28	515.0	486.0	868.2	253.3	0.6	0.2	28.0	472.8	557.2
ST70	0.31	46.58	694.3	684.0	906.0	470.2	−0.1	−0.4	15.4	663.1	725.6
ST71	2.31	43.21	590.6	576.1	1176.3	327.2	1.3	4.4	24.9	547.7	633.5
ST72	−5.35	36.15	759.6	751.3	1886.0	307.9	1.7	4.3	41.6	667.4	851.9
ST73	20.77	38.92	906.2	909.3	1616.7	438.9	0.6	1.5	23.6	843.7	968.7
ST74	25.91	40.85	520.3	500.0	891.7	324.2	0.7	0.0	27.4	478.7	561.9
ST75	21.28	37.91	812.3	786.4	1331.5	402.8	0.4	0.1	25.9	750.9	873.8
ST76	23.70	38.00	410.2	412.0	908.2	150.6	1.2	5.2	29.9	374.4	446.0
ST77	28.08	36.40	689.0	666.0	1328.4	294.1	0.9	0.9	33.5	621.6	756.4
ST78	24.48	38.96	472.3	446.5	1142.6	150.1	1.2	2.4	40.7	416.1	528.6
ST79	23.70	37.89	348.6	359.2	571.5	10.9	−0.5	0.4	33.4	314.6	382.5
ST80	25.18	35.33	467.3	477.2	714.6	272.8	0.0	−0.7	23.0	435.8	498.8

Table A1. Cont.

ID	Long	Lat	Mean	Med	Max	Min	Sk	Ku	CV%	LCL	UCL
ST81	18.91	39.61	1026.1	1015.7	1561.9	624.6	0.5	0.4	21.0	963.1	1089.1
ST82	22.41	39.61	428.0	430.3	704.3	227.6	0.3	1.1	21.7	400.9	455.0
ST83	21.70	36.83	628.4	629.1	1017.3	68.6	−0.5	0.7	32.5	568.7	688.1
ST84	26.60	39.06	621.3	650.0	927.6	240.5	−0.3	−0.2	25.8	574.4	668.2
ST85	25.38	37.10	368.0	351.0	698.7	178.0	0.7	0.2	33.6	331.9	404.1
ST86	26.91	37.70	679.6	660.7	1042.4	374.7	0.2	−0.6	25.1	629.7	729.6
ST87	24.11	35.48	644.8	634.2	1099.0	262.2	0.4	−0.6	30.8	586.8	702.8
ST88	22.96	40.51	429.2	419.1	754.1	210.0	0.5	0.9	24.6	398.3	460.0
ST89	22.40	37.53	728.5	696.7	1334.5	359.9	0.6	1.0	26.2	672.7	784.3
ST90	34.39	31.49	486.9	445.8	1020.2	180.2	1.0	0.5	41.3	428.2	545.6
ST91	35.58	32.65	379.1	375.9	759.9	154.9	0.6	1.3	30.8	344.9	413.2
ST92	34.78	31.23	189.5	179.7	346.7	64.7	0.4	−0.6	39.1	167.9	211.2
ST93	34.81	32.00	525.4	505.8	1104.8	233.0	1.1	2.4	31.3	477.3	573.4
ST94	35.09	33.00	614.6	616.6	934.9	355.3	0.1	−0.5	22.8	573.7	655.5
ST95	34.70	31.70	536.8	487.2	991.9	195.5	0.6	0.1	32.4	485.9	587.7
ST96	35.27	32.83	465.1	475.0	894.1	159.6	0.3	0.9	31.1	422.9	507.4
ST97	35.15	31.47	666.4	679.7	982.7	295.0	−0.1	−0.8	27.3	613.1	719.6
ST98	35.21	31.86	525.9	508.1	934.3	223.0	0.4	0.2	30.1	479.7	572.1
ST99	34.50	31.43	490.1	476.5	902.5	187.3	0.5	0.2	32.2	444.1	536.2
ST100	34.53	31.56	533.1	525.3	1175.2	199.9	1.1	2.2	34.9	478.8	587.5
ST101	34.80	30.60	76.4	73.5	158.4	19.8	0.5	−0.5	51.1	65.0	87.9
ST102	34.46	32.04	524.3	495.2	1175.2	190.2	1.2	2.3	35.8	469.4	579.2
ST103	16.13	39.34	452.2	428.2	975.9	126.0	0.5	0.4	40.1	399.3	505.2
ST104	16.78	41.13	516.9	544.1	779.0	178.3	−0.3	−0.4	28.5	473.8	559.9
ST105	9.70	45.66	1035.4	1019.2	1697.0	405.9	0.1	−0.8	31.2	941.1	1129.7
ST106	11.30	44.53	738.5	749.0	1091.4	430.6	0.1	−0.7	22.2	690.7	786.4
ST107	17.95	40.65	576.0	621.0	946.8	109.9	−0.5	0.2	32.3	521.7	630.3
ST108	9.05	39.25	417.9	422.8	836.7	164.1	0.7	0.8	35.6	374.4	461.3
ST109	14.65	41.56	676.3	663.7	1356.9	248.4	0.8	1.1	35.0	607.2	745.4
ST110	9.71	39.93	397.4	372.2	846.0	43.1	0.5	0.5	39.8	351.1	443.6
ST111	8.16	43.95	659.7	673.4	1115.1	295.9	0.0	0.1	27.3	607.1	712.3
ST112	15.05	37.46	566.8	462.4	1338.6	224.3	1.0	0.3	52.0	480.7	653.0
ST113	15.13	36.68	567.2	543.8	1247.7	174.2	0.6	0.3	43.8	494.5	639.8
ST114	11.20	43.80	871.1	824.0	1518.0	580.8	1.1	1.5	22.5	813.8	928.5
ST115	8.85	44.25	1204.8	1244.8	2174.4	367.2	0.3	0.3	32.6	1090.1	1319.4
ST116	11.06	42.75	640.3	612.9	1145.0	196.4	0.2	0.0	33.3	578.0	702.7
ST117	15.55	38.20	899.6	879.3	1738.2	463.3	0.8	1.7	27.9	826.2	973.0
ST118	9.11	45.28	936.1	908.8	1462.6	501.0	0.2	−0.4	24.7	868.6	1003.6
ST119	15.95	41.70	589.4	554.7	875.9	287.5	0.4	0.2	19.9	555.1	623.6
ST120	19.55	39.37	1020.1	1011.0	1635.8	624.6	0.7	0.7	21.7	955.4	1084.8
ST121	13.10	38.18	956.7	666.8	4206.7	227.3	2.4	5.2	92.7	697.6	1215.8
ST122	11.96	36.81	672.1	570.0	1724.2	61.7	1.3	1.6	51.9	570.1	774.0
ST123	14.20	42.43	668.0	685.5	960.0	240.0	−0.6	1.2	20.2	628.6	707.3
ST124	10.38	43.68	937.0	920.2	1764.8	487.7	1.0	1.3	29.6	855.8	1018.2
ST125	12.95	40.91	645.5	635.6	1223.5	278.4	0.3	−0.5	34.3	580.8	710.3
ST126	12.55	41.78	842.6	765.9	2531.0	321.9	2.7	11.0	42.6	737.6	947.5
ST127	18.35	39.81	533.5	527.3	1019.3	61.7	0.6	0.8	37.3	475.3	591.7
ST128	14.37	41.09	635.8	644.7	1350.0	68.8	0.1	1.0	38.2	564.8	706.8
ST129	12.50	37.91	578.3	454.4	1695.2	223.7	1.9	3.8	56.8	482.4	674.2
ST130	25.25	39.93	516.3	482.3	971.2	211.8	0.5	0.1	32.9	466.6	565.9
ST131	13.75	45.65	912.5	900.8	1382.6	484.9	0.1	−0.3	22.6	852.3	972.6
ST132	12.33	45.50	800.8	776.7	1946.5	61.7	1.1	2.5	42.3	701.9	899.7
ST133	10.86	45.38	793.5	808.4	1177.9	294.5	−0.2	0.3	23.3	739.0	848.0
ST134	14.30	40.85	939.2	840.0	2117.6	257.6	1.0	1.4	38.2	834.3	1044.2
ST135	−8.63	42.23	1748.7	1808.2	2381.5	967.7	−0.3	−0.6	20.9	1642.1	1855.2
ST136	−0.80	37.78	289.7	290.1	628.1	105.4	0.7	0.4	41.0	255.0	324.4
ST137	−3.78	40.38	427.4	440.7	628.1	250.4	0.1	−0.8	23.1	398.6	456.3
ST138	−3.46	40.48	372.9	367.3	529.3	192.0	0.0	−0.6	22.3	348.6	397.2
ST139	35.98	31.98	269.9	227.0	603.3	101.3	1.0	0.3	49.1	231.2	308.6

Table A1. Cont.

ID	Long	Lat	Mean	Med	Max	Min	Sk	Ku	CV%	LCL	UCL
ST140	35.85	32.54	425.2	429.0	778.2	104.7	0.1	0.1	31.9	385.6	464.8
ST141	38.20	32.56	80.3	78.0	250.0	7.8	1.4	3.2	59.0	66.5	94.2
ST142	35.48	33.81	716.8	717.5	1099.5	352.0	0.0	−0.8	24.9	664.6	768.9
ST143	35.80	34.45	763.0	785.7	1355.6	396.1	0.4	0.1	28.1	700.3	825.7
ST144	20.26	32.10	265.1	243.6	591.6	55.3	1.2	1.6	41.3	233.1	297.0
ST145	15.05	32.41	246.7	235.2	455.2	89.3	0.3	−0.8	40.7	217.3	276.0
ST146	10.98	31.86	135.0	124.5	570.0	22.5	2.3	7.3	76.8	104.7	165.3
ST147	8.75	36.95	1237.3	1162.5	2364.5	654.0	1.1	1.4	29.2	1131.7	1342.9
ST148	16.58	31.20	176.5	176.0	380.0	42.9	0.8	0.6	44.2	153.7	199.4
ST149	13.15	32.66	276.6	275.0	574.4	52.3	0.5	−0.2	45.2	240.0	313.1
ST150	14.48	35.85	587.5	554.6	1361.7	133.9	0.8	2.3	37.5	523.1	651.9
ST151	−8.03	31.61	220.2	208.5	509.0	61.7	0.8	0.9	41.9	193.2	247.1
ST152	−7.58	33.36	290.3	268.5	707.9	61.7	1.0	1.3	47.7	249.9	330.8
ST153	−1.93	34.78	267.9	269.1	422.9	106.2	−0.1	−0.4	27.8	246.1	289.6
ST154	−6.77	34.04	491.0	494.3	1209.1	61.7	1.3	2.7	44.5	427.2	554.8
ST155	−5.90	35.73	626.9	590.4	1643.6	61.7	1.2	3.7	42.6	548.7	705.0
ST156	−6.73	41.80	743.8	742.1	1243.1	435.5	0.5	−0.6	28.4	682.2	805.5
ST157	−7.96	37.01	484.5	465.6	1157.0	173.0	1.5	2.9	39.7	428.3	540.6
ST158	−9.09	38.43	762.5	775.4	1591.0	416.0	0.8	1.2	32.7	689.7	835.4
ST159	13.56	45.51	917.5	940.3	1462.4	61.7	−0.8	2.7	26.4	846.8	988.3
ST160	13.71	46.50	1516.5	1493.8	2083.3	1135.1	0.3	−0.4	15.1	1449.5	1583.6
ST161	−2.50	36.80	194.0	198.5	551.5	64.9	1.9	7.1	42.3	170.0	218.0
ST162	−1.85	38.95	359.4	333.7	615.0	184.9	0.6	−0.3	27.3	330.7	388.1
ST163	−0.50	38.36	310.4	282.7	653.1	108.9	1.1	0.9	39.2	274.8	345.9
ST164	−2.38	36.85	195.0	198.6	551.5	64.9	1.9	7.1	42.0	171.1	218.9
ST165	2.38	41.57	749.8	709.9	1286.7	464.7	0.6	−0.6	29.5	685.2	814.4
ST166	−0.55	38.28	288.6	258.1	739.0	114.0	1.6	3.0	45.2	250.5	326.7
ST167	−4.51	40.65	399.7	387.8	678.9	242.8	0.9	1.0	23.9	371.8	427.5
ST168	−6.81	38.88	450.3	444.1	774.3	228.8	0.7	0.2	29.8	411.1	489.6
ST169	2.07	41.25	619.0	577.4	988.0	346.2	1.0	0.4	25.0	573.8	664.1
ST170	2.06	41.28	579.5	541.1	1025.5	323.9	0.9	0.8	28.0	532.1	626.8
ST171	25.96	31.71	129.0	119.3	421.6	13.5	1.6	3.3	64.5	104.7	153.3
ST172	−6.03	43.55	546.7	551.2	751.7	322.6	−0.1	0.5	16.8	519.9	573.5
ST173	−6.33	39.46	530.9	515.6	958.7	287.9	0.5	0.2	28.6	486.6	575.3
ST174	−0.06	39.95	447.6	443.9	1024.9	218.8	1.3	4.0	32.8	404.7	490.4
ST175	−3.91	38.98	402.5	383.9	709.3	168.3	0.5	0.4	26.7	371.1	433.8
ST176	−4.83	37.85	559.3	527.4	1179.4	300.4	1.5	2.9	34.0	503.6	614.9
ST177	−2.13	40.06	502.5	488.3	734.1	266.2	0.2	−0.8	23.0	468.8	536.3
ST178	−1.41	41.11	404.5	409.6	659.1	171.4	0.1	0.2	25.2	374.8	434.3
ST179	2.50	41.58	639.2	578.9	1641.6	288.5	1.8	4.6	39.3	565.7	712.7
ST180	2.76	41.90	707.9	686.8	1143.4	313.0	0.4	−0.5	28.4	649.2	766.6
ST181	−3.78	37.18	368.1	349.1	687.7	186.5	0.8	0.6	29.7	336.2	400.0
ST182	35.78	30.16	41.5	37.0	117.0	6.0	0.9	0.5	60.1	34.2	48.8
ST183	−6.91	37.28	502.1	475.3	1057.1	236.0	0.9	1.3	34.0	452.2	552.0
ST184	1.38	38.88	420.7	411.0	878.2	196.8	1.0	1.8	32.2	381.2	460.2
ST185	−0.40	39.50	361.7	354.5	661.7	181.0	0.8	0.8	28.4	331.6	391.7
ST186	−6.06	36.75	564.4	550.2	1412.2	250.0	1.6	5.5	36.3	504.4	624.3
ST187	−0.33	42.08	491.1	497.7	691.0	277.4	0.0	−0.4	19.1	463.6	518.6
ST188	−5.65	42.58	525.5	509.2	798.5	300.2	0.3	−0.6	23.1	490.0	561.0
ST189	0.62	41.62	346.7	324.8	516.9	180.1	0.3	−0.9	25.2	321.1	372.2
ST190	−2.33	42.45	412.5	399.6	630.4	240.1	0.4	−0.2	20.9	387.3	437.8
ST191	−3.55	40.45	375.7	368.4	567.1	213.5	0.2	−0.8	24.7	348.7	402.8
ST192	−3.71	40.30	370.4	369.6	578.3	216.1	0.2	−0.5	23.9	344.5	396.3
ST193	−3.40	40.24	423.7	413.9	609.2	251.7	0.1	−0.9	22.9	395.4	452.1
ST194	−4.48	36.66	508.9	454.2	1207.0	204.0	1.7	3.1	43.6	444.1	573.7
ST195	−2.95	35.28	388.3	364.7	690.4	204.7	0.9	0.1	31.6	352.5	424.1
ST196	4.23	39.86	556.4	568.7	780.5	275.2	−0.2	−0.7	22.8	519.3	593.5
ST197	−1.88	40.85	463.4	462.3	657.4	268.6	0.1	−0.9	23.4	431.7	495.1
ST198	−5.61	37.15	545.6	545.2	1033.8	219.7	0.7	0.6	31.8	494.8	596.3

Table A1. Cont.

ID	Long	Lat	Mean	Med	Max	Min	Sk	Ku	CV%	LCL	UCL
ST199	−1.23	37.95	291.3	292.5	547.0	115.2	0.3	−0.4	33.7	262.6	319.9
ST200	−4.01	40.78	1293.1	1229.1	2011.0	805.7	0.4	−0.7	22.7	1207.3	1378.9
ST201	2.73	39.55	416.6	410.9	559.6	227.3	−0.3	−0.7	21.4	390.5	442.7
ST202	−1.38	42.49	720.2	736.7	1062.9	490.3	0.3	−0.2	18.7	680.9	759.4
ST203	−6.58	42.56	657.9	671.6	952.3	376.7	−0.1	−0.9	21.1	617.3	698.5
ST204	1.16	41.15	493.9	495.5	770.0	249.4	0.1	−0.7	24.7	458.2	529.6
ST205	−6.35	36.56	518.1	493.2	1219.5	194.0	1.4	4.5	34.2	466.3	570.0
ST206	−5.50	40.95	367.8	363.6	547.0	219.4	0.1	−0.7	21.0	345.2	390.3
ST207	−1.39	42.46	1204.8	1244.8	2174.4	367.2	0.3	0.3	32.6	1090.1	1319.4
ST208	−5.39	40.57	382.6	378.4	576.9	205.1	0.2	−0.5	23.3	356.5	408.6
ST209	−4.11	40.95	457.1	448.9	812.2	288.2	1.0	2.0	22.2	427.4	486.7
ST210	−3.63	42.35	532.9	511.0	940.6	254.5	0.7	−0.1	31.9	483.2	582.7
ST211	−2.46	41.76	518.8	502.5	859.6	344.8	1.0	1.7	19.7	489.0	548.7
ST212	13.50	45.83	989.4	950.5	1481.7	513.6	0.4	−0.4	22.7	923.8	1055.0
ST213	−5.90	37.41	349.9	365.2	543.0	159.6	−0.2	−0.3	24.5	324.8	375.0
ST214	0.50	40.81	500.0	482.9	768.2	251.0	0.3	0.0	23.9	465.1	534.9
ST215	−0.46	39.50	436.0	405.3	1043.1	159.5	1.3	3.9	35.7	390.5	481.5
ST216	−4.76	41.65	432.4	426.6	698.7	205.5	0.2	−0.1	23.7	402.5	462.3
ST217	−0.45	39.58	465.8	430.0	1043.1	184.0	1.0	1.5	37.4	414.9	516.8
ST218	35.00	32.80	554.3	557.7	821.5	272.6	−0.1	−0.3	25.1	513.7	595.0
ST219	−5.73	41.51	381.1	378.9	578.3	219.7	0.1	−1.0	24.4	353.9	408.2
ST220	−1.01	41.66	321.7	317.6	542.2	182.9	0.5	0.1	25.3	297.9	345.4
ST221	40.91	34.41	120.2	118.8	272.9	9.2	0.5	0.5	46.3	103.4	137.1
ST222	37.21	36.18	312.2	317.5	499.3	109.3	−0.2	0.0	30.4	283.5	341.0
ST223	37.47	35.21	191.1	178.5	420.8	47.5	1.0	1.4	39.3	168.4	213.8
ST224	36.51	33.41	120.0	119.1	272.9	9.2	0.4	0.4	46.3	103.8	136.2
ST225	36.10	32.60	271.1	221.9	825.3	56.3	1.8	3.7	61.5	221.9	320.4
ST226	40.15	35.31	134.6	132.3	262.8	30.1	0.1	−0.6	44.8	116.4	152.9
ST227	36.61	35.93	490.8	489.7	722.5	215.1	−0.1	−0.6	27.3	450.2	531.3
ST228	36.75	35.11	305.1	325.5	606.4	116.4	0.3	0.9	31.4	277.1	333.1
ST229	40.75	36.50	240.6	233.8	477.6	80.5	0.5	0.1	38.5	212.6	268.6
ST230	35.93	35.40	775.8	780.7	1191.5	329.2	0.1	−0.7	28.9	710.2	841.3
ST231	36.25	32.85	269.4	259.7	521.5	94.9	0.6	0.5	33.0	242.5	296.3
ST232	38.00	36.81	298.6	283.0	545.0	164.9	0.8	0.5	29.9	271.7	325.6
ST233	41.21	37.05	338.4	349.8	667.2	82.0	0.1	−0.7	45.0	294.0	382.9
ST234	36.47	33.05	163.0	154.5	393.3	49.1	0.7	0.8	46.4	140.1	185.8
ST235	35.76	35.53	699.9	692.2	1104.6	362.6	0.2	−1.1	29.2	640.2	759.7
ST236	37.20	36.31	317.7	320.2	501.6	129.0	−0.1	0.0	27.2	291.6	343.8
ST237	36.71	34.03	139.2	122.6	465.6	34.0	2.1	4.2	67.9	110.7	167.8
ST238	38.30	34.55	123.2	122.1	271.4	20.2	0.4	0.9	39.3	108.5	137.8
ST239	39.01	35.93	170.4	176.5	369.7	41.7	0.3	0.1	41.4	149.1	191.8
ST240	36.13	34.81	986.5	1019.4	1821.6	432.2	0.2	−0.1	31.0	894.1	1078.9
ST241	37.03	35.00	279.1	277.5	479.0	85.0	0.1	1.1	27.5	255.9	302.3
ST242	36.58	32.70	300.7	296.8	486.3	109.2	0.2	−0.5	30.2	273.2	328.1
ST243	35.88	34.88	809.9	805.0	1378.6	365.4	0.2	−0.4	30.2	735.9	884.0
ST244	38.95	36.70	254.5	261.4	452.1	38.9	−0.3	0.6	33.4	228.7	280.2
ST245	8.81	34.41	197.1	143.1	800.4	21.1	1.9	4.5	77.3	152.6	241.6
ST246	10.23	36.83	441.2	449.3	851.4	61.7	0.0	−0.1	37.4	393.0	489.4
ST247	10.10	33.88	179.0	135.6	659.4	31.6	1.8	3.9	69.6	142.6	215.5
ST248	8.80	36.48	443.3	440.4	817.6	61.7	0.0	−0.7	40.3	391.1	495.6
ST249	10.10	35.66	283.2	278.9	587.0	61.7	0.5	0.1	40.7	249.6	316.9
ST250	11.08	36.85	485.5	468.3	847.9	61.7	0.0	−0.6	39.2	430.0	541.1
ST251	10.75	35.66	336.3	311.2	687.8	61.7	0.5	−0.5	47.1	290.0	382.7
ST252	7.88	33.88	96.5	81.8	330.5	8.6	1.7	2.5	75.1	75.4	117.7
ST253	9.78	37.24	563.6	561.6	1008.9	61.7	−0.2	−0.4	37.6	501.7	625.4
ST254	10.72	34.69	199.7	190.5	499.9	46.0	0.9	1.8	46.3	172.7	226.7
ST255	11.09	33.51	236.5	211.2	572.8	64.7	1.1	0.9	49.4	202.4	270.7
ST256	35.41	37.00	684.2	645.2	1078.4	311.5	0.3	−0.9	30.1	624.1	744.2
ST257	30.53	38.75	422.4	437.0	680.0	270.4	0.7	2.0	19.2	398.6	446.1

Table A1. Cont.

ID	Long	Lat	Mean	Med	Max	Min	Sk	Ku	CV%	LCL	UCL
ST258	27.85	38.91	556.6	549.1	866.0	286.4	0.4	−0.2	22.8	519.6	593.7
ST259	32.00	36.55	1102.5	1072.0	1769.0	552.8	0.4	−0.5	28.0	1012.3	1192.7
ST260	22.40	38.90	513.6	520.4	932.9	229.7	0.4	0.5	28.2	471.2	556.0
ST261	30.73	36.86	1074.3	1103.0	1890.0	288.5	0.2	0.2	30.3	979.2	1169.4
ST262	27.85	37.85	609.5	634.0	948.0	134.4	−0.4	0.2	28.7	558.4	660.7
ST263	27.91	39.61	566.8	552.5	911.9	323.5	0.5	0.3	21.1	531.8	601.8
ST264	16.88	40.43	481.8	481.0	850.1	170.0	0.2	−0.5	32.7	435.7	527.9
ST265	22.01	37.06	755.1	762.0	1116.0	322.1	−0.4	0.4	21.3	708.0	802.2
ST266	29.06	40.18	670.2	632.0	1181.1	460.0	1.5	4.5	19.1	632.8	707.6
ST267	26.40	40.13	579.8	556.0	901.0	371.0	0.6	−0.4	22.7	541.4	618.2
ST268	28.32	37.92	691.6	686.3	1140.0	144.5	−0.2	0.4	28.2	634.7	748.4
ST269	29.08	37.78	565.8	559.0	830.7	327.8	0.3	0.0	21.3	530.6	601.0
ST270	40.18	37.88	487.2	475.0	768.6	258.0	0.4	−0.2	24.2	452.7	521.7
ST271	26.56	41.66	593.5	566.0	963.2	388.1	0.9	0.5	22.9	553.9	633.1
ST272	39.28	38.60	406.4	387.0	735.4	199.1	0.7	1.2	26.8	374.7	438.2
ST273	34.05	37.50	306.4	300.0	473.4	138.0	−0.1	0.6	21.8	286.8	325.9
ST274	28.26	36.85	881.5	859.1	1823.1	416.5	1.2	3.0	30.2	803.7	959.4
ST275	26.88	39.06	626.4	608.5	926.7	372.7	0.3	−0.5	21.4	587.2	665.6
ST276	30.56	39.78	388.4	380.2	630.2	196.9	0.6	0.7	24.3	360.8	416.0
ST277	30.15	36.30	940.0	911.0	1556.0	365.0	0.4	0.2	27.3	865.0	1015.1
ST278	37.36	37.08	531.7	517.0	992.0	237.5	0.5	0.4	28.9	486.9	576.6
ST279	36.16	36.58	741.6	753.0	1010.0	492.0	0.2	0.0	16.3	706.3	776.9
ST280	30.55	37.75	518.9	526.0	803.0	246.9	−0.1	−0.3	23.3	483.6	554.3
ST281	28.81	40.96	662.8	615.7	1214.4	351.5	1.1	1.1	31.1	602.6	723.1
ST282	27.01	38.51	698.4	683.0	1133.1	362.0	0.4	−0.3	27.0	643.3	753.5
ST283	34.50	37.60	337.9	329.2	467.0	183.0	0.1	−0.5	21.1	317.0	358.7
ST284	35.43	38.81	378.1	372.0	614.0	233.6	0.6	0.6	21.2	354.8	401.5
ST285	34.16	39.15	372.8	363.0	497.0	240.0	0.0	−0.9	18.5	352.7	393.0
ST286	32.54	37.96	333.6	347.7	574.5	177.0	0.3	0.4	24.9	309.3	357.8
ST287	29.96	39.41	552.7	538.0	851.1	328.7	0.3	−0.1	20.4	519.7	585.6
ST288	38.08	38.43	345.5	345.4	676.9	1.1	−0.2	1.1	38.2	307.0	384.1
ST289	28.36	37.21	1146.9	1158.0	1760.0	509.0	0.0	0.4	22.5	1071.5	1222.2
ST290	34.68	37.96	343.0	341.0	475.0	205.0	0.0	−0.2	19.1	323.9	362.1
ST291	33.93	36.38	560.1	561.0	1007.0	299.0	0.4	−0.4	30.7	509.8	610.4
ST292	29.08	40.96	697.9	676.0	1047.2	432.0	0.2	−0.5	21.7	653.6	742.2
ST293	27.55	40.98	590.7	580.1	879.3	248.2	0.1	0.4	22.3	552.2	629.1
ST294	26.70	39.30	642.3	661.1	972.1	306.0	0.0	−0.4	24.3	596.7	687.9
ST295	38.76	37.13	444.1	438.1	855.0	203.0	0.9	0.9	33.0	401.2	486.9
ST296	29.40	38.68	542.6	534.7	876.2	346.3	0.6	1.0	19.3	512.0	573.3
ST297	36.93	37.60	743.5	718.0	1416.6	443.1	1.3	2.5	25.7	687.6	799.4
ST298	34.80	39.81	598.3	580.0	858.0	405.5	0.5	−0.2	18.0	566.8	629.7
ST299	27.43	37.03	684.8	673.3	1091.4	355.4	0.2	−0.9	28.9	626.9	742.6
ST300	42.00	37.93	695.2	694.0	1046.4	446.0	0.4	−0.3	21.8	650.9	739.5
ST301	34.57	31.67	464.7	433.1	823.9	165.7	0.5	−0.2	35.1	417.1	512.3
ST302	34.59	32.27	597.4	563.2	1106.9	252.1	0.9	1.7	30.4	544.4	650.5
ST303	5.06	36.71	719.9	747.8	1084.7	307.5	−0.3	−0.4	25.6	665.9	773.8
ST304	6.95	36.88	740.1	719.1	1148.9	491.6	0.3	−0.4	21.3	694.1	786.0
ST305	12.23	41.80	731.9	701.3	1234.9	345.5	0.3	−0.4	30.1	667.6	796.2
ST306	10.68	34.71	215.4	206.2	382.0	94.7	0.5	−0.2	33.4	194.4	236.4
ST307	27.30	38.40	709.0	706.3	1088.0	361.0	0.3	−0.3	24.4	658.4	759.6
ST308	34.60	36.80	631.6	590.8	1023.7	280.5	0.3	−0.6	29.6	576.9	686.3
ST309	34.53	38.76	422.6	417.4	589.0	287.2	0.2	−0.4	16.6	402.1	443.2
ST310	38.28	37.75	648.8	602.0	1171.0	350.2	1.0	0.6	29.1	593.6	704.0
ST311	20.88	37.75	699.6	696.0	1325.0	0.0	−0.6	1.4	37.3	623.3	775.9
ST312	14.28	37.56	604.0	563.8	1631.0	269.6	2.0	6.1	40.9	531.9	676.1

Long: Longitude; Lat: Latitude; Mean: Mean value, Max: Maximum value, Min: Minimum value; SK: Skewness; Ku: Kurtosis; CV%: Coefficient of Variation %; LCL: Lower Control Limit; UCL: Upper Control Limit.

Table A2. Main statistical characteristics of mean annual temperature over the MED during 1975–2019.

ID	Long	Lat	Mean	Med	Max	Min	Sk	Ku	CV%	LCL	UCL
ST01	7.48	36.50	17.7	17.8	18.6	16.6	−0.6	0.3	2.7	17.6	17.8
ST02	1.20	36.12	19.2	19.2	21.0	17.8	0.1	−0.3	4.0	19.0	19.4
ST03	3.25	36.68	17.5	17.8	18.8	14.5	−1.2	1.9	4.9	17.3	17.8
ST04	2.14	36.18	17.0	17.0	18.0	15.5	−0.4	−0.8	4.2	16.8	17.2
ST05	−0.60	35.63	17.8	17.9	18.6	16.4	−0.5	−0.8	3.6	17.6	18.0
ST06	18.08	42.65	16.8	16.6	18.4	15.4	0.3	−0.7	4.4	16.6	17.0
ST07	15.36	44.55	9.3	9.2	11.3	7.5	0.1	−0.7	9.9	9.0	9.6
ST08	16.45	43.16	16.8	16.8	18.3	15.5	0.2	−0.4	4.0	16.6	17.0
ST09	16.20	44.03	13.3	13.2	15.2	12.0	0.3	0.3	4.9	13.2	13.5
ST10	16.90	42.76	16.0	16.0	17.5	14.7	0.1	−0.5	4.3	15.8	16.2
ST11	15.23	45.26	10.5	10.5	12.5	8.7	−0.1	−0.8	9.0	10.3	10.8
ST12	18.38	45.32	11.5	11.4	13.3	9.7	0.1	−0.5	7.4	11.2	11.7
ST13	14.27	45.20	14.3	14.3	16.0	12.7	0.1	−0.9	5.8	14.1	14.6
ST14	16.43	43.51	16.5	16.5	17.9	15.1	0.0	−0.8	4.5	16.3	16.8
ST15	16.38	46.30	10.8	10.6	12.5	9.0	−0.1	−0.8	8.7	10.5	11.0
ST16	15.12	44.07	15.4	15.3	17.0	14.1	0.1	−0.7	4.7	15.2	15.6
ST17	15.98	45.81	13.0	13.1	15.7	10.3	0.1	−1.1	10.6	12.6	13.4
ST18	14.59	44.49	4.1	4.1	5.9	2.4	−0.1	−0.6	19.7	3.9	4.4
ST19	32.98	34.58	19.8	19.7	21.1	18.7	0.2	0.0	2.7	19.6	19.9
ST20	32.92	34.93	18.2	18.1	21.0	16.5	1.0	1.2	5.2	17.9	18.5
ST21	33.36	34.88	19.8	19.9	21.4	18.3	0.0	−0.6	3.8	19.6	20.0
ST22	33.00	34.70	19.7	19.7	21.5	17.7	0.1	−0.4	4.6	19.4	19.9
ST23	33.40	35.15	19.5	19.2	21.4	17.8	0.4	−0.5	4.4	19.2	19.7
ST24	32.48	34.71	19.9	19.6	22.9	17.4	0.5	−0.5	6.6	19.5	20.3
ST25	32.43	35.03	18.7	18.8	20.5	16.6	−0.3	−0.6	4.7	18.4	18.9
ST26	29.95	31.20	20.7	20.6	22.1	19.5	0.1	−0.6	3.2	20.5	20.9
ST27	27.21	31.33	20.0	20.0	21.1	19.3	0.4	−0.3	2.5	19.9	20.2
ST28	32.29	31.26	21.7	21.6	23.4	20.4	0.3	−0.3	3.1	21.5	21.9
ST29	8.80	41.91	15.5	15.7	17.1	13.9	−0.2	−0.3	4.6	15.3	15.7
ST30	1.40	43.64	13.5	13.5	14.8	11.7	−0.2	−0.7	5.7	13.3	13.7
ST31	9.48	42.55	16.1	16.0	17.1	14.8	−0.2	−0.4	3.5	15.9	16.2
ST32	1.20	45.90	11.0	11.1	12.9	9.5	0.0	−0.6	8.0	10.8	11.3
ST33	−1.46	35.01	17.5	17.6	18.5	16.0	−0.7	0.3	3.1	17.4	17.7
ST34	9.28	42.33	16.0	16.0	16.9	15.0	−0.2	−0.1	2.8	15.9	16.2
ST35	6.43	43.50	12.6	12.5	13.7	11.2	0.0	−0.9	5.3	12.4	12.8
ST36	5.56	43.04	15.5	15.5	17.1	14.0	0.1	−0.6	5.0	15.3	15.8
ST37	3.16	45.78	11.7	11.7	13.5	10.0	0.0	−0.8	7.5	11.5	12.0
ST38	6.50	44.56	11.1	11.2	13.4	9.4	0.5	0.1	7.7	10.9	11.4
ST39	1.40	44.75	12.8	12.7	14.1	11.2	−0.1	−0.8	5.9	12.5	13.0
ST40	5.33	45.36	12.4	12.3	13.4	11.3	0.1	−1.0	5.0	12.2	12.5
ST41	12.61	44.03	14.0	14.0	15.6	12.5	0.0	−0.6	5.1	13.8	14.2
ST42	5.23	43.45	15.5	15.6	16.9	14.0	−0.1	−0.8	4.7	15.3	15.8
ST43	−0.70	44.83	13.8	13.8	15.1	12.2	−0.2	−1.0	5.9	13.6	14.0
ST44	3.01	44.11	11.0	10.9	12.3	9.3	0.0	−0.8	6.9	10.7	11.2
ST45	3.58	44.11	5.3	5.3	6.6	3.8	−0.2	−0.8	14.4	5.1	5.5
ST46	−0.50	43.91	13.6	13.5	14.7	12.3	−0.1	−1.0	5.1	13.4	13.8
ST47	4.73	44.58	13.9	13.9	15.4	12.3	−0.1	−0.7	5.7	13.6	14.1
ST48	3.96	43.58	15.2	15.1	16.5	13.8	−0.2	−0.9	4.7	14.9	15.4
ST49	7.20	43.65	16.1	16.1	17.2	14.8	−0.2	−0.8	3.8	15.9	16.2
ST50	4.40	43.86	14.9	14.7	16.1	13.7	0.2	−0.9	4.1	14.7	15.1
ST51	4.83	44.13	14.2	14.2	15.1	12.9	−0.3	−0.8	4.3	14.0	14.4
ST52	2.89	42.69	15.8	15.9	16.9	14.4	−0.2	−0.9	4.1	15.6	16.0
ST53	14.91	37.41	17.5	17.4	18.8	16.5	0.6	0.2	3.0	17.4	17.7
ST54	3.68	43.40	15.1	15.1	16.6	13.6	−0.1	−0.7	5.3	14.9	15.3
ST55	1.10	43.00	12.4	12.3	13.4	11.3	0.1	−1.0	5.0	12.2	12.5
ST56	5.35	43.31	15.0	15.1	16.4	13.8	−0.3	−0.8	4.6	14.8	15.2
ST57	0.00	43.18	12.6	12.5	13.8	11.3	0.1	−0.9	4.9	12.4	12.8
ST58	−7.66	33.56	18.0	18.2	19.4	16.9	0.0	−1.1	3.8	17.8	18.2
ST59	3.34	45.76	11.7	11.7	12.9	10.1	−0.1	−0.9	6.5	11.4	11.9

Table A2. Cont.

ID	Long	Lat	Mean	Med	Max	Min	Sk	Ku	CV%	LCL	UCL
ST60	7.51	47.60	10.5	10.6	12.3	9.0	0.0	−0.4	7.2	10.3	10.8
ST61	2.87	42.77	15.7	15.8	16.7	14.4	−0.3	−0.9	3.8	15.5	15.9
ST62	−1.25	44.63	14.1	14.3	17.2	10.2	−0.8	0.4	12.6	13.6	14.6
ST63	6.66	43.25	15.7	15.8	17.1	14.4	0.0	−0.7	4.4	15.5	15.9
ST64	−0.41	43.38	13.2	13.1	14.8	11.9	0.3	−0.2	4.8	13.0	13.3
ST65	15.28	40.01	17.0	17.1	18.7	15.6	0.3	0.3	4.0	16.8	17.2
ST66	6.15	43.09	16.0	16.0	16.9	14.4	−0.7	1.0	3.1	15.8	16.1
ST67	1.30	45.80	11.2	11.0	12.4	10.0	0.2	−1.0	6.1	11.0	11.4
ST68	8.79	41.92	15.5	15.6	16.6	13.9	−0.5	−0.3	4.1	15.3	15.7
ST69	6.61	36.28	15.4	15.5	16.4	13.3	−0.8	0.3	4.8	15.2	15.6
ST70	0.31	46.58	11.9	11.8	13.5	10.4	0.2	−0.6	6.4	11.6	12.1
ST71	2.31	43.21	13.8	14.0	14.9	12.3	−0.3	−0.8	4.9	13.6	14.0
ST72	−5.35	36.15	18.4	18.4	19.3	17.4	−0.5	0.8	2.2	18.3	18.5
ST73	20.77	38.92	17.2	17.1	18.6	16.3	0.3	−0.7	3.3	17.1	17.4
ST74	25.91	40.85	14.8	14.6	17.0	13.4	0.7	−0.3	6.1	14.6	15.1
ST75	21.28	37.91	16.9	16.8	18.0	16.0	0.1	−1.0	3.3	16.8	17.1
ST76	23.70	38.00	18.1	18.2	19.6	15.0	−1.1	2.0	5.4	17.8	18.4
ST77	28.08	36.40	19.3	19.3	20.7	17.4	−0.3	0.9	3.3	19.1	19.5
ST78	24.48	38.96	17.2	17.1	18.4	16.3	0.4	−0.8	3.5	17.0	17.3
ST79	23.70	37.89	18.4	18.5	19.8	14.2	−2.5	8.4	5.6	18.1	18.7
ST80	25.18	35.33	15.2	15.1	16.7	14.3	0.6	−0.3	4.0	15.1	15.4
ST81	18.91	39.61	17.3	17.1	18.8	16.0	0.3	−0.6	4.1	17.0	17.5
ST82	22.41	39.61	11.2	9.2	16.3	7.9	0.7	−1.5	30.0	10.2	12.1
ST83	21.70	36.83	18.0	18.0	18.8	17.3	0.1	−0.6	2.2	17.9	18.1
ST84	26.60	39.06	17.7	17.5	19.5	16.2	0.4	−0.8	4.8	17.4	17.9
ST85	25.38	37.10	18.5	18.4	20.5	17.3	0.6	0.2	3.6	18.3	18.7
ST86	26.91	37.70	18.9	18.8	20.3	16.9	−0.2	−0.4	4.0	18.7	19.1
ST87	24.11	35.48	18.4	18.4	19.5	17.4	0.2	−0.4	2.7	18.2	18.5
ST88	22.96	40.51	15.4	15.4	17.0	14.0	0.1	−1.1	5.1	15.2	15.6
ST89	22.40	37.53	13.7	13.7	16.5	11.9	0.9	0.4	7.7	13.4	14.0
ST90	34.39	31.49	20.5	20.5	22.3	19.1	0.3	−0.2	3.5	20.2	20.7
ST91	35.58	32.65	19.2	19.1	21.7	17.7	0.6	0.4	4.7	18.9	19.5
ST92	34.78	31.23	20.2	20.2	23.4	18.6	0.7	1.1	4.9	19.9	20.5
ST93	34.81	32.00	19.2	19.1	21.7	17.7	0.6	0.4	4.7	18.9	19.5
ST94	35.09	33.00	19.3	19.2	21.4	17.9	0.3	0.1	3.8	19.0	19.5
ST95	34.70	31.70	20.1	20.1	22.1	18.7	0.2	−0.3	3.8	19.9	20.3
ST96	35.27	32.83	20.1	20.0	22.1	18.7	0.3	0.0	3.6	19.9	20.3
ST97	35.15	31.47	17.4	17.5	19.5	15.3	−0.3	−0.3	5.4	17.1	17.6
ST98	35.21	31.86	18.0	18.0	20.4	16.3	0.2	0.7	4.5	17.8	18.2
ST99	34.50	31.43	20.3	20.3	22.3	18.9	0.3	−0.2	3.8	20.1	20.5
ST100	34.53	31.56	20.3	20.3	22.5	18.6	0.1	−1.2	5.1	20.0	20.6
ST101	34.80	30.60	19.2	19.1	21.3	17.9	0.4	0.6	3.6	19.0	19.4
ST102	34.46	32.04	20.9	20.9	23.1	18.0	0.0	−0.5	5.3	20.6	21.2
ST103	16.13	39.34	16.0	15.7	18.4	14.2	0.6	0.0	5.8	15.7	16.2
ST104	16.78	41.13	16.1	16.1	17.5	15.0	0.2	−0.7	3.7	16.0	16.3
ST105	9.70	45.66	13.2	13.2	15.0	11.5	0.1	−0.7	6.8	12.9	13.4
ST106	11.30	44.53	14.7	14.8	17.0	13.2	0.0	−0.7	6.2	14.5	15.0
ST107	17.95	40.65	17.1	17.1	18.1	15.7	−0.3	−0.7	3.8	16.9	17.3
ST108	9.05	39.25	17.2	17.3	18.4	15.9	−0.4	−0.7	3.8	17.0	17.4
ST109	14.65	41.56	12.5	12.6	14.2	10.6	−0.5	0.1	6.1	12.3	12.7
ST110	9.71	39.93	17.3	17.3	18.2	16.0	−0.3	−0.9	3.6	17.1	17.5
ST111	8.16	43.95	15.6	15.5	16.8	14.1	−0.1	−0.9	4.6	15.4	15.8
ST112	15.05	37.46	17.4	17.4	18.4	16.2	−0.1	−0.8	3.2	17.3	17.6
ST113	15.13	36.68	18.7	18.9	20.4	17.2	0.1	0.2	3.8	18.5	18.9
ST114	11.20	43.80	15.6	15.7	16.8	14.3	−0.4	−0.2	3.7	15.4	15.8
ST115	8.85	44.25	16.1	16.3	17.4	14.8	−0.3	−1.0	4.4	15.9	16.3
ST116	11.06	42.75	15.3	15.3	16.9	13.7	−0.1	−0.5	4.8	15.1	15.5
ST117	15.55	38.20	18.9	18.9	19.7	17.8	−0.8	0.2	2.4	18.7	19.0
ST118	9.11	45.28	15.5	14.6	18.3	13.1	0.4	−1.5	10.9	15.0	15.9

Table A2. Cont.

ID	Long	Lat	Mean	Med	Max	Min	Sk	Ku	CV%	LCL	UCL
ST119	15.95	41.70	12.0	12.1	13.8	10.5	−0.1	−0.1	6.3	11.8	12.3
ST120	19.55	39.37	17.7	17.8	18.8	16.7	0.0	−0.7	3.1	17.6	17.9
ST121	13.10	38.18	18.8	18.8	19.6	17.8	−0.4	−0.1	2.1	18.7	18.9
ST122	11.96	36.81	18.6	18.6	19.9	17.0	−0.2	−0.3	3.8	18.4	18.8
ST123	14.20	42.43	15.1	15.2	16.1	13.7	−0.4	−0.8	4.4	14.9	15.3
ST124	10.38	43.68	15.3	15.4	16.9	13.5	−0.2	−0.4	5.1	15.1	15.6
ST125	12.95	40.91	16.8	16.8	18.2	15.3	0.0	−0.6	4.0	16.6	17.0
ST126	12.55	41.78	15.7	15.6	17.1	14.2	−0.1	−0.8	4.7	15.5	15.9
ST127	18.35	39.81	17.1	17.1	18.3	15.8	−0.1	0.1	3.0	16.9	17.2
ST128	14.37	41.09	17.1	17.2	18.2	15.8	−0.4	−0.2	3.4	17.0	17.3
ST129	12.50	37.91	17.9	18.0	18.7	16.5	−0.8	0.9	2.6	17.8	18.1
ST130	25.25	39.93	15.9	15.8	17.3	14.8	0.3	−0.8	4.2	15.7	16.1
ST131	13.75	45.65	15.1	15.2	16.4	13.4	−0.2	−0.7	4.8	14.9	15.3
ST132	12.33	45.50	13.6	13.6	15.3	12.1	0.0	−0.6	5.9	13.3	13.8
ST133	10.86	45.38	13.5	13.4	15.3	11.7	0.1	−0.9	6.8	13.3	13.8
ST134	14.30	40.85	16.5	16.6	17.9	14.4	−0.4	−0.4	5.3	16.2	16.8
ST135	−8.63	42.23	14.1	14.0	15.3	13.0	0.3	−0.9	4.6	13.9	14.3
ST136	−0.80	37.78	16.4	16.5	18.1	14.5	−0.1	−0.7	5.8	16.2	16.7
ST137	−3.78	40.38	15.0	15.0	16.6	13.5	−0.1	−0.5	5.2	14.7	15.2
ST138	−3.46	40.48	14.6	14.6	15.7	13.2	−0.2	−0.7	4.7	14.4	14.8
ST139	35.98	31.98	17.7	17.7	20.1	16.0	0.3	0.6	4.5	17.5	18.0
ST140	35.85	32.54	20.0	19.8	22.1	18.4	0.3	0.0	3.8	19.8	20.2
ST141	38.20	32.56	19.4	19.4	22.0	16.4	−0.2	2.0	4.9	19.1	19.6
ST142	35.48	33.81	20.6	20.8	22.6	18.7	−0.2	−0.9	4.8	20.3	20.9
ST143	35.80	34.45	18.5	18.6	21.2	16.5	0.3	−0.6	6.5	18.2	18.9
ST144	20.26	32.10	20.2	20.2	21.1	19.3	0.0	−0.1	2.2	20.0	20.3
ST145	15.05	32.41	20.6	20.6	21.8	19.4	−0.1	−0.8	2.9	20.4	20.7
ST146	10.98	31.86	20.8	20.8	22.0	19.3	−0.3	−0.3	3.1	20.6	21.0
ST147	8.75	36.95	18.3	18.5	20.0	16.7	−0.1	−0.8	4.8	18.0	18.6
ST148	16.58	31.20	21.0	21.0	23.3	19.4	0.5	1.1	3.5	20.8	21.3
ST149	13.15	32.66	20.6	20.6	21.9	19.3	0.0	−0.8	3.4	20.4	20.8
ST150	14.48	35.85	18.8	18.8	19.7	17.5	−0.5	−0.4	2.9	18.6	18.9
ST151	−8.03	31.61	20.0	20.0	21.5	18.1	−0.4	−0.1	3.6	19.8	20.2
ST152	−7.58	33.36	17.6	17.7	18.7	16.3	−0.3	−0.8	3.5	17.4	17.7
ST153	−1.93	34.78	17.0	17.0	18.6	15.4	0.0	−0.8	5.0	16.7	17.2
ST154	−6.77	34.04	17.4	17.4	18.2	16.7	0.2	−0.8	2.5	17.2	17.5
ST155	−5.90	35.73	17.9	17.9	19.0	16.9	−0.1	−0.6	2.9	17.8	18.1
ST156	−6.73	41.80	12.8	12.8	14.3	11.4	0.0	−0.5	4.9	12.6	13.0
ST157	−7.96	37.01	17.8	17.9	18.9	15.8	−0.6	1.2	3.6	17.6	18.0
ST158	−9.09	38.43	17.5	17.5	18.5	16.4	0.0	−1.0	3.2	17.3	17.6
ST159	13.56	45.51	13.6	13.7	14.9	11.2	−0.8	1.8	5.1	13.4	13.8
ST160	13.71	46.50	7.4	7.5	9.1	5.5	−0.1	−1.0	13.5	7.2	7.7
ST161	−2.50	36.80	19.0	19.1	20.0	17.7	−0.6	0.1	2.8	18.9	19.2
ST162	−1.85	38.95	14.3	14.4	15.6	12.7	−0.3	−0.5	5.3	14.1	14.5
ST163	−0.50	38.36	18.3	18.4	19.2	17.1	−0.3	−0.9	3.2	18.1	18.4
ST164	−2.38	36.85	19.0	19.1	20.0	17.9	−0.3	−0.4	2.7	18.9	19.2
ST165	2.38	41.57	14.6	14.7	15.9	13.2	−0.1	−0.3	4.2	14.4	14.7
ST166	−0.55	38.28	18.2	18.3	19.3	17.0	−0.4	0.0	2.9	18.1	18.4
ST167	−4.51	40.65	11.1	11.2	12.9	9.2	0.0	−0.8	8.3	10.8	11.3
ST168	−6.81	38.88	17.1	17.0	18.4	15.9	0.0	−0.5	3.7	16.9	17.3
ST169	2.07	41.25	15.8	15.9	16.7	14.4	−0.4	−0.8	4.0	15.6	16.0
ST170	2.06	41.28	16.2	16.4	17.8	14.8	−0.1	−1.4	5.9	15.9	16.5
ST171	25.96	31.71	17.0	16.9	18.9	15.5	0.4	0.2	4.3	16.7	17.2
ST172	−6.03	43.55	10.7	10.8	12.1	9.2	−0.2	−0.9	6.9	10.5	10.9
ST173	−6.33	39.46	16.4	16.3	17.7	15.0	0.0	0.2	3.5	16.2	16.6
ST174	−0.06	39.95	17.6	17.8	18.8	15.9	−0.4	−0.9	4.6	17.3	17.8
ST175	−3.91	38.98	15.5	15.7	17.0	13.0	−0.8	0.3	6.3	15.2	15.8
ST176	−4.83	37.85	18.2	18.2	19.5	16.9	−0.1	−0.7	3.6	18.0	18.3
ST177	−2.13	40.06	13.2	13.2	15.0	11.7	0.2	−0.7	6.6	13.0	13.5

Table A2. Cont.

ID	Long	Lat	Mean	Med	Max	Min	Sk	Ku	CV%	LCL	UCL
ST178	-1.41	41.11	13.0	13.1	14.2	11.6	-0.3	-0.7	5.3	12.8	13.2
ST179	2.50	41.58	15.6	16.0	17.4	13.2	-0.4	-0.9	7.2	15.3	15.9
ST180	2.76	41.90	14.8	14.8	16.2	13.2	-0.1	-0.8	5.1	14.6	15.0
ST181	-3.78	37.18	15.5	15.4	17.5	14.2	0.5	-0.3	5.0	15.3	15.7
ST182	35.78	30.16	17.8	17.8	20.1	15.9	0.1	0.8	4.7	17.5	18.0
ST183	-6.91	37.28	18.3	18.3	19.2	17.1	-0.3	0.4	2.3	18.2	18.4
ST184	1.38	38.88	18.2	18.2	19.1	17.1	-0.3	-0.6	2.7	18.0	18.3
ST185	-0.40	39.50	15.6	15.6	16.9	14.2	-0.2	-0.5	4.1	15.4	15.8
ST186	-6.06	36.75	18.1	18.2	19.3	16.9	-0.2	-0.1	2.9	18.0	18.3
ST187	-0.33	42.08	14.1	14.2	15.6	12.9	0.0	-0.7	5.0	13.9	14.3
ST188	-5.65	42.58	11.1	11.1	12.2	10.0	0.1	-0.2	4.4	11.0	11.3
ST189	0.62	41.62	15.1	15.1	16.3	13.9	0.0	-0.8	4.1	15.0	15.3
ST190	-2.33	42.45	14.0	14.0	14.9	12.8	-0.1	-1.1	4.4	13.8	14.1
ST191	-3.55	40.45	14.6	14.5	16.0	12.9	0.2	-0.4	5.0	14.4	14.8
ST192	-3.71	40.30	14.4	14.3	16.2	12.7	0.3	-0.2	5.6	14.2	14.6
ST193	-3.40	40.24	15.1	15.1	16.7	13.7	0.1	-0.4	4.9	14.9	15.3
ST194	-4.48	36.66	18.6	18.6	19.9	17.3	-0.1	-1.0	3.6	18.4	18.8
ST195	-2.95	35.28	19.0	19.0	19.9	17.9	-0.1	-0.9	2.7	18.8	19.1
ST196	4.23	39.86	17.2	17.3	18.2	15.7	-0.5	-0.7	3.8	17.0	17.4
ST197	-1.88	40.85	10.6	10.6	11.7	9.3	-0.1	-0.9	6.2	10.4	10.8
ST198	-5.61	37.15	17.9	18.0	19.3	16.4	-0.3	-0.6	4.1	17.7	18.1
ST199	-1.23	37.95	18.3	18.3	19.4	17.1	-0.1	-0.4	3.3	18.1	18.5
ST200	-4.01	40.78	7.0	7.0	8.7	5.4	0.0	-0.2	11.3	6.8	7.2
ST201	2.73	39.55	16.6	16.7	17.9	15.1	-0.4	-0.8	4.5	16.4	16.8
ST202	-1.38	42.49	13.0	13.0	14.2	11.7	0.1	-0.9	5.2	12.8	13.2
ST203	-6.58	42.56	13.1	13.0	14.5	12.2	0.2	-1.0	4.8	12.9	13.3
ST204	1.16	41.15	16.2	16.4	17.8	14.5	-0.1	-0.6	4.5	16.0	16.4
ST205	-6.35	36.56	18.1	18.2	19.3	16.9	-0.3	-0.2	3.0	18.0	18.3
ST206	-5.50	40.95	12.1	12.1	13.3	10.8	-0.1	-0.7	5.2	11.9	12.3
ST207	-1.39	42.46	12.9	12.9	14.2	11.4	-0.1	-0.8	5.6	12.7	13.1
ST208	-5.39	40.57	12.7	12.7	16.5	10.7	0.7	0.8	9.2	12.4	13.1
ST209	-4.11	40.95	12.3	12.3	13.7	11.0	0.0	-0.8	5.8	12.1	12.5
ST210	-3.63	42.35	19.1	19.4	20.4	17.8	-0.2	-1.1	3.9	18.9	19.4
ST211	-2.46	41.76	11.1	11.1	12.4	9.9	0.0	-1.0	5.9	10.9	11.3
ST212	13.50	45.83	13.5	13.4	15.0	12.0	0.2	-0.5	5.5	13.3	13.7
ST213	-5.90	37.41	15.9	15.8	17.4	14.5	0.1	-0.6	4.7	15.7	16.1
ST214	0.50	40.81	17.8	17.8	18.9	16.6	-0.1	-0.9	3.5	17.6	18.0
ST215	-0.46	39.50	17.6	17.6	18.9	16.3	-0.2	-0.9	3.7	17.4	17.8
ST216	-4.76	41.65	12.7	12.7	14.3	9.9	-0.7	1.8	6.4	12.4	12.9
ST217	-0.45	39.58	18.3	18.4	19.5	17.0	-0.3	-0.9	3.5	18.1	18.5
ST218	35.00	32.80	19.8	19.9	21.7	18.3	0.2	-0.9	4.7	19.5	20.1
ST219	-5.73	41.51	13.2	13.1	14.7	12.0	0.1	-0.9	5.3	13.0	13.4
ST220	-1.01	41.66	15.6	15.5	17.0	14.2	0.0	-0.8	4.7	15.4	15.8
ST221	40.91	34.41	20.7	20.7	22.2	19.1	-0.2	-0.9	4.1	20.5	21.0
ST222	37.21	36.18	17.8	17.9	19.5	16.3	-0.1	0.3	3.6	17.7	18.0
ST223	37.47	35.21	18.2	18.3	19.5	16.5	-0.3	-0.1	4.0	18.0	18.4
ST224	36.51	33.41	17.2	17.4	19.3	15.2	-0.1	-0.4	5.3	16.9	17.4
ST225	36.10	32.60	17.7	17.7	19.9	16.3	0.4	1.3	3.9	17.5	17.9
ST226	40.15	35.31	20.4	20.4	22.3	18.6	0.0	0.6	3.6	20.2	20.6
ST227	36.61	35.93	17.7	17.9	19.2	16.1	-0.4	0.0	3.8	17.5	17.9
ST228	36.75	35.11	18.4	18.5	21.0	16.0	0.1	-0.5	6.0	18.0	18.7
ST229	40.75	36.50	19.0	18.8	22.5	16.6	0.6	-0.3	7.3	18.6	19.4
ST230	35.93	35.40	19.2	19.2	20.6	17.7	-0.1	0.5	2.8	19.1	19.4
ST231	36.25	32.85	17.3	17.5	19.8	15.6	0.2	-0.2	5.2	17.1	17.6
ST232	38.00	36.81	17.8	17.9	19.8	15.9	-0.2	0.0	4.4	17.6	18.1
ST233	41.21	37.05	19.5	19.4	21.6	17.3	0.3	-0.3	5.2	19.2	19.8
ST234	36.47	33.05	16.3	16.3	19.1	14.5	0.4	-0.1	6.5	16.0	16.6
ST235	35.76	35.53	19.8	19.7	21.5	18.1	0.3	0.2	3.5	19.6	20.0
ST236	37.20	36.31	17.1	17.1	19.6	15.0	0.3	-0.2	5.8	16.8	17.4

Table A2. Cont.

ID	Long	Lat	Mean	Med	Max	Min	Sk	Ku	CV%	LCL	UCL
ST237	36.71	34.03	13.7	13.8	16.1	12.2	0.4	0.5	6.2	13.5	14.0
ST238	38.30	34.55	19.4	19.3	21.2	17.8	0.2	0.2	3.7	19.1	19.6
ST239	39.01	35.93	19.0	19.0	21.2	17.0	0.1	−0.4	4.9	18.7	19.3
ST240	36.13	34.81	18.7	18.7	20.2	17.1	0.0	0.3	3.3	18.5	18.9
ST241	37.03	35.00	17.7	17.4	20.8	15.5	0.6	−0.3	7.1	17.3	18.1
ST242	36.58	32.70	16.2	16.1	17.6	14.7	−0.3	0.0	4.2	16.0	16.4
ST243	35.88	34.88	19.9	19.8	22.1	18.4	0.6	0.3	3.9	19.7	20.2
ST244	38.95	36.70	17.5	17.6	20.9	15.4	0.7	1.3	6.0	17.2	17.9
ST245	8.81	34.41	19.9	19.9	21.8	17.8	0.0	0.3	4.4	19.7	20.2
ST246	10.23	36.83	19.0	19.1	20.1	17.2	−0.6	−0.7	4.1	18.8	19.2
ST247	10.10	33.88	20.3	20.2	21.5	18.7	0.1	−0.2	3.3	20.1	20.5
ST248	8.80	36.48	18.6	18.7	21.1	16.4	0.0	0.2	5.3	18.3	18.9
ST249	10.10	35.66	20.2	20.2	21.8	18.1	−0.2	−1.1	4.7	20.0	20.5
ST250	11.08	36.85	18.8	18.9	19.7	17.1	−0.9	0.0	3.6	18.6	19.0
ST251	10.75	35.66	19.6	19.6	20.8	18.0	−0.3	−0.7	3.4	19.4	19.8
ST252	7.88	33.88	22.2	22.3	23.4	20.7	−0.2	−0.2	2.8	22.0	22.4
ST253	9.78	37.24	18.3	18.4	19.7	16.8	0.1	−0.4	3.9	18.1	18.5
ST254	10.72	34.69	19.6	19.7	20.7	18.0	−0.5	−0.6	3.3	19.4	19.8
ST255	11.09	33.51	20.7	20.8	21.8	19.1	−0.3	−1.0	3.6	20.4	20.9
ST256	35.41	37.00	18.8	18.8	20.3	17.3	−0.1	−0.3	3.5	18.6	19.0
ST257	30.53	38.75	11.5	11.4	13.9	9.4	0.3	0.6	7.4	11.2	11.7
ST258	27.85	38.91	16.5	16.3	19.4	14.5	0.8	0.7	6.0	16.2	16.8
ST259	32.00	36.55	20.0	19.5	22.8	18.3	0.6	−0.9	6.4	19.6	20.3
ST260	22.40	38.90	16.6	16.7	18.4	15.4	0.4	−0.2	4.2	16.4	16.8
ST261	30.73	36.86	18.6	18.7	20.3	17.3	0.1	−1.1	4.3	18.4	18.9
ST262	27.85	37.85	17.9	18.0	19.2	16.4	0.0	−0.9	4.1	17.7	18.1
ST263	27.91	39.61	14.6	14.7	15.8	13.2	−0.4	−0.3	4.3	14.4	14.8
ST264	16.88	40.43	16.3	16.3	19.3	13.0	−0.5	0.8	8.0	15.9	16.7
ST265	22.01	37.06	17.6	17.7	18.8	16.6	0.1	−0.8	2.9	17.5	17.8
ST266	29.06	40.18	15.1	15.0	17.4	13.6	0.5	0.2	5.5	14.9	15.4
ST267	26.40	40.13	15.3	15.1	17.0	14.0	0.4	−0.8	4.9	15.0	15.5
ST268	28.32	37.92	17.6	17.6	18.6	16.6	0.0	−0.4	2.8	17.5	17.8
ST269	29.08	37.78	16.9	16.9	18.6	15.1	−0.1	−0.8	5.1	16.6	17.1
ST270	40.18	37.88	15.8	15.9	17.7	13.2	−0.5	2.2	5.0	15.6	16.1
ST271	26.56	41.66	14.0	13.8	16.8	12.7	0.8	0.8	6.3	13.7	14.2
ST272	39.28	38.60	13.1	13.3	15.7	10.2	−0.2	1.0	8.2	12.8	13.4
ST273	34.05	37.50	12.6	12.0	16.7	9.3	0.7	0.0	13.2	12.1	13.0
ST274	28.26	36.85	19.4	19.3	21.9	17.6	0.6	1.2	4.3	19.2	19.7
ST275	26.88	39.06	17.1	16.8	19.2	15.6	1.0	0.3	5.6	16.8	17.3
ST276	30.56	39.78	10.9	10.9	12.7	9.1	0.2	−0.5	7.6	10.7	11.2
ST277	30.15	36.30	19.7	19.3	23.3	17.9	1.0	0.1	7.1	19.3	20.1
ST278	37.36	37.08	15.8	15.9	17.4	14.1	−0.3	−0.4	5.1	15.6	16.0
ST279	36.16	36.58	20.4	20.3	22.1	18.8	0.3	0.1	3.6	20.2	20.6
ST280	30.55	37.75	12.3	12.3	13.9	10.6	−0.1	0.1	6.2	12.0	12.5
ST281	28.81	40.96	15.4	15.3	16.8	14.1	0.2	−1.0	4.8	15.2	15.6
ST282	27.01	38.51	18.0	18.0	19.6	15.5	−0.5	1.0	4.6	17.8	18.2
ST283	34.50	37.60	11.0	11.0	14.1	8.9	0.2	−0.6	11.4	10.7	11.4
ST284	35.43	38.81	10.5	10.5	12.9	7.7	0.0	0.7	9.9	10.2	10.8
ST285	34.16	39.15	11.4	11.4	13.9	7.7	−0.6	2.2	9.8	11.1	11.8
ST286	32.54	37.96	11.7	11.8	14.2	9.5	0.3	0.8	7.7	11.5	12.0
ST287	29.96	39.41	11.7	11.2	15.4	9.3	0.9	0.1	12.0	11.3	12.1
ST288	38.08	38.43	13.6	13.6	15.5	11.5	−0.3	1.1	5.5	13.4	13.9
ST289	28.36	37.21	15.2	15.2	16.3	13.9	−0.1	−0.5	3.9	15.0	15.3
ST290	34.68	37.96	11.5	11.5	13.9	8.7	−0.1	1.3	8.1	11.3	11.8
ST291	33.93	36.38	20.2	19.8	23.3	18.1	0.7	−0.5	6.5	19.8	20.6
ST292	29.08	40.96	14.8	14.6	16.8	13.4	0.6	−0.7	6.4	14.6	15.1
ST293	27.55	40.98	14.1	14.0	15.6	12.9	0.1	−1.0	5.2	13.9	14.4
ST294	26.70	39.30	17.1	16.9	19.2	15.7	0.4	−0.9	5.5	16.9	17.4

Table A2. Cont.

ID	Long	Lat	Mean	Med	Max	Min	Sk	Ku	CV%	LCL	UCL
ST295	38.76	37.13	18.7	18.6	20.5	16.7	−0.2	0.1	4.3	18.4	18.9
ST296	29.40	38.68	12.6	12.5	14.2	10.8	0.2	−0.1	5.8	12.3	12.8
ST297	36.93	37.60	17.0	17.0	18.9	15.2	0.0	−0.4	4.8	16.8	17.2
ST298	34.80	39.81	9.7	9.7	11.8	7.8	0.1	−0.3	8.9	9.4	9.9
ST299	27.43	37.03	18.6	18.8	20.1	15.8	−0.8	1.3	4.5	18.3	18.8
ST300	42.00	37.93	18.6	18.8	20.1	15.8	−0.8	1.3	4.5	18.3	18.8
ST301	34.57	31.67	20.1	20.1	22.1	18.7	0.2	−0.2	3.7	19.9	20.3
ST302	34.59	32.27	19.9	19.7	22.0	18.6	0.4	−0.1	3.8	19.7	20.1
ST303	5.06	36.71	17.7	17.8	18.6	16.3	−0.7	−0.4	3.4	17.5	17.9
ST304	6.95	36.88	18.4	18.6	19.6	16.8	−0.6	−0.5	3.9	18.2	18.7
ST305	12.23	41.80	15.9	15.9	16.8	15.0	0.1	−0.6	3.0	15.7	16.0
ST306	10.68	34.71	19.5	19.7	20.6	17.9	−0.6	−0.5	3.6	19.3	19.7
ST307	27.30	38.40	17.9	18.0	19.6	14.9	−0.9	1.7	5.4	17.6	18.2
ST308	34.60	36.80	19.6	19.8	21.5	18.0	0.0	−1.0	4.7	19.3	19.9
ST309	34.53	38.76	10.9	10.8	14.0	9.1	0.8	1.7	8.5	10.7	11.2
ST310	38.28	37.75	17.1	17.1	19.3	14.3	−0.2	0.8	5.7	16.8	17.4
ST311	20.88	37.75	18.0	18.1	19.5	12.3	−2.3	8.8	6.9	17.6	18.3
ST312	14.28	37.56	14.7	14.5	21.6	11.6	2.3	6.2	14.0	14.1	15.3

Long: Longitude; Lat: Latitude; Mean: Mean value, Max: Maximum value, Min: Minimum value; SK: Skewness; Ku: Kurtosis; CV%: Coefficient of Variation %; LCL: Lower Control Limit; UCL: Upper Control Limit.

References

- Haile, G.G.; Tang, Q.; Moghari, S.M.H.; Liu, X.; Gebremicael, T.G.; Leng, G.; Kebede, S.; Xu, X.; Yun, X. Projected impacts of climate change on drought patterns over East Africa. *Earth's Future* **2020**, *8*, e2020EF001502. [\[CrossRef\]](#)
- Cook, B.; Seager, R.; Williams, P.; Puma, M.J.; McDermid, S.; Kelley, M.; Nazarenko, L. Climate Change Amplification of natural drought variability: The Historic mid-twentieth-century North American drought in a warmer. *J. Clim.* **2019**, *32*, 5417–5436. [\[CrossRef\]](#)
- Pérez, G.R.; Vico, G. Effects of Temperature and Water Availability on Northern European Boreal Forests. *Front. For. Glob. Chang.* **2020**, *3*. [\[CrossRef\]](#)
- Wang, M.; Zhi, D.; Chaoyang, W.; Lisheng, S.; Mingguo, M.; Puja, Y.; Bingqing, L.; Xuguang, T. Divergent responses of ecosystem water-use efficiency to extreme seasonal droughts in Southwest China. *Sci. Total. Environ.* **2021**, *760*. [\[CrossRef\]](#) [\[PubMed\]](#)
- Jiao, W.; Tian, C.; Chang, Q.; Novick, K.A.; Wang, L. A new multi-sensor integrated index for drought monitoring. *Agric. For. Meteorol.* **2019**, *268*, 74–85. [\[CrossRef\]](#)
- Singh, R.M.; Shukla, P. Drought characterization using Drought indices and El Niño effects. *Natl. Acad. Sci. Lett.* **2020**, *43*, 339–342. [\[CrossRef\]](#)
- He, B.; Change, J.; Wang, W.; Zhou, S.; Chen, C. Spatio-temporal evolution and non-stationary characteristics of meteorological drought in inland arid areas. *Ecol. Indic.* **2021**, *126*, 107644. [\[CrossRef\]](#)
- Yang, P.; Xia, J.; Zhang, Y.; Zhan, C.; Cai, W.; Zhang, S.; Wang, W. Quantitative study on characteristics of hydrological drought in arid area of Northwest China under changing environment. *J. Hydrol.* **2021**, *597*, 126343. [\[CrossRef\]](#)
- Srinivasarao, C.H.; Rao, K.V.; Gopinath, A.; Prasad, G.; Runachalam, A.; Ramana, D.B.V.; Ravindra Chary, G.; Gangaiah, B.; Venkateswarlu, B.; Mohapatra, T. Chapter Two—Agriculture contingency plans for managing weather aberrations and extreme climatic events: Development, implementation and impacts in India. *Adv. Agron.* **2020**, *159*, 35–91.
- Mondala, S.K.; Huang, J.; Wang, Y.; Su, B.; Zhai, J.; Tao, H.; Wang, G.; Fischer, T.; Wen, S.; Jiang, T. Doubling of the population exposed to drought over South Asia: CMIP6 multi-model-based analysis. *Sci. Total Environ.* **2021**, *771*, 145186. [\[CrossRef\]](#) [\[PubMed\]](#)
- Mishra, A.; Bruno, E.; Zilberman, D. Compound natural and human disasters: Managing drought and COVID-19 to sustain global agriculture and food sectors. *Sci. Total Environ.* **2021**, *754*, 142210. [\[CrossRef\]](#) [\[PubMed\]](#)
- Phillips, C.A.; Caldas, A.; Cleetus, R.; Dahl, K.A.; Barreto, J.D.; Licker, R.; Merner, L.D.; Partida, P.O.J.; Phelan, A.L.; Spanger-Siegfried, E.; et al. Compound climate risks in the COVID-19 pandemic. *Nat. Clim. Chang.* **2020**, *10*, 586–588. [\[CrossRef\]](#)
- Schwartz, S.A. Climate change, Covid-19, preparedness, and consciousness. *Explore* **2020**, *16*, 141–144. [\[CrossRef\]](#) [\[PubMed\]](#)
- Parsons, D.J.; Keyb, D.; Tanguyc, M.; Holman, I.P. Regional variations in the link between drought indices and reported agricultural impacts of drought. *Agric. Syst.* **2019**, *173*, 119–129. [\[CrossRef\]](#)
- Esit, M.; Kumar, S.; Pandey, A.; Lawrence, D.M.; Rangwala, I.; Yeager, S. Seasonal to multi-year soil moisture drought forecasting. *Clim. Atmos. Sci.* **2021**, *4*. [\[CrossRef\]](#)
- Cammarano, D.; Ceccarellib, S.; Grando, S.; Romagosa, I.; Benbelkaceme, A.; Akarf, T.; Yassin, A.; Pecchionihi, N.; Franciai, E.; Ronga, D. The impact of climate change on barley yield in the Mediterranean basin. *Eur. J. Agron.* **2019**, *106*, 1–11. [\[CrossRef\]](#)

17. Sardans, J.; Urbin, F.; Grau, O.; Asensio, D.; Ogaya, R.; Peñuelas, J. Long-term drought decreases ecosystem C and nutrient storage in a Mediterranean holm oak forest. *Environ. Exp. Bot.* **2020**, *177*, 104135. [[CrossRef](#)]
18. Crausbay, S.D.; Ramirez, A.R.; Carter, S.L.; Cross, M.S.; Hall, K.R.; Bathke, D.J.; Betancourt, J.L.; Colt, S.; Cravens, A.E.; Dalton, M.S.; et al. Defining Ecological Drought for the Twenty-First Century. *Bull. Am. Meteorol. Soc.* **2017**, *98*, 2543–2550. [[CrossRef](#)]
19. Stott, P.A.; Christidis, N.; Otto, F.E.L.; Sun, Y.; Van Oderlinden, J.P.; Vautard, R.; von Storch, V.; Walton, P.; Yiou, P.; Zwiers, F.W. Attribution of extreme weather and climate-related events. *Wiley Interdiscip. Rev. Clim. Chang.* **2016**, *7*, 23–41. [[CrossRef](#)]
20. Diffenbaugh, N.S.; Singh, D.; Mankin, J.S.; Horton, D.E.; Swain, D.L.; Touma, D.; Charland, A.; Liu, Y.; Haugen, M.; Tsiang, M.; et al. Quantifying the influence of global warming on unprecedented extreme climate events. *Proc. Natl. Acad. Sci. USA* **2017**, *114*, 4881–4886. [[CrossRef](#)] [[PubMed](#)]
21. Crausbay, S.D.; Betancourt, J.; Bradford, J.; Cartwright, J.; Dennison, W.C.; Dunham, J.; Enquist, C.A.F.; Frazier, A.G.; Hall, K.; Littell, J.S.; et al. Unfamiliar territory: Emerging themes for ecological drought research and management. *One Earth* **2020**, *3*, 337–353. [[CrossRef](#)]
22. Hasan, A.G.; Fullen, M.A.; Oloke, D. Problems of drought and its management in Yobe State, Nigeria. *Weather. Clim. Extrem.* **2019**, *23*, 100192. [[CrossRef](#)]
23. Zhao, T.; Dai, A. The Magnitude and Causes of Global Drought Changes in the Twenty-First Century under a Low–Moderate Emissions Scenario. *Bull. Am. Meteorol. Soc.* **2015**, *28*, 4490–4512. [[CrossRef](#)]
24. Zhao, T.; Dai, A. Uncertainties in historical changes and future projections of drought. Part II: Model-simulated historical and future drought changes. *Clim. Chang.* **2016**, *144*, 535–548. [[CrossRef](#)]
25. Lu, Y.J.; Cai, H.J.; Jiang, T.T.; Sun, S.K.; Wang, Y.B.; Zhao, J.; Yu, K.; Sun, J. Assessment of global drought propensity and its impacts on agricultural water use in future climate scenarios. *Agric. For. Meteorol.* **2019**, *278*, 107623. [[CrossRef](#)]
26. McEvoy, J.; Bathke, D.J.; Burkardt, N.; Cravens, A.E.; Haigh, T.; Hall, K.R.; Hayes, M.J.; Jedd, T.; Podebradska, M.; Wickham, E. Ecological drought: Accounting for the non-human impacts of water shortage in the Upper Missouri Headwaters Basin, Montana, USA. *Resources* **2018**, *7*, 14. [[CrossRef](#)]
27. Lionello, P.; Scarascia, L. The relation between climate change in the Mediterranean region and global warming. *Reg. Environ. Chang.* **2018**, *18*, 1481–1493. [[CrossRef](#)]
28. Spinoni, J.; Barbosa, P.; De Jager, A.; McCormick, N.; Naumann, G.; Vogt, J.V.; Magni, D.; Masante, D.; Mazzeschi, M. A new global database of meteorological drought events from 1951 to 2016. *J. Hydrol. Reg. Stud.* **2019**, *22*, 100593. [[CrossRef](#)]
29. Vogel, J.; Paton, E.; Aich, V.; Bronstert, A. Increasing compound warm spells and droughts in the Mediterranean Basin. *Weather Clim. Extrem.* **2021**, *32*, 100312. [[CrossRef](#)]
30. Malhi, Y.; Girardin, C.; Metcalfe, D.B.; Doughty, C.E.; Aragão, L.E.O.C.; Rifai, S.W.; Oliveras, I.; Shenkin, A.; Aguirre-Gutiérrez, J.; Dahlsjö, C.A.L.; et al. The global ecosystems monitoring network: Monitoring ecosystem productivity and carbon cycling across the tropics. *Biol. Conserv.* **2021**, *253*, 108889. [[CrossRef](#)]
31. Soares, P.M.M.; Cardoso, R.M.; Lima, D.C.A.; Miranda, P.M.A. Future precipitation in Portugal: High-resolution projections using WRF model and EURO-CORDEX multi-model ensembles. *Clim. Dyn.* **2017**, *49*, 2503–2530. [[CrossRef](#)]
32. Trambly, Y.; Koutroulis, A.; Samaniego, L.; Vicente-Serrano, S.M.; Volaire, F.; Boone, A.; Page, M.L.; Llasat, M.C.; Albergel, C.; Burak, S.; et al. Challenges for drought assessment in the Mediterranean region under future climate scenarios. *Earth Sci. Rev.* **2020**, *210*, 103348. [[CrossRef](#)]
33. IPCC. Global Warming of 1.5 °C. An IPCC Special Report on the Impacts of Global Warming of 1.5 °C Above Pre-Industrial Levels and Related Global Greenhouse Gas Emission Pathways. In *The Context of Strengthening the Global Response to the Threat of Climate Change, Sustainable Development, and Efforts to Eradicate Poverty*; Masson-Delmotte, P., Zhai, H.O., Pörtner, D., Roberts, D., Skea, J., Shukla, P.R., Pirani, A., Moufouma-Okia, W., Péan, C., Pidcock, R., et al., Eds.; 2018; in press.
34. Ding, Y.; Mu, C.; Wu, T.; Hu, G.; Zou, D.; Wang, D.; Li, W.; Wu, X. Increasing cryospheric hazards in a warming climate. *Earth Sci. Rev.* **2020**, *213*, 103500. [[CrossRef](#)]
35. Lionello, P.; Gacic, M.; Gomis, D.; Garcia-Herrera, R.; Giorgi, F.; Planton, S.; Trigo, R.; Theocharis, A.; Tsimplis, M.N.; Ulbrich, U.; et al. Program focuses on climate of the Mediterranean region. *Eos Trans. Am. Geophys. Union* **2012**, *93*, 105–106. [[CrossRef](#)]
36. Michaelides, S.; Karacostas, T.; Sanchez, J.L.; Retalis, A.; Pytharoulis, I.; Homar, V.; Romero, R.; Zanis, P.; Giannakopoulos, C.; Bühl, J.; et al. Reviews and perspectives of high impact atmospheric processes in the Mediterranean. *Atmos. Res.* **2018**, *208*, 4–44. [[CrossRef](#)]
37. Hertig, E.; Trambly, Y. Regional downscaling of Mediterranean droughts under past and future climatic conditions. *Glob. Planet Chang.* **2017**, *151*, 36–48. [[CrossRef](#)]
38. Cook, B.I.; Anchukaitis, K.J.; Touchan, R.; Meko, D.M.; Cook, E.R. Spatiotemporal drought variability in the Mediterranean over the last 900 years. *J. Geophys. Res. Atmos.* **2016**, *121*, 2060–2074. [[CrossRef](#)] [[PubMed](#)]
39. Vicente-Serrano, S.M. Differences in spatial patterns of drought on different timescales: An analysis of the Iberian Peninsula. *Water Resour. Manag.* **2006**, *20*, 37–60. [[CrossRef](#)]
40. Caloiero, T.; Veltri, S.; Frustaci, F. Drought Analysis in Europe and in the Mediterranean Basin Using the Standardized Precipitation Index. *Water* **2018**, *10*, 1043. [[CrossRef](#)]
41. Klein Tank, A.M.G.; Wijngaard, J.B.; Konnen, G.P.; Böhm, R.; Demarée, G.; Gocheva, A.; Mileta, M.; Pashiardis, S.; Hejkrlik, L.; Kern-Hansen, C.; et al. Daily dataset of 20th-century surface air temperature and precipitation series for the European Climate Assessment. *Int. J. Climatol.* **2002**, *22*, 1441–1453. [[CrossRef](#)]

42. Menne, M.J.; Durre, I.; Vose, R.S.; Gleason, B.E.; Houston, T.G. An overview of the global historical climatology network daily database. *J. Atmos. Ocean. Technol.* **2012**, *29*, 897–910. [[CrossRef](#)]
43. Szentimrey, T. Theoretical questions of daily data homogenization. *Időjárás* **2013**, *117*, 113–122.
44. Szentimrey, T. Multiple Analysis of Series for Homogenization (MASH). In Proceedings of the Second Seminar for Homogenization of Surface Climatological Data, Budapest, Hungary, 9–13 November 1998; WMO: Budapest, Hungary, 1999; pp. 27–46.
45. Haied, N.; Foufou, A.; Chaab, S.; Azlaoui, M.; Khadri, K.; Benzahia, K.; Benzahia, I. Drought assessment and monitoring using meteorological indices in a semi-arid region. *Energy Procedia* **2017**, *119*, 518–529. [[CrossRef](#)]
46. Adnan, S.; Ullah, K.; Shuanglin, L.; Gao, S.; Hayat Khan, A.; Mahmood, R. Comparison of various drought indices to monitor drought status in Pakistan. *Clim. Dyn.* **2018**, *51*, 1885–1899. [[CrossRef](#)]
47. Xu, L.; Abbaszadeh, P.; Moradkhani, H.; Chen, N.; Zhang, X. Continental drought monitoring using satellite soil moisture, data assimilation and an integrated drought index. *Remote Sens. Environ.* **2020**, *250*, 112028. [[CrossRef](#)]
48. Hong, M.; Lee, S.H.; Lee, S.J.; Choi, J.Y. Application of high-resolution meteorological data from NCAM-WRF to characterize agricultural drought in small-scale farmlands based on soil moisture deficit. *Agric. Water Manag.* **2021**, *243*, 106494. [[CrossRef](#)]
49. Heim, R.R. A review of twentieth-century drought indices used in the United States. *Bull. Am. Meteorol. Soc.* **2002**, *83*, 1149–1165. [[CrossRef](#)]
50. Alvalá, R.C.S.; Cunha, A.P.N.A.; Britos, S.S.B.; Seluchi, M.E.; Marengo, J.A.; Moraes, L.L.M.; Carvalho, M.A. Drought monitoring in the Brazilian Semiarid region. *An. Acad. Bras. Ciências* **2019**, *91*. [[CrossRef](#)]
51. McKee, T.B.; Doesken, N.J.; Kleist, J. The relationship of drought frequency and duration to time scales. In *Proceeding of the 8th Conference on Applied Climatology, Anaheim, CA, USA, 17–22 January 1993*; American Meteorological Society: Boston, MA, USA, 1993; pp. 179–184.
52. McKee, T.B.; Doesken, N.J.; Kleist, J. Drought monitoring with Multiple Time scales. In *Proceeding of the Ninth Conference on Applied Climatology, Dallas, TX, USA, 15–20 January 1995*; American Meteorological Society: Dallas, TX, USA, 1995; pp. 233–236.
53. Guttman, N.B. Accepting the standardized precipitation index: A calculation algorithm. *J. Am. Water Resour. Assoc.* **1999**, *35*, 311–322. [[CrossRef](#)]
54. Turco, M.; Jerez, S.; Donat, M.G.; Toreti, A.; Vicente-Serrano, S.M.; Doblas-Reyes, F.J. A global probabilistic dataset for monitoring meteorological droughts. *Bull. Am. Meteorol. Soc.* **2020**, *101*, E1628–E1644. [[CrossRef](#)]
55. Vicente-Serrano, S.M.; Begueria, S.; Lopez-Moreno, J.I. A multi-scalar drought index sensitive to global warming: The standardized precipitation evapotranspiration index. *J. Clim.* **2010**, *23*, 1696–1718. [[CrossRef](#)]
56. Begueria, S.; Vicente-Serrano, S.M.; Reig, F.; Latorre, B. Standardized Precipitation Evapotranspiration Index (SPEI) Revisited: Parameter fitting, evapotranspiration models, tools, datasets and drought monitoring. *Int. J. Climatol.* **2014**, *34*, 3001–3023. [[CrossRef](#)]
57. Tsakiris, G.; Vangelis, H. Establishing a drought index incorporating evapotranspiration. *Eur. Water* **2005**, *9*, 3–11.
58. Tsakiris, G.; Pangalou, D.; Vangelis, H. Regional Drought Assessment Based on the Reconnaissance Drought Index (RDI). *Water Resour. Manag.* **2007**, *21*, 821–833. [[CrossRef](#)]
59. Zhang, J.; Shen, Y. Spatio-temporal variations in extreme drought in China during 1961–2015. *J. Geogr. Sci.* **2019**, *29*, 67–83. [[CrossRef](#)]
60. Zhao, R.; Wang, H.; Chen, J.; Fu, G.; Zhang, C.; Yang, H. Quantitative analysis of nonlinear climate change impact on drought based on the standardized precipitation and evapotranspiration index. *Ecol. Indic.* **2021**, *121*, 107107. [[CrossRef](#)]
61. Scocco, P.; Piermarteri, K.; Malfatti, A.; Tardella, F.M.; Catorci, A. Increase of drought stress negatively affects the sustainability of extensive sheep farming in sub-Mediterranean climate. *J. Arid Environ.* **2016**, *128*, 50–58. [[CrossRef](#)]
62. González-Hidalgo, J.C.; Vicente-Serrano, S.M.; Peña-Angulo, D.; Salinas, C.; Tomas-Burguera, M.; Begueria, S. High-resolution spatio-temporal analyses of drought episodes in the western Mediterranean basin (Spanish mainland, Iberian Peninsula). *Acta Geophys.* **2018**, *66*, 381–392. [[CrossRef](#)]
63. Wu, D.; Li, Z.; Zhu, Y.; Li, X.; Wu, Y.; Fang, S. A new agricultural drought index for monitoring the water stress of winter wheat. *Agric. Water Manag.* **2021**, *244*, 106599. [[CrossRef](#)]
64. Hargreaves, G.H.; Samani, Z.A. Reference crop evapotranspiration from temperature. *Trans. ASAE* **1985**, *1*, 96–99. [[CrossRef](#)]
65. Samani, Z.A. Estimating Solar Radiation and Evapotranspiration Using Minimum Climatological Data. *J. Irrig. Drain. Eng.* **2000**, *126*, 265–267. [[CrossRef](#)]
66. Sheffield, J.; Wood, E.F.; Roderick, M.L. Little change in global drought over the past 60 years. *Nature* **2012**, *491*, 435–438. [[CrossRef](#)]
67. Dai, A. Characteristics and trends in various forms of the Palmer Drought Severity Index during 1900–2008. *J. Geophys. Res. Atmos.* **2011**, *116*, D12. [[CrossRef](#)]
68. Van der Schrier, G.; Barichivich, J.; Briffa, K.R.; Jones, P.D. A scPDSI-based global dataset of dry and wet spells for 1901–2009. *J. Geophys. Res. Atmos.* **2013**, *118*, 4025–4048. [[CrossRef](#)]
69. Valipour, M.; Bateni, S.M.; Gholami Sefidkouhi, M.A.; Raeini-Sarjaz, M.; Singh, V.P. Complexity of Forces Driving Trend of Reference Evapotranspiration and Signals of Climate Change. *Atmosphere* **2020**, *1*, 1081. [[CrossRef](#)]
70. Begueria, S.; Vicente-Serrano, S.M. SPEI: Calculation of the Standardised Precipitation-Evapotranspiration Index. Available online: <https://cran.r-project.org/package=SPEI> (accessed on 5 June 2020).

71. Yang, P.; Zhang, Y.; Xia, J.; Sun, S. Identification of drought events in the major basins of central Asia based on a combined climatological deviation index from grace measurements. *Atmos. Res.* **2020**, *244*, 105105. [[CrossRef](#)]
72. Sepulcre-Cantó, G.; Horion, S.; Singleton, A.; Carrao, H.; Vogt, J. Development of a Combined Drought Indicator to detect agricultural drought in Europe. *Nat. Hazards Earth Syst. Sci.* **2012**, *12*, 3519–3531. [[CrossRef](#)]
73. Naumann, G.; Alfieri, A.; Wyser, K.; Mentaschi, L.; Betts, R.A.; Carrao, H.; Soinoni, J.; Vogt, J.; Feyen, L. Global Changes in Drought Conditions Under Different Levels of Warming. *Geophys. Res. Lett.* **2018**, *45*, 3285–3296. [[CrossRef](#)]
74. Cammalleri, C.; Arias-Muñoz, C.; Barbosa, P.; De Jager, A.; Magni, D.; Musante, D.; Mazzeschi, M.; McCormick, N.; Naumann, G.; Spinoni, J.; et al. A revision of the Combined Drought Indicator (CDI) used in the European Drought Observatory (EDO). *Nat. Hazards Earth Syst. Sci.* **2021**, *21*, 481–495. [[CrossRef](#)]
75. Hao, Z.; Hao, F.; Singh, V.P.; Xia, Y.; Ouyang, W.; Shen, X. A theoretical drought classification method for the multivariate drought index based on distribution properties of standardized drought indices. *Adv. Water Resour.* **2016**, *92*, 240–247. [[CrossRef](#)]
76. Spinoni, J.; Vogt, J.V.; Naumann, G.; Barbosa, P.; Dosio, A. Will drought events become more frequent and severe in Europe? *Int. J. Climatol.* **2018**, *38*, 1718–1736. [[CrossRef](#)]
77. Zhu, J.; Zhou, L.; Huang, S. A hybrid drought index combining meteorological, hydrological, and agricultural information based on the entropy weight theory. *Arab. J. Geosci.* **2018**, *11*. [[CrossRef](#)]
78. Stagge, J.H.; Kohn, I.; Tallaksen, L.M.; Stahl, K. Modeling drought impact occurrence based on meteorological drought indices in Europe. *J. Hydrol.* **2015**, *530*, 37–50. [[CrossRef](#)]
79. Hao, Z.; Singh, V.P. Drought characterization from a multivariate perspective: A review. *J. Hydrol.* **2015**, *527*, 668–678. [[CrossRef](#)]
80. Dai, A.; Zhao, T.; Chen, J. Climate change and drought: A precipitation and evaporation perspective. *Curr. Clim. Chang. Rep.* **2018**, *4*, 301–312. [[CrossRef](#)]
81. Salehnia, N.; Alizadeh, A.; Sanaeinejad, H.; Bannayan, M.; Zarrin, A.; Hoogenboom, G. Estimation of meteorological drought indices based on AgMERRA precipitation data and station-observed precipitation data. *J. Arid Land* **2017**, *9*, 797–809. [[CrossRef](#)]
82. Tadić, L.; Bonacci, O.; Brleković, T. An example of principal component analysis application on climate change assessment. *Theor. Appl. Climatol.* **2019**, *138*, 1049–1062. [[CrossRef](#)]
83. Lopez-Bustins, J.A.; Serrano, E.; Ayarzagüena, B.; Sanchez-Lorenzo, A. Spatial and temporal temperature trends in the lower stratosphere during the extended boreal winter from reanalysis. *Int. J. Climatol.* **2015**, *35*, 3888–3901. [[CrossRef](#)]
84. Kaiser, H.F. An index of factorial simplicity. *Psychometrika* **1974**, *39*, 31–36. [[CrossRef](#)]
85. North, G.R.; Bell, T.L.; Cahalan, R.F.; Moeng, R.F. Sampling errors in the estimation of empirical orthogonal functions. *Mon. Weather Rev.* **1982**, *110*, 699–706. [[CrossRef](#)]
86. Henriques, A.G.; Santos, M.J.J. Regional drought distribution model. *Phys. Chem. Earth Part B Hydrol. Ocean. Atmos.* **1999**, *24*, 19–22. [[CrossRef](#)]
87. Spinoni, J.; Naumann, G.; Vogt, J.V.; Barbosa, P. The biggest drought events in Europe from 1950 to 2012. *J. Hydrol. Reg. Stud.* **2015**, *3*, 509–524. [[CrossRef](#)]
88. Wilhite, D.A.; Sivakumar, M.V.; Pulwarty, R. Managing drought risk in a changing climate: The role of national drought policy. *Weather Clim. Extrem.* **2014**, *2*, 4–13. [[CrossRef](#)]
89. Krichak, S.O.; Breitgand, J.S.; Gualdi, S.; Feldstein, S.B. Teleconnection–extreme precipitation relationships over the Mediterranean region. *Theor. Appl. Climatol.* **2014**, *117*, 679–692. [[CrossRef](#)]
90. Yao, J.; Tuoliewubieke, D.; Chen, J.; Huo, W.; Hu, W. Identification of Drought Events and Correlations with Large-Scale Ocean–Atmospheric Patterns of Variability: A Case Study in Xinjiang, China. *Atmosphere* **2019**, *10*, 94. [[CrossRef](#)]
91. Ionita, M.; Boroneant, C.; Chelcea, S. Seasonal modes of dryness and wetness variability over Europe and their connections with large scale atmospheric circulation and global sea surface temperature. *Clim. Dyn.* **2015**, *45*, 2803–2829. [[CrossRef](#)]
92. Cardil, A.; Rodrigues, M.; Ramirez, J.; de-Miguel, S.; Silva, C.A.; Mariani, M.; Ascoli, D. Coupled Effects of Climate Teleconnections on Drought, Santa Ana Winds and Wildfires in Southern California. *Sci. Total Environ.* **2020**, *765*, 142788. [[CrossRef](#)]
93. Ionita, M.; Tallaksen, L.M.; Kingston, D.G.; Stagge, J.H.; Laaha, G.; Van Lanen, H.A.J.; Scholz, P.; Chelcea, S.M.; Haslinger, K. The European 2015 drought from a climatological perspective. *Hydrol. Earth Syst. Sci.* **2017**, *21*, 1397–1419. [[CrossRef](#)]
94. Hurrell, J.W. Decadal trends in the North Atlantic Oscillation: Regional Temperatures and Precipitation. *Science* **1995**, *269*, 676–679. [[CrossRef](#)]
95. Redolat, D.; Monjo, R.; Lopez-Bustins, J.A.; Martin-Vide, J. Upper-level Mediterranean oscillation index and seasonal variability of rainfall and temperature. *Theor. Appl. Climatol.* **2019**, *135*, 1059–1077. [[CrossRef](#)]
96. Martín-Vide, J.; Lopez-Bustins, J.A. The Western Mediterranean Oscillation and rainfall in the Iberian Peninsula. *Int. J. Climatol.* **2006**, *26*, 1455–1475. [[CrossRef](#)]
97. Barnston, A.G.; Livezey, R.E. Classification, seasonality and persistence of low-frequency atmospheric circulation patterns. *Mon. Weather Rev.* **1987**, *115*, 1083–1126. [[CrossRef](#)]
98. Bueh, C.; Nakamura, H. Scandinavian pattern and its climatic impact. *Q. J. R. Meteorol. Soc.* **2007**, *133*, 2117–2131. [[CrossRef](#)]
99. Hoell, A.; Barlow, M.; Saini, R. The leading pattern of intrapersonal and interannual Indian Ocean precipitation variability and its relationship with Asian circulation during the boreal cold season. *J. Clim.* **2012**, *25*, 7509–7526. [[CrossRef](#)]
100. Barlow, M.; Zaitchik, B.; Paz, S.; Black, E.; Evans, J.; Hoell, A. A Review of Drought in the Middle East and Southwest Asia. *J. Clim.* **2016**, *29*, 8547–8574. [[CrossRef](#)]

101. Garcia-Herrera, R.; Garrido-Perez, J.M.; Barriopedro, D.; Ordonez, C.; Vicente-Serrano, S.M.; Nieto, R.; Gimeno, L.; Sori, R.; Yiou, P. The European 2016/17 Drought. *J. Clim.* **2019**, *32*, 3169–3187. [CrossRef]
102. García-Herrera, R.; Díaz, J.; Trigo, R.M.; Luterbacher, J.; Fischer, E.M. A Review of the European Summer Heat Wave of 2003. *Crit. Rev. Environ. Sci. Technol.* **2010**, *40*, 267–306. [CrossRef]
103. Mitchell, D.; Kurnhuber, K.; Huntingford, C.; Uhe, P. The day the 2003 European heatwave record was broken. *Lancet Planet. Health* **2019**, *3*, e290–e292. [CrossRef]
104. Touchan, R.; Anchukaitis, K.J.; Meko, D.M.; Sabir, M.; Attalah, S.; Aloui, A. Spatiotemporal drought variability in northwestern Africa over the last nine centuries. *Clim. Dyn.* **2011**, *37*, 237–252. [CrossRef]
105. Touchan, R.; Anchukaitis, K.J.; Meko, D.M.; Attalah, S.; Baisan, C.; Aloui, A. Long term context for recent drought in northwestern Africa. *Geophys. Res. Lett.* **2008**, *35*, L13705. [CrossRef]
106. Gleick, P.H. Water, Drought, Climate Change, and Conflict in Syria. *Cover Weather Clim. Soc.* **2014**, *6*, 331–340. [CrossRef]
107. Mathbout, S.; Lopez-Bustins, J.A.; Martin-Vide, J.; Bech, J.; Rodrigoc, F.S. Spatial and temporal analysis of drought variability at several time scales in Syria during 1961–2012. *Atmos. Res.* **2018**, *200*, 153–168. [CrossRef]
108. Lelieveld, J.; Hadjinicolaou, P.; Kostopoulou, E.; Chenoweth, J.; El Maayar, M.; Giannakopoulos, C.; Hannides, C.; Lange, M.A.; Tanarhte, M.; Tyrlis, E.; et al. Climate change and impacts in the Eastern Mediterranean and the Middle East. *Clim. Chang.* **2012**, *114*, 667–687. [CrossRef] [PubMed]
109. Körner, C.; Sarris, D.; Christodoulakis, D. Long-term increase in climatic dryness in the East-Mediterranean as evidenced for the island of Samos. *Reg. Environ. Chang.* **2005**, *5*, 27–36. [CrossRef]
110. Varol, T.; Ertuğrul, M. Climate change and forest fire trend in the Aegean and Mediterranean regions of Turkey. *Fresenius Environ. Bull.* **2016**, *24*, 3436–3444.
111. Tabari, H.; Willems, P. More prolonged droughts by the end of the century in the Middle East. *Environ. Res. Lett.* **2018**, *13*, 104005. [CrossRef]
112. Hanel, M.; Rakovec, O.; Markonis, Y.; Máca, P.; Samaniego, L.; Kysely, J.; Kumar, R. Revisiting the recent European droughts from a long-term perspective. *Sci. Rep.* **2018**, *8*. [CrossRef]
113. Zhong, L.; Hua, L.; Yan, Z. Datasets of meteorological drought events and risks for the developing countries in Eurasia. *Big Earth Data* **2020**, *4*, 191–223. [CrossRef]
114. Inbar, M.; Bruins, H.J. Environmental Impact of Multi-Annual Drought in the Jordan Kinneret Watershed, Israel. *Land Degrad. Dev. Geogr. Perspect.* **2004**, *15*, 243–256. [CrossRef]
115. Buttafuoco, G.; Caloiero, T. Drought events at different timescales in southern Italy (Calabria). *J. Maps.* **2014**, *10*, 529–537. [CrossRef]
116. Polemio, M.; Casarano, D. Rainfall and drought in southern Italy (1821–2001). *Basis Civiliz. Water Sci.* **2004**, *286*, 217–227.
117. Barriopedro, D.; Fischer, E.M.; Luterbacher, J.; Trigo, R.M.; Garcia-Herrera, R. The hot summer of 2010: Redrawing the temperature record map of Europe. *Science* **2011**, *332*, 220–224. [CrossRef] [PubMed]
118. Djebbar, A.; Goosse, H.; Klein, K. Robustness of the link between precipitation in North Africa and standard Modes of atmospheric variability during the last millennium. *Climate* **2020**, *8*, 62. [CrossRef]
119. Pal, J.S.; Giorgi, F.; Bi, X. Consistency of recent European summer precipitation trends and extremes with future regional climate projections. *Geophys. Res. Lett.* **2004**, *31*, L13202. [CrossRef]
120. Peters, W.; Bastos, A.; Ciais, P.; Vermeulen, A. A historical, geographical and ecological perspective on the 2018 European summer drought. *Philos. Trans. R. Soc.* **2020**, *B 375*, 20190505. [CrossRef]
121. FAO. *Drought Characterization and Management in Central Asia Region and Turkey*; FAO Water Reports no. 44; FAO, FAO Sub-Regional Office for Central Asia: Ankara, Turkey, 2017; Available online: <http://www.fao.org/resilience/resources/resources-detail/en/c/1113629/> (accessed on 20 June 2018).
122. Ouassou, A.; Ameziane, T.; Ziyad, A.; Belghiti, M. Application of the Drought Management Guidelines in Morocco. In MEDROPLAN Mediterranean Drought Preparedness and Mitigation Planning; Morocco, 2005; Chapter 19. Available online: https://projects.iamz.ciheam.org/medroplan/guidelines/archivos/Guidelines_Chapter19.pdf (accessed on 21 June 2021).
123. Payab, A.H.; Türker, U. Analyzing temporal–spatial characteristics of drought events in the northern part of Cyprus. *Environ. Dev. Sustain.* **2018**, *20*, 1553–1574. [CrossRef]
124. Khan, N.; Hadipou, R.S.; Shahid, S.; Ismail, T.; Ahmed, K.; Chung, E.S.; Nawaz, N.; Wang, X. Spatial distribution of secular trends in rainfall indices of peninsular Malaysia in the presence of long-term persistence. *Meteorol. Appl.* **2019**, *26*, 655–670. [CrossRef]
125. Selby, J.; Dahi, O.S.; Fröhlich, C.; Hulme, M. Climate change and the Syrian civil war revisited. *Polit Geogr.* **2017**, *60*, 232–244. [CrossRef]
126. Kelley, C.P.; Mohtadi, S.; Cane, M.A.; Seager, R.; Kushnir, Y. Climate change in the Fertile Crescent and implications of the recent Syrian drought. *Proc. Natl. Acad. Sci. USA* **2015**, *112*, e3241–e3246. [CrossRef] [PubMed]
127. Rateb, A.; Scanlon, A.R.; Kuo, C.Y. Multi-decadal assessment of water budget and hydrological extremes in the Tigris-Euphrates Basin using satellites, modeling, and in-situ data. *Sci. Total Environ.* **2021**, *766*, 144337. [CrossRef] [PubMed]
128. Gumus, V.; Algin, H.M. Meteorological and hydrological drought analysis of the Seyhan-Ceyhan River Basins, Turkey. *Meteorol. Appl.* **2017**, *24*, 62–73. [CrossRef]
129. Spinoni, J.; Antofie, T.; Barbosa, P.; Bihari, Z.; Lakatos, M.; Szalai, S.; Szentimrey, T.; Vogt, J. An overview of drought events in the Carpathian region in 1961–2010. *Adv. Sci.* **2013**, *10*, 21–32. [CrossRef]

130. Sepulcre-Canto, G.; Vogt, J.V.; Arboleda, A.; Antofie, T. Assessment of the EUMETSAT LSA-SAF evapotranspiration product for drought monitoring in Europe. *Int. J. Appl. Earth Obs. Geoinf.* **2014**, *30*, 190–202. [[CrossRef](#)]
131. Mihajlović, D. Monitoring the 2003–2004 meteorological droughts over Pannonian part of Croatia. *Int. J. Climatol.* **2006**, *26*, 2213–2225. [[CrossRef](#)]
132. Falloon, P.; Betts, R. Climate impacts on European agriculture and water management in the context of adaptation and mitigation—the importance of an integrated approach. *Sci. Total Environ.* **2010**, *408*, 5667–5687. [[CrossRef](#)] [[PubMed](#)]
133. Tselepidaki, I.; Zarifis, B.; Asimakopoulos, D.N. Low precipitation over Greece during 1989–1990. *Theor. Appl. Climatol.* **1992**, *46*, 115–121. [[CrossRef](#)]
134. Page, M.; Zribi, M. Analysis and Predictability of Drought In Northwest Africa Using Optical and Microwave Satellite Remote Sensing Products. *Sci. Rep.* **2019**, *9*. [[CrossRef](#)]
135. Le Meddi, H.; Meddi, M.; Assani, A.A. Study of Drought in Seven Algerian Plains. *Arab. J. Sci. Eng.* **2014**, *39*, 339–359. [[CrossRef](#)]
136. Vernar, D.; Tréguer, D.; Redwood, J.; Christensen, J.; McDonnell, R.; Elbert, C. *Climate Variability, Drought, and Drought Management in Morocco's Agricultural Sector*; The World Bank: Morocco, 2018.
137. Rita, A.; Camarero, J.J.; Nole, A.; Borghetti, M.; Brunetti, M.; Pergola, N.; Serio, C.; Vicente-Serrano, S.M.; Tramutoli, V.; Ripullone, F. The impact of drought spells on forests depends on site conditions: The case of 2017 summer heat wave in southern Europe. *Glob. Chang. Biol.* **2020**, *26*, 851–863. [[CrossRef](#)]
138. Buras, A.; Rammig, A.; Zang, C.S. Quantifying impacts of the 2018 drought on European ecosystems in comparison to 2003. *Biogeosciences* **2020**, *17*, 1655–1672. [[CrossRef](#)]
139. Fragaszy, S.R.; Jedd, T.; Wall, N.; Knutson, C.; Fraj, M.B.; Bergaoui, K.; Svoboda, M.; Hayes, M.; McDonnell, R. Drought Monitoring in the Middle East and North Africa (MENA) Region: Participatory Engagement to Inform Early Warning Systems. *Cover Bull. Am. Meteorol. Soc.* **2020**, *101*, E1148–E1173. [[CrossRef](#)]
140. Dimitrakopoulos, A.P.; Vlahou, M.; Anagnostopoulou, C.G.; Mitsopoulos, I.D. Impact of drought on wildland fires in Greece: Implications of climatic change? *Clim. Chang.* **2011**, *109*, 331–347. [[CrossRef](#)]
141. Quintana Seguí, P.; Martin, E.; Sanchez, E.; Zribi, M.; Vennetier, M.; Vicente-Serrano, S.M.; Vidal, J.P. Drought: Observed trends, future projections. In *The Mediterranean under Climate Change*; Thiebault, S., Moatti, J.P., Eds.; IRD Editions: Marseille, France, 2016; pp. 123–131. Available online: <https://hal.archives-ouvertes.fr/hal-01401386> (accessed on 21 July 2021).
142. Nicholson, S.E.; Funk, C.; Fink, A.H. Rainfall over the African continent from the 19th through the 21st century. *Glob. Planet. Chang.* **2018**, *165*, 114–127. [[CrossRef](#)]
143. Schilling, J.; Freier, K.P.; Hertig, E.; Scheffran, J. Climate change, vulnerability and adaptation in North Africa with focus on Morocco. *Agric. Ecosyst. Environ.* **2012**, *156*, 12–26. [[CrossRef](#)]
144. IPCC. Climate change 2014: Synthesis report. In *Contribution of Working Groups I, II and III to the Fifth Assessment Report of the Intergovernmental Panel on Climate Change*; Core Writing Team, Pachauri, R.K., Meyer, L.A., Eds.; IPCC: Geneva, Switzerland, 2014; 151p.
145. Seim, A.; Treydte, K.; Trouet, V.; Frank, D.; Fonti, P.; Tegel, W.; Panayotov, M.; Fernández-Donado, L.; Krusic, P.; Büntgen, U. Climate sensitivity of Mediterranean pine growth reveals distinct east-west dipole. *Int. J. Climatol.* **2015**, *35*, 2503–2513. [[CrossRef](#)]
146. Homdee, T.; Pongput, K.; Kanae, S. A comparative performance analysis of three standardized climatic drought indices in the Chi River basin, Thailand. *Agric. Nat. Resour.* **2016**, *3*, 211–219. [[CrossRef](#)]
147. Pathak, A.A.; Dodamani, B.M. Trend analysis of rainfall, rainy days and drought: A case study of Ghataprabha River Basin, India. *Modeling Earth Syst. Environ.* **2020**, *6*, 1357–1372. [[CrossRef](#)]
148. Pei, Z.; Fang, S.; Wang, L.; Yang, W. Comparative Analysis of Drought Indicated by the SPI and SPEI at Various Timescales in Inner Mongolia, China. *Water* **2020**, *12*, 1925. [[CrossRef](#)]
149. Krichak, S.O.; Alpert, P. Decadal trends in the East Atlantic West Russia pattern and the Mediterranean precipitation. *Int. J. Climatol.* **2005**, *25*, 183–193. [[CrossRef](#)]
150. Yosef, Y.; Sarroni, H.; Alpert, P. Trends in daily rainfall intensity over Israel 1950/1–2003/4. *Open Atmos. Sci. J.* **2009**, *3*, 196–203. [[CrossRef](#)]
151. Hannaford, J.; Lloyd-Hughes, B.; Keef, C.; Parry, S.; Prudhomme, C. Examining the large-scale spatial coherence of European drought using regional indicators of precipitation and streamflow deficit. *Hydrol. Process* **2011**, *25*, 1146–1162. [[CrossRef](#)]